2. Type of Mathematical Model:

☒ Process Model ☐ Abstraction Model ☐ System Model

DOC.20030819.0003

Describe Intended Use of Model:

This model will assess the impacts of igneous intrusion event on the Total Repository System Performance.

3. Title:

Igneous Intrusion Impacts on Waste Packages and Waste Forms

4. DI (including Rev. No. and Change No., if applicable):

MDL-EBS-GS-000002 REV 00

5. Total Attachments:		6. Attachment Numbers - No. of Pages in Each:	
Five (5)		I-8; II-8; III-4; IV-CD-ROM; V-2	

	Printed Name	Signature	Date
7. Originator:	Patricia Bernot	SIGNATURE ON FILE	8/15/03
8. CSO:	David Stahl	SIGNATURE ON FILE	8/15/03
9. Checker:	Steve Alcorn	SIGNATURE ON FILE	8/15/03
10. QER:	Judy Gebhart	SIGNATURE ON FILE	8/15/03
11. Responsible Manager/Lead:	Howard Adkins	SIGNATURE ON FILE	08-15-03
12. Responsible Manager:	Thomas W. Doering	SIGNATURE ON FILE	8-16-03

13. Remarks:

This report was written by Patricia Bernot, John Case, Dash Sayala, and Terry Steinborn.

This report was checked by Steve Alcorn, Susan LeStrange, Emma Thomas, and Kaveh Zarrabi.

2. Title:
Igneous Intrusion Impacts on Waste Packages and Waste Forms

3. DI (including Rev. No. and Change No., if applicable):
MDL-EBS-GS-000002 REV 00

4. Revision / Change Number:	5. Description of Revision/Change:
REV 00	Initial Issue.

CONTENTS

CONTENTS (Continued)

FIGURES

TABLES

INTENTIONALLY LEFT BLANK

ACRONYMS

DR   dissolution rate

EBS   engineered barrier system

FEP   feature, event, or process

TSPA   Total System Performance Assessment
TSPA-LA   Total System Performance Assessment for the License Application

INTENTIONALLY LEFT BLANK

1. PURPOSE

The purpose of this model report is to assess the potential impacts of igneous intrusion on waste packages and waste forms in the emplacement drifts at the Yucca Mountain Repository. The model is based on conceptual models and includes an assessment of deleterious dynamic, thermal, hydrologic, and chemical impacts. This constitutes the waste package and waste form impacts submodel of the Total System Performance Assessment for the License Application (TSPA-LA) model assessing the impacts of a hypothetical igneous intrusion event on the repository total system performance. This submodel is carried out in accordance with *Technical Work Plan for Waste Form Degradation Modeling, Testing, and Analyses in Support of SR and LA* (BSC 2003a) and *Total System Performance Assessment-License Application Methods and Approaches* (BSC 2002a). The technical work plan is governed by the procedures of AP-SIII.10Q, *Models*. Any deviations from the technical work plan are documented in the following sections as they occur.

The TSPA-LA approach to implementing the models for waste package and waste form response during igneous intrusion is based on identification of damage zones. Zone 1 includes all emplacement drifts intruded by the basalt dike, and Zone 2 includes all other emplacement drifts in the repository that are not in Zone 1. This model report will document the following model assessments:

- Impacts of magma intrusion on the components of engineered barrier system (e.g., drip shields and cladding) of emplacement drifts in Zone 1, and the fate of waste forms.

- Impacts of conducting magma heat and diffusing magma gases on the drip shields, waste packages, and cladding in the Zone 2 emplacement drifts adjacent to the intruded drifts.

- Impacts of intrusion on Zone 1 in-drift thermal and geochemical environments, including seepage hydrochemistry.

The scope of this model only includes impacts to the components stated above, and does not include impacts to other engineered barrier system (EBS) components such as the invert and waste package pallet.

Information regarding the impacts of magma leaving the repository are not dealt with in this model report but are discussed in *Characterize Eruptive Processes at Yucca Mountain, Nevada* (BSC 2001a).

2. QUALITY ASSURANCE

Quality Assurance Program Applicability: Development of this model report has been determined to be subject to the Yucca Mountain Project's quality assurance program because it will be used to support performance assessments and relates to items on *Q-List* (YMP 2001, Attachment I).

Electronic Management of Data: The technical work plan contains the Process Control Evaluation used to evaluate the control of electronic management of data (BSC 2003a,

Attachment III) during the modeling and documentation activities, and this evaluation determined that the methods identified in the implementing procedures are adequate. No deviations from these methods were performed.

3. USE OF SOFTWARE

This section describes the computer software used to conduct the modeling of thermal and chemical impacts of igneous intrusion. All applicable products are obtained from Software Configuration Management and have been verified appropriate for the application. A brief description of the computer software is included in Table 3-1. More in-depth descriptions of the software are included in Sections 3.1 and 3.2. The software products are run on standard computers listed in Table 3-2.

Table 3-1. Computer Software Used in the Igneous Intrusion Impacts Model

Software Name	Version	Software Tracking Number (Qualification Status)	Description and Components Used	Input and Output Files (Included in Attachment I)
EQ3/6	Version 7.2b	LLNL: UCRL-MA-110662 (Qualified on Windows 95)	EQ3NR: a speciation-solubility code	input: *.3i pickup: *.3p output: *.3o
			EQPT: a data file preprocessor	input: data0.* output: data1.*
EQ6	Version 7.2bLV	10075-7.2bLV-00 (Qualified on Windows 95)	EQ6: a reaction path code which models water/rock interaction or fluid mixing in either a pure reaction progress mode or a time mode	input: *.6i pickup: *.6p output: *.6o *.elem_aqu.txt *.elem_min.txt *.elem_tot.txt *.min_info.txt *.bin
ASPRIN	Version 1	10487-1.0-00 (Qualified on Windows 95)	Performs post-processing of numerical information from EQ6	input: *.bin output: *.xls
Microsoft Excel	97 SR-1 and SR-2	Commercial off-the-shelf software: Exempt in accordance with AP-SI.1Q, Section 2.1.	Used in this document for graphical representation and arithmetical manipulations	input: *.6o output: *.xls

Table 3-2. Computers Used

Computer Make	CPU #	Operating System	Software Used
Dell Optiplex GX300	117728	Windows 95	EQ3/6 V7.2b, EQ6 V7.2bLV, Microsoft Excel, ASPRIN
Dell Optiplex GX260	152393	Windows 2000	Microsoft Excel
Dell Optiplex GX260	501475	Windows 2000	Microsoft Excel

3.1 QUALIFIED SOFTWARE

3.1.1 EQ3/6 Version 7.2b

The major components of the EQ3/6 package (EQ3/6 V7.2b, STN: LLNL UCRL-MA-110662) include: EQ3NR, a speciation-solubility code; EQ6, a reaction path code which models water/rock interaction or fluid mixing in either a pure reaction progress mode or a time mode; EQPT, a data file preprocessor; EQLIB, a supporting software library; and several supporting thermodynamic data files. The software deals with the concepts of thermodynamic equilibrium, thermodynamic disequilibrium, and reaction kinetics. EQPT takes a formatted data file (a "data0" file) and writes an unformatted near-equivalent called a "data1" file, which is actually the form read by EQ3NR and EQ6. EQ3NR is useful for analyzing groundwater chemistry data, calculating solubility limits, and determining whether certain reactions are in states of partial equilibrium or disequilibrium. EQ3NR is also required to initialize an EQ6 calculation.

EQ6 represents the consequences of exposing an aqueous solution to a set of reactants, which react irreversibly. It can also represent fluid mixing and the consequences of changes in temperature. This code operates both in a pure reaction progress frame and in a time frame. In a time frame calculation, the user specifies rate laws for the progress of the irreversible reactions. Otherwise, only relative rates are specified. EQ3NR and EQ6 use a hybrid Newton-Raphson technique to make thermodynamic calculations. This is supported by a set of algorithms that create and optimize starting values. EQ6 uses an ordinary differential equation integration algorithm to solve rate equations in time mode.

3.1.2 EQ6 Version 7.2bLV

EQ6 7.2bLV (EQ6 V7.2bLV, STN: 10075-7.2bLV-00) is the only version of EQ6 capable of incorporating radioactive decay, and is the only version capable of passing time-varying aqueous compositions from run to run. Although EQ6 7.2bLV was the version of EQ6 used for this calculation, these two new features were not employed.

3.1.3 ASPRIN

ASPRIN Version 1 (ASPRIN V1.0, STN: 10487-1.0-00) performs post-processing of numerical information from an output data file created by EQ6 (*.bin). Although originally designed to calculate the isotopic inventory of radionuclides, this program is also able to extract output data (i.e., moles left of materials, solution composition, etc.) from the binary file produced as EQ6 V7.2bLV output.

3.2 EXEMPT SOFTWARE

Microsoft Excel (Versions SR-1 and SR-2) is a problem-solving environment used in calculations and analyses. It is also used to tabulate and chart results. The user-defined expressions, inputs, and results are documented in sufficient detail to allow an independent repetition of computations. Thus, Microsoft Excel is used as a worksheet and not as software routines. The formulae and algorithms used for Microsoft Excel, including the inputs and outputs, are given in the attachments.

4. INPUTS

All of the information in the following subsections is used as direct input to the Igneous Intrusion Impacts Model. Discussion of input uncertainties is included in Section 6.6.

4.1   DATA AND PARAMETERS

A summary of input data and parameters used in the model and related analyses are presented in Table 4-1. Details of all input data are given in subsequent sections of Section 4. All calculated inputs are presented in Section 6 within their respective sections. Discussion of uncertainty in the input parameters is addressed in Section 6.

Table 4-1. A Summary of Input Parameters and Data

Model component	Input	Reference document	Section
Intrusive impacts on waste package and waste forms	Initial intrusive magma conditions	BSC 2001a	Section 6.5
Intrusive heat flow / conduction and volatile gas diffusion	Thermal conductivities, porosity and density of rock units (Values in Table 4-2 of this report)	DTN: SN0208T0503102.007	Attachment I & IV Corresponding results presented in Section 6.5.2
	Heat capacity (Values in Table 4-2 of this report)	DTN: SN0303T0510902.002	
	Thermal diffusivity & specific heat of water	Incropera and DeWitt, 2002, p. 58, 59, and 924, Table A.6	
Total volume of magma in an intruded drift	Number of different types and dimensions of waste packages in a drift:	BSC 2003b BSC 2003c	Attachment II & IV Corresponding results presented in Section 6.5.2
	Dimensions of emplacement drift spacing between drifts	BSC 2003d BSC 2003e	
Volatile gas diffusion Total volatile gas moles and composition	Composition of volatile gas	DTN:LA0107GV831811.001	

Table 4-1. A Summary of Input Parameters and Data (Continued)

Model component	Input	Reference document	Section
Bounding the water content of basalt magma Total moles of volatile gases exsolving from magma Basalt characteristics	Mean chemical composition of basalt (Values in Table 4-5 of this report) Water content of basalt magma Mole percent volatile gas constituents (Values in Table 4-3 of this report)	DTN: LA0107GV831811.001	Attachment IV Corresponding results presented in Section 6.5.3
Reaction of seepage water with cooled basalt in EQ6	Dissolution of nepheline (Table 4-7 of this report)	Tole et al. 1986	
	Dissolution of albite (Table 4-7 of this report)	Chou and Wollast 1985	
	Dissolution of anorthite, enstatite, and quartz (Values in Tables 4.7 and 4-8 of this report)	Brady and Walther 1989	
	Dissolution of olivine (Values in Table 4-8 of this report)	Wogelius and Walther 1991	
	Dissolution of diopside (Values in Table 4-8 of this report)	Brantley and Chen 1995; Schott et al. 1981; Knauss et al. 1993	
	Dissolution of quartz (Values in Table 4-8 of this report)	Brady and Walther 1990	
	Densities of minerals (Values in Table 4-6 of this report)	Roberts et al. 1990	
	Basaltic composition in oxides (Values in Table 4-5 of this report)	DTN: LA0107GV831811.001	
	Density of minerals (Table 4-6 of this report)	Roberts et al. 1990	
	Atomic weights of elements	Parrington et al. 1996	
EQ3 input water compositions	Bin 8 seepage water (Table 4-9 of this report)	DTN: MO0304SPAEBSCB.001	
	Bin 11 seepage water (Table 4-10 of this report)	DTN: MO0304SPAEBSCB.001	
	J-13 well water (Table 4-10 of this report)	DTN: MO0006J13WTRCM.000	

4.1.1   Inputs for Heat Flow Calculations and Model Simulations

The primary thermal conductivity statistics are contained in Table 4-2.

Table 4-2. Summary of Primary Thermal Conductivity Statistics

Stratigraphic Unit	Bulk Dry Rock Mass Thermal Conductivity (W/m·K)	Bulk Wet Rock Mass Thermal Conductivity (W/m·K)	Matrix Porosity	Lithophysal Porosity	Dry Bulk Density (kg/m^3)	Specific Heat Capacity of Solids J/(g·K)
	k_{rm}	k_{rm}	ϕ_m	ϕ_L	ρ_{bd}	C_p
Tptpul	1.18	1.77	0.17	0.12	1830	0.93
Tptpmn	1.42	2.07	0.13	0.03	2150	0.93
Tptpll	1.28	1.89	0.15	0.09	1980	0.93
Tptpln	1.49	2.13	0.11	0.03	2210	0.93

DTN: SN0208T0503102.007, SN0303T0510902.002

NOTE: Porosity is the ratio of void volume to total rock volume, and has units of m^3 void/m^3 rock.

The following equations (from Attachment I) and parameter were used for the heat flow analysis in Attachment I:

- **Equation I-1**: Equation for one-dimensional unsteady heat conduction in a rod model, subject to constant heat content (Chapman 1974, p. 137).

- **Equation I-2**: Equation for finite difference expression approximations to first and second order derivatives for the radial heat conduction (Carnahan et al. 1990, p. 462).

- **Equation I-8**: Equation for volumetric heat capacity (BSC 2003f, Equation II-15).

- **Equation I-11**: Equation for grain density of solids (BSC 2002b, p. 41, Equation 6-4).

- Liquidus temperature of intruding magma = 1046 to 1169°C (DTN: LA0107GV831811.001).

The sources for the conductivity, porosity, dry bulk density and heat capacity listed in Table 4-2, and the temperature of the intruding magma are appropriate input for this report because they come from project data completed under the same quality program. The use of the equations by *Heat Transfer* (Chapman 1974) and *Applied Numerical Methods* (Carnahan et al. 1990) for the heat conduction model are appropriate because they are well-accepted thermodynamic handbooks, and the model for one-dimensional flow is conservative because it predicts the maximum heat flow by neglecting flow in the axial direction. The equations for volumetric heat capacity and grain density are appropriate input for this report because they come from project documents completed under the same quality program.

4.1.2 Inputs for Volatile Gas Calculations and Flow Model Simulations

The data used for calculation of volatile gas flow are found in Tables 4-3 and 4-4. Volatile components (volatile water and other gases) exsolved from intrusive magma are taken from DTN: LA0107GV831811.001. Owing to the absence of current volcanic activity in the Yucca Mountain region, direct measurement of gases is not possible. Therefore, the results of an extensive study on gases released from mafic volcanic centers (found in DTN:LA0107GV831811.001) are considered a proper surrogate.

Table 4-3. Mole Percent Concentration of Volatile Gases and Associated Uncertainty Estimates

Volatile Gases	Mean	Square Root of the Sum of the Squares	Standard Deviation
H_2O	73.16	17.97	19.81
H_2	1.17	0.89	0.67
CO_2	14.28	16.03	15.32
CO	0.57	0.59	0.75
SO_2	9.45	8.90	8.95
S_2	0.41	0.63	0.40
HCl	0.87	0.21	1.12
HF	0.17	0.04	0.08
H_2S	0.74	1.04	0.69

DTN: LA0107GV831811.001

Table 4-4. Parameters Used in Gas Flow Model

Parameter	Value	Source
Porosity of backfill	0.545	BSC 2001b, Table 4-1
Porosity of rock matrix	0.154	DTN: LB990861233129.001
Gaseous diffusivity	2.13E-5 m^2/sec	Lichtner et al. 1999
Universal gas constant	0.08205 atm × liters/(mole × K)	Weast 1984
Viscosity of water vapor	241.2 micro poises at 400°C	Weast 1984, p. F-44
Intrinsic permeability of mafic intrusion in rock matrix	Various (see source)	DTN: LB0207REVUZPRP.002
Porosity of magma	3-35	Domenico and Schwartz 1990, Table 2.1
Equation for pressure	Equation 1	BSC 2001a
Emplacement drift diameter	5.5 meters	BSC 2003d
Emplacement drift length	Various (see source)	BSC 2003e
Diameters of waste packages	Various (see source)	BSC 2003b
Length of waste package	Various (see source)	BSC 2003b
Number of types of waste packages	Various (see source)	BSC 2003c
Drift spacing	81 meters	BSC 2003d

The sources for the porosity for the backfill and rock matrix and the permeability of the mafic intrusion are appropriate input for this report because they come from project documents completed under the same quality program. The use of *A Natural Analog for Thermal-Hydrological-Chemical Coupled Processes at the Proposed Nuclear Waste Repository at Yucca Mountain, Nevada* (Lichtner et al. 1999) for the gaseous diffusivity is appropriate because the work was performed at Los Alamos National Laboratory, under a comparable quality program. The values for the universal gas constant, the viscosity of water, and the porosity of the magma from *CRC Handbook of Chemistry and Physics* (Weast 1984) and *Physical and Chemical*

Hydrogeology (Domenico and Schwartz 1990) are appropriate because these references are considered to be handbooks.

The information from the various IEDs (Information Exchange Drawing) is appropriate to calculate the volume of the drift available for a magma intrusion, because it is the latest design information, obtained from RPD (Repository Design) via the approved mechanism, an IED.

4.1.3   Inputs for EQ6 Simulation of Water/Basalt Reaction Hydrochemistry

4.1.3.1   Composition for Intruded Basalt Material

The basalt characteristics in Table 4-5 serve as the basis for the calculations of basalt/water interaction. The densities of normalized minerals are included in Table 4-6. The converted values (for normalized minerals) used for EQ6 calculations are located in Section 6.5.3. This composition was taken from an analysis of 45 samples taken from the Lathrop Wells Cone. This cone is the youngest volcanic center in the Crater Flat region next to Yucca Mountain and is, therefore, considered indicative of the composition of an intrusive body. The mineral densities used in the model calculations come from an accepted data source and so are considered appropriate for use in the model.

Table 4-5. Basalt Characteristics

Basalt Composition[a]			
Oxide	**Mean Wt%**	**Oxide**	**Mean Wt%**
SiO_2	48.5	K_2O	1.84
Al_2O_3	16.74	TiO_2	1.93
Fe_2O_3	1.74	P_2O_5	1.22
MgO	5.83	MnO	0.17
CaO	8.6	FeO	8.9
Na_2O	3.53	**Total**	99
Pore fraction = 0.17 [b]			
Saturation = 0.12 [c]			

Sources: [a] DTN: LA0107GV831811.001
[b] DTN: SN0208T0503102.007
[c] DTN: LB0307AMRU0120.001

Table 4-6. Mineral Densities

Mineral	Density (g/cm^{3})	Mineral	Density (g/cm^{3})
Anorthite	2.74-2.76 (p. 32)	Fayalite	4.32 (p. 268)
Albite	2.60-2.63 (p. 12)	Quartz	2.33 (p. 199)
Nepheline	2.55-2.665 (p. 603)	Diopside	3.22-3.38 (p. 228)
Sanidine	2.56-2.62 (p. 754)	Enstatite	3.209-3.431 (p. 250)
Rutile	4.23 (p. 746-747)		

Source: Roberts et al. 1990

NOTE: All density values are for measured density.

4.1.3.2 Dissolution Rates of Basalt Materials/Minerals

The dissolution rates of minerals come from various literature sources and are presented in Tables 4-7 and 4-8 below. These values are used in Microsoft Excel spreadsheets in Attachment IV to calculate EQ6 dissolution rates for minerals. These calculated rates are presented in Section 6.5.3 and Attachment III. All of the values for mineral dissolution come from peer-reviewed journals and are thus considered appropriate for use in this model.

Table 4-7. Dissolution Rates of Aluminosilicate Minerals

Albite[a]		Anorthite[b]		Nepheline[c]	
pH	Log DR (mols/cm^2·s)	pH	Log DR (mols/cm^2·s)	pH	Log DR (mols/cm^2·s)
1.2	-14.25	3	-13.30	3	-10.39
2.1	-14.60	3	-13.90	5	-12.40
2.5	-14.86	3.1	-13.00	7	-12.68
2.95	-15.26	3.25	-13.50	11	-11.89
3.05	-15.18	3.5	-14.30	—	—
3.5	-15.44	4	-15.00	—	—
4.1	-15.50	4.5	-15.20	—	—
5.1	-15.82	5	-15.50	—	—
5.4	-15.78	5.5	-15.50	—	—
5.5	-15.68	5.5	-15.60	—	—
5.6	-15.82	6	-15.70	—	—
5.6	-15.92	6	-15.00	—	—
7.8	-15.86	6	-14.80	—	—
8	-15.70	6.5	-15.70	—	—
9.45	-15.30	7	-15.70	—	—
9.55	-15.22	7.25	-15.60	—	—
10	-15.18	9.5	-14.80	—	—
10	-15.04	10	-14.70	—	—
10.7	-15.00	12	-14.20	—	—
11.2	-14.60	—	—	—	—
11.6	-14.64	—	—	—	—
12.3	-14.40	—	—	—	—

Sources: [a] Chou and Wollast 1985, Figure 5
[b] Brady and Walther 1989, Figure 4
[c] Tole et al. 1986, based on release of sodium

NOTES: DR = dissolution rate.

Table 4-8. Dissolution Rates of Olivine, Quartz, and Pyroxene Minerals

Olivine[a]		Quartz[b]		Diopside[c]		Enstatite[d]	
pH	Log DR (mols/cm^2·s)	pH	Log DR (mols/cm^2·s)	pH	Log DR (mols/cm^2·s)	pH	Log DR (mols/cm^2·s)
4.1	-13.07	2.15	-16.05	2.4	-12.30	1	-12.30
5.7	-13.78	4.09	-16.10	3	-12.60	2	-13.00
12	-14.36	4.03	-16.23	4	-13.30	4	-14.30
10.4	-14.74	5.5	-16.44	4.5	-13.90	6	-15.15
7.4	-13.80	8.33	-15.85	5	-14.10	8.4	-15.20
9.9	-14.46	10.27	-15.47	5.6	-14.50	9.4	-14.95
9.9	-14.58	12.3	-14.78	6	-14.80	10.1	-14.40
9.9	-14.38	11	-15.14	6	-14.90	12.2	-13.60
3.7	-12.27	11.04	-14.99	7.6	-15.00	—	—
10.8	-15.27	9.02	-15.85	9.4	-15.20	—	—
3	-12.79	10.9	-15.27	12.1	-15.20	—	—
5	-12.73	12.3	-14.81	1	-13.50	—	—
5.7	-14.34	10.3	-15.50	1.5	-12.10	—	—
2	-11.99	10.3	-15.51	2	-12.20	—	—
9.1	-14.54	6.9	-15.90	1	-12.20	—	—
3.7	-12.31	—	—	—	—	—	—
2.5	-12.21	—	—	—	—	—	—
4.4	-12.52	—	—	—	—	—	—
3.1	-12.34	—	—	—	—	—	—
4	-12.42	—	—	—	—	—	—
3	-12.29	—	—	—	—	—	—
3.5	-12.30	—	—	—	—	—	—
3.1	-11.88	—	—	—	—	—	—
5.3	-12.77	—	—	—	—	—	—
10.8	-14.27	—	—	—	—	—	—

Sources: [a] Wogelius and Walther 1991, Table 2
[b] Brady and Walther 1990, Table I (pH < 8) and Table III (pH > 8)
[c] Brantley and Chen 1995, Table 1
[d] Brady and Walther 1989, Figure 5

4.1.3.3   Composition and Flow Rate of Incoming Water

The composition of the water running through the basalt block (Table 4-9) is taken as that resembling Bin 8 seepage water from DTN: MO0304SPAEBSCB.001. The rational for considering Bin 8 seepage water is that Bin 8 seepage water has the highest time-integrated probability of occurrence (55 percent, DTN: MO0304SPAEBSCB.001). The flow rate was derived from a flux of 0.4 mm/year (DTN: LB0307AMRU0120.001). The low flow rate is selected because optimal chemical reaction of seepage water with the fractured basalt is not possible with higher flow rates of incoming seepage water. The water composition parameters and their values (DTN: MO0304SPAEBSCB.001) are given in Table 4-9.

Table 4-9. Water Composition and Redox Conditions Used in the EQ3 for Base-Case

EQ3NR Input Composition Values			
Element	Basis Switch	Concentration	Units
redox	—	-0.7 [a]	$LogfO_2$
Na^+	—	7.31E-03	moles/kg
$SiO_2(aq)$	—	1.79E-03	moles/kg
Ca^{++}		5.73E-04	moles/kg
K^+	—	2.76E-04	moles/kg
Mg^{++}	—	8.51E-05	moles/kg
H^+	—	7.94	pH
HCO_3^-	$CO_2(g)$	-2.198	Log fugacity
F^-	—	6.43E-04	moles/kg
Cl^-	—	5.61E-04	moles/kg
NO_3^-	$NH_3(aq)$	3.97E-05	moles/kg
SO_4^{--}	—	3.55E-04	moles/kg
AlO_2	—	1.50E-09	moles/kg
$HFeO_2(aq)$	—	1.49E-12	moles/kg

DTN: MO0304SPAEBSCB.001

NOTE: [a] Equilibrium atmospheric levels of oxygen.

It also needs to be noted that the EQ6 cases were run at log fCO_2 = -3 and at 25°C. These are the expected atmospheric conditions to prevail in the repository environment (BSC 2002c).

4.1.3.4   Sensitivity Cases

This section provides the inputs for the uncertainty cases presented in Section 6.5.3. The seven sensitivity cases involve changing base-case parameters such as water type, flow rate of water (flux=3.8 mm/year, DTN: LB0307AMRU0120.001), available reactive surface area of minerals, saturation index (fraction of pore saturation), and pore fraction (0.13, DTN: SN0208T0503102.007). Two of the uncertainty cases look at the effect that different water compositions have on the chemistry of the basalt/water interaction. The composition of the two modeled water types are presented below in Table 4-10. EQ3NR output for input into EQ6 is listed in Table 6.9.

Table 4-10. Water Composition and Redox Conditions Used in the EQ3 for Uncertainty Cases

		EQ3NR Input Composition Values			
Species	Basis Switch	Bin 11 Seepage Water[a]		J-13 Well Water[b]	
		Concentration	Units	Concentration	Units
redox	—	-0.7[c]	LogfO$_2$	-0.7[c]	LogfO$_2$
Na$^+$	—	4.80E-03	moles/kg	45.8	mg/L
SiO$_2$(aq)	—	1.19E-02	moles/kg	60.97	mg/L
Ca^{++}		3.34E-04	moles/kg	13.0	mg/L
K$^+$	—	7.50E-04	moles/kg	5.04	mg/L
Mg^{++}	—	6.34E-06	moles/kg	2.01	mg/L
H$^+$	—	7.76	pH	8.1	mg/L
HCO$_3^-$	CO$_2$(g)	-2.392	Log fugacity	-3	Log fugacity
F$^-$	—	1.38E-03	moles/kg	2.18	mg/L
Cl$^-$	—	5.61E-04	moles/kg	7.14	mg/L
NO$_3^-$	NH$_3$(aq)	3.97E-05	moles/kg	8.78	mg/L
SO$_4^{--}$	—	3.55E-04	moles/kg	18.4	mg/L
AlO$_2$	—	1.50E-09	moles/kg	—	—
HfeO$_2$(aq)	—	1.49E-12	moles/kg	—	—

NOTES: [a] DTN: MO0304SPAEBSCB.001
[b] DTN: MO0006J13WTRCM.000
[c] Equilibrium atmospheric levels of oxygen.

4.1.4 General EQ6 Inputs That Apply to All EQ6 Cases in This Model

4.1.4.1 Thermodynamic Database

The thermodynamic database used for the EQ6 calculations was the "data0.slt" file used at 25ºC, which is the qualified database ("data0.ymp.R2," DTN: MO0302SPATHDYN.000), but with commercial spent nuclear fuel and Savannah River Laboratory Glass included as "Minerals" and with 34 gas species deleted. The changes made to the database were not made specifically for this report, but for general use in EQ6 calculations of waste package corrosion. The underlying reason for deleting 34 gas species is that the EQ6 constraints only accommodate a limited number of gas species to be read from the database and the deleted gas species are not usually required for these types of calculations. The database can be found on Attachment IV. The "data0.ymp.R2" database is used in this model as it is the most comprehensive database available for modeling of aqueous systems.

4.1.4.2 Atomic Weights

Atomic weights were taken from *Atomic Mass Adjustment, Mass List for Analysis* (Audi and Wapstra 1995) and *Nuclides and Isotopes, Chart of the Nuclides* (Parrington et al. 1996).

4.2 CRITERIA

Project Requirements Document (Canori and Leitner 2003) identifies the high-level requirements for the Yucca Mountain Project. The requirements that pertain to this modeling report, and their link to 10 CFR Part 63, are shown below.

1. **PRD-002/T-014** (page 3-14) **Performance Objectives for the Geologic Repository After Permanent Closure** (Regulation 10 CFR 63.113):

   This section specifies the repository performance objectives that must be met following permanent closure. It includes a requirement for multiple barriers and limits on radiological exposure.

2. **PRD-002/T-015** (page 3-14) **Requirements for Performance Assessment** (Regulation 10 CFR 63.114):

   This section specifies the technical requirements to be used in performing a performance assessment. It includes requirements for calculations, including data related to site geology, hydrology, and variability in the models, and deterioration or degradation processes, including waste form degradation.

The following acceptance criteria from *Yucca Mountain Review Plan, Final Report* (NRC 2003) were identified as applicable to this technical product. Section 8.4 identifies information in this report that addresses the acceptance criteria associated with the integrated sub-issue of Mechanical Disruption of Engineered Barriers.

Mechanical Disruption of Engineered Barriers Acceptance Criteria (NRC 2003, Section 2.2.1.3.2.3):

- Acceptance Criterion 1: System description and model integration are adequate.

- Acceptance Criterion 2: Data are sufficient for model justification.

- Acceptance Criterion 3: Data uncertainty is characterized and propagated through the model abstraction.

- Acceptance Criterion 4: Model uncertainty is characterized and propagated through the model abstraction.

- Acceptance Criterion 5: Model abstraction output is supported by objective comparisons.

4.3 CODES AND STANDARDS

ASTM C 1174-97, *Standard Practice for Prediction of the Long-Term Behavior of Materials, Including Waste Forms, Used in Engineered Barrier Systems (EBS) for Geological Disposal of High-Level Radioactive Waste*, is used to support the model development methodology, to categorize the models developed with respect to their usage for TSPA-LA, and to relate the information and data used to develop the model to the requirements of the standard.

5. ASSUMPTIONS

This section identifies relevant assumptions, along with their respective rationale, that are essential for process modeling and assessing the impacts of igneous intrusion on waste packages and waste forms.

5.1 ASSUMPTIONS SPECIFIC TO INTRUSIVE EVENT AND IMPACTS

5.1.1 Assumption 1: Volume of Magma

Assumption: The volume of the magma is assumed to be equal to the total volume of the emplacement drift minus the volume of the waste packages.

Rationale: This assumption yields maximum volumes and masses of magma in Zone 1 drifts, because it conservatively assumes that the free volume of the engineered barrier system is reduced to zero. This volume is used for calculating the molar volumes of exolved gases, and modeling the gas diffusion and heat conduction between Zones 1 and 2 emplacement drifts.

Confirmation Status: This assumption is considered to be a conservative because it leads to a high source term for modeling gas diffusion and heat conduction between Zones 1 and 2 emplacement drifts. Therefore, it requires no further confirmation.

Use in the Model: This assumption is used in Section 6.5.2.2.

5.1.2 Assumption 2: Quantity of Water Exuded by the Magma

Assumption: A quantity of water corresponding to 2 weight percent would be exuded from the intruded magma. This water, containing other corrosive gases, would be available for diffusion away from the intruded drifts.

Rationale: According to Section 6.2.2 of *Characterize Eruptive Processes at Yucca Mountain, Nevada* (BSC 2001a), there is a uniform probability that the dissolved water content of basalt magma would be between 1 and 3 weight percent, reflecting that this is most likely range of water contents. The probability decreases linearly for water contents from 3 to 4 weight percent dissolved water, so that it is zero at 4 weight percent. Likewise, the probability decreases to zero at a water content of zero. The upper limit is based on the expectation that at water contents above about 4 weight percent, basaltic magma would crystallize underground rather than erupt. The upper bound of 4 weight percent dissolved water would initially exist in the intrusive magma at depths around 9 km (BSC 2001a, Figure 1). As the magma ascends, it decompresses at lower pressures and as a result, crystallization begins along with exudation of water vapor. At the pressure corresponding to the repository level the dissolved water content of the intruded magma is reduced to zero at the maximum temperature of 1169ºC or to 0.5 weight percent at a temperature of 1150ºC. Based on these considerations, a total volatile water mass of 2 weight percent is assumed. These water masses are derived from Figure 1 of *Characterize Eruptive Processes at Yucca Mountain, Nevada* (BSC 2001a).

Confirmation Status: The 2 weight percent water is the average of the range of most likely values. Concentrations of corrosive gases exuded from magma are in proportion to the amount

of water exuded (BSC 2001a, Table 3). Assumption of a high water content (2 percent for a magma at 1150ºC) leads to correspondingly high concentrations of corrosive gases available for diffusion into Zone 2 drifts and is conservative. Therefore, it requires no further confirmation.

Use in the Model: This assumption is used in Section 6.5.2.2.

5.1.3   Assumption 3: Permeability of Metamorphic Aureole and Cooled Basalt

Assumption: The permeability of any contact metamorphic aureole surrounding the intruded drifts is assumed to be as great as that of the bulk host rock. The basalt is assumed to fracture during cooling so that it too provides no barrier to flow.

Rationale: Natural analogs indicate that at the contacts of basalt dikes with tuffs of the types found at Yucca Mountain, there is extensive fusion and devitrification of glass to clays (Lichtner et al. 1999, pp. 8 and 9). This indicates there could be lower permeabilities in such a contact metamorphic aureole. However, it is not certain how uniformly such an aureole would form around a basalt-filled drift at Yucca Mountain, so it is assumed that hydraulic properties of the aureole are the same as those of the host rock.

In the case of the intrusive, the basalt magma would crack during magma cooling and degassing, providing paths for water flow. Maximum fracturing would occur at the flow margins, particularly the top resulting in greater permeability at the margins than in the center of the flow. However, the amount of fracturing and the resulting permeability variation is unknown so it is assumed that fracturing is uniform throughout the flow. It is further assumed that the fracturing is extensive enough that the basalt no barrier to flow.

Confirmation Status: This assumption is conservative in that it permits maximum water flow through basalt-filled drifts. Therefore, it does not require confirmation.

Use in the Model: This assumption is used in Section 6.5.3.

5.2   ASSUMPTIONS SPECIFIC TO VOLATILE GAS FLOW MODEL SIMULATIONS

5.2.1   Assumption 4: Advective Flow from Magma to the Drift

Assumption: The advective flow of volatile gases from the magma in the emplacement drifts is two-dimensional linear flow with the volatile gases traveling to the adjacent emplacement drifts on either side of the magma-filled drift.

Rationale: The two-dimensional advective linear flow is more effective from a high-pressure state to a low-pressure state. The linear flow is conservative because by ignoring the radial movement, transport of more volatile gases to the Zone 2 drifts is facilitated. This assumption is used in Section 6.5.2.2.

Confirmation Status: This assumption is conservative because it permits maximum movement of volatile gases to Zone 2. Therefore, it does not require confirmation.

Use in the Model: This assumption is used in Section 6.5.2.2.

5.2.2   Assumption 5: Source of Initial Pressure

Assumption: The initial pressure is that resulting from the elevated gas temperature, not the magma intrusion pressure.

Rationale: The full volume of volatile gasses will not be immediately available for movement after the intrusion, but would evolve slower than the magma movement because the exsolving of gases takes place according to the cooling rates of the magma.   The initial gas pressure was calculated at several hundred atmospheres from the number of moles of gas in the magma, the initial gas volume, and the temperature.   The temperature calculation presented in the report shows that there would only be a local temperature and therefore rock mass perturbation near the drift, and that is would be expected that the rock mass fracture properties in the vadose zone would not be significantly altered. Since the fractures are relatively free of water, the system is an open system.   Any gas pressure from the magma intrusion would be expected to relieve quickly with time. The gas flow analysis using rock mass properties support this conclusion. It would not be realistic to expect the gas pressures to be lithostatic.

Confirmation Status: Initial pressure resulting from elevated gas temperatures is considered realistic due to an open system quickly relieving gas pressure.   Therefore, no further confirmation needed.

Use in the Model: This assumption is used in Section 6.5.2.2.

5.3   ASSUMPTIONS SPECIFIC TO HEAT FLOW AND EQ3/6 SIMULATIONS

5.3.1   Assumption 6: Glass Degradation Rate

Assumption: It is assumed that the "basalt glass" material will have the same constant degradation rate as high-level radioactive waste glass (BSC 2001c) at a pH of 8.

Rationale: Since it is unknown exactly how this material would dissolve, the glass rate is considered a good surrogate because the dissolution rate chosen lies within the range of dissolution rates of the minerals within the basalt at a pH of 7 to 9. Also, a constant rate at pH 8 was considered viable since the pH of the incoming water (Bin 8 seepage water) lies below 8 and the pH of water, after equilibration with basalt as minerals, ranges from approximately 8.6 to 9.5.

Confirmation Status: No further verification needed.

Use in the Model: This assumption is used in Section 6.5.3.

5.3.2   Assumption 7: Block Size in Fractures

Assumption: It is assumed that basalt will fragment into meter sized blocks.

Rationale: Since it is unknown exactly how the basalt will fracture, meter sized blocks is considered a good surrogate. Intrusion into a emplacement drift can be correlated to cooling of basaltic materials in volcanic necks. Upon cooling, the magma tends to cool in large blocks or form columnar jointing (also usually in the meter scale).

Confirmation Status: Using the meter sized blocks is considered realistic. Therefore, no further confirmation needed.

Use in the Model: This assumption is used in Section 6.5.3.

5.3.3   Assumption 8: Thermal Properties of the Magma

Assumption: It is assumed that the thermal properties: thermal conductivity and diffusivity of the magma are the same as the welded tuff.

Rationale: The exact properties of the magma intruded into the emplacement drift are unknown. The assumption that the thermal properties (thermal conductivity and diffusivity) of the in-drift magma is at least as great as the drift wall rocks is reasonable for this type of order of magnitude analysis.

Confirmation Status: Attachment I shows that the results are sensitive to these parameters. Therefore, no further confirmation is needed.

Use in the Model: This assumption is used in Section 6.5.2.

6. MODEL DISCUSSION

6.1   MODELING OBJECTIVES

The main objective of this model is to assess the potential impacts of igneous intrusion on waste packages and waste forms in the emplacement drifts at the Yucca Mountain Repository. The model is based on conceptual models and includes an assessment of deleterious dynamic, thermal, hydrologic, and chemical conditions.

The TSPA-LA approach to implementing the models for waste package and waste form response during igneous intrusion is based on identification of damage zones. Zone 1 includes all emplacement drifts intruded by the basalt dike, and Zone 2 includes all other emplacement drifts in the repository that are not in Zone 1. This model report will document the following model assessments for implementation into TSPA damage zones as:

- Mechanical and thermal impacts of basalt magma intrusion on the waste packages and waste forms of the intersected emplacement drifts of Zone 1.

- Temperature and pressure trends of basaltic magma intrusion intersecting the Zone 1 and their potential effects on waste packages and waste forms in Zone 2 emplacement drifts.

- Deleterious volatile gases, exsolving from the intruded basalt magma and their potential effects on waste packages of Zone 2 emplacement drifts.

- Post-intrusive physical-chemical environment and seepage water alteration by reaction with intruded basalt.

The scope of this model only includes impacts to the components stated above, and does not include impacts to other engineered barrier system (EBS) components such as the invert and waste package pallet.

Information regarding the impacts of magma leaving the repository are not dealt with in this model report but are discussed in *Characterize Eruptive Processes at Yucca Mountain, Nevada* (BSC 2001a).

Due to lack of solid information (and data) on these processes in a repository environment, the model has used conservative assumptions and input values. Therefore, the model outputs are conservative and representative as bounding.

The objectives of the model assessments will be realized through model simulations, sensitivity analysis and corroboration with the relevant natural and industrial analogs or published data. These assessments and their results and limitations are provided in Sections 6.5, 6.6, 6.7, 7, and 8.

6.2   INCLUDED FEATURES, EVENTS AND PROCESSES

In support of TSPA-LA, one feature, event, or process (FEP) is considered (FEP 1.2.04.04.0A, Interaction of igneous intrusion with engineered barrier system components). The disposition of this FEP is summarized in Table 6-1.

Table 6-1. Included FEP for This Model Report and Its Disposition in TSPA-LA

FEP Number	License Application FEP Title	Section Where Disposition is Described
1.2.04.04.0A	**Igneous intrusion interacts with EBS components**	6.5.1, 6.5.2, and 6.7
	Description: An igneous intrusion in the form of a dike occurs through the repository, intersecting the repository drifts. Magma, pyroclastics, and volcanic gases enter the drift and interact with the EBS components including the drip shields, the waste packages, and the invert. This leads to accelerated drip shield and waste package failure (e.g., attack by magmatic volatiles, damage by flowing or fragmented magma, thermal effects) and dissolution or volatilization of waste.	
	Summary of Disposition in TSPA-LA: An igneous intrusion (basalt magma) occurs in the repository, intersecting Zone 1 emplacement. Damage to engineered barrier system components (waste packages, drip shield, and cladding), so that they no longer provide containment for the waste forms, and entraining of waste form by magma. The use of these results as used in total system performance assessment (TSPA) for modeling of Zone1 is described further in Section 6.5.1.	
	Potential impact of heat conduction and deleterious volatile gases diffusion from cooling magma on the engineered barrier system components and waste forms in the Zone 2- emplacement drifts is included in Section 6.5.2 on heat and gas flow. Potential impacts of heat conduction were assessed by numerical simulations of non-steady state heat conduction with radial flow modeling. The assessment of volatile gas was done by two-dimensional diffusion modeling using Fick's second law of diffusion. These will be implemented in the TSPA-LA impacts on engineered barrier system capability of Zone 2 emplacement drifts as indicated in Section 6.7.	
	The temporal evolution of hydrochemistry of interacted seepage water (Section 6.5.2) was calculated using EQ3/6. The temporal hydrochemistry will be applied to in-drift TSPA-LA sub-models, such as waste form degradation models, radionuclide dissolved concentrations model, and waste form colloidal model, as indicated in Section 6.7.	

6.3   BASE-CASE CONCEPTUAL MODEL

The base-case conceptual model is based on the igneous intrusion and consequential processes; these are outlined in the following:

- Intrusion of basaltic magma dike into Zone 1 emplacement drifts.

- Damage to drip shield, cladding, and waste packages in Zone 1 results in these components providing no further protection for the waste forms.

- Embedding of materials into magma intruded into Zone 1 drifts.

- Post-intrusive perturbations to the in-drift environment due to magma cooling includes heat loss by conduction, degassing, and fracturing of intrusive body. During the post intrusive perturbations, the intrusive would cool and the deleterious volatile gases, exsolving from the intruded magma, would diffuse through the host rock (tuff) with out any chemical interaction and reach the waste packages in Zone 2 emplacement drifts.

- Reversion to normal in-drift environmental conditions, with re-establishment of seepage flow. Seepage water entering the intruded drifts would react and equilibrate with the cooled and fractured basalt.

6.4   ALTERNATE CONCEPTUAL MODELS

The model that serves as the base-case for this model report is necessarily very simple because of the lack of solid information about the precise conditions that are most likely to occur given the occurrence of a highly unlikely igneous intrusion event.

Alternatives that may be relevant for igneous intrusive event impacts on the waste packages and waste forms are discussed in the remainder of Section 6.4.

6.4.1   Reaction Between Waste Forms and Basalt

The base case model does not consider the effects of reactions between the waste forms and the basalt and its reactive exudates. Thus, the concentrations of radioelements dissolving from waste within the basalt are considered to be the same as those developed from waste in drifts not affected by magma intrusion.

The spent fuel within the fuel rods is a hard ceramic material with a high melting point temperature of 2800°C; therefore, the commercial and defense spent nuclear fuel wastes exposed to hot magma are not expected to melt under temperatures no higher than the maximum magma temperature of 1169°C. However, when the waste canisters/assemblies and fuel claddings are damaged, the fuel pellets/rods may be assimilated into the cooling basalt magma. Under this scenario, two types of processes are expected: a) interaction between waste forms and the magma and b) interaction between the waste forms and the metal of waste canisters/assemblies and cladding in the presence of hot magma.

In the first case, (a), oxidation of UO_2 fuel in the presence of water-rich volatiles exuding from cooling basalt magma may occur (Einziger et al. 1991). In addition, radionuclides in the waste

could be incorporated into crystallizing silicate mineral phases such as soddyite [$(UO_2)_2(SiO_4) \times 2 H_2O$].

In the second case, (b), chemical interactions may occur between fuel and metals/alloys of damaged waste canisters/assemblies and claddings in the presence of the cooling magma that may result in the formation of new phases. This type of interaction is demonstrated by experiments conducted between UO_2 and Zircaloy-4 under isothermal and transient temperatures of 1000 to 1700°C and at 1 to 80 bars pressures for a duration of 1-150 minutes (Hofmann and Kerwin-Peck 1984). The authors show that under reducing conditions, oxygen from UO_2 is transported to the Zircaloy via the gas phase and as a result, uranium metal is formed. Uranium then diffuses to react with zirconium to start forming a layer of U-Zr alloy at about 800°C - 1150°C. Subsequently, several other solid solution layers of interactive U-Zr and Zr-oxides are formed at lower temperatures.

Dissolved Concentration Limits of Radioactive Elements (BSC 2003g, Section 6.7.2) illustrates that the solubility of soddyite is lower than that of schoepite, which is considered to be the phase controlling the concentration of uranium in fluids transiting the nominal repository. By analogy, if this alternate model accounting for fuel-basalt chemical interactions were adopted, it is likely that it would lead to lower dissolved actinide concentrations in water passing through basalt-filled drifts than are now used in the base-case model which does not consider such reactions.

It is to be expected that phases that could result from interaction between dispersed waste and waste package materials would be refractory and of limited solubility. However, the exact properties of these phases are not known. Therefore, this alternative conceptual model will not be analyzed further in this model.

6.4.2   Reaction Between Corrosion Products and Basalt

Igneous intrusion could also support chemical reactions within the waste packages and the drift. As magma intrudes into the drift, it could compromise the integrity of the waste packages and could cause a "thermite-type reaction" between aluminum and iron oxide (from corrosion of waste package components) by the following reaction:

$$2Al(s) + Fe_2O_3(s) \rightarrow Al_2O_3(s) + 2Fe(l)$$
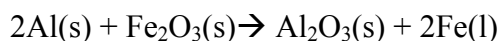
These types of reactions are known to be extremely exothermic and the activation energy for this reaction could be provided by the temperature increase in the drift by intruded magma. The $\Delta H°_{rxn}$ (heat of reaction) is about -847.6 kJ/mole and the temperatures from this reaction can exceed 1500°C producing molten iron. However, there are several parameters that make occurrence of this type of reactions less likely:

- The requirement for this reaction is to bring iron oxide in contact with aluminum. If during magma intrusion (magma acts as a continuous medium), iron oxide and aluminum were to come into contact with each other and the magma, they would likely react with the magma components to form secondary phases. If this were the dominant process, then a thermite type reaction would be unlikely.

- The density of magma is about 2.7 g/cm^3 and all oxides of iron exhibit density higher than magma. As a result, iron oxides in contact with magma would probably sink in the magma, due to the density difference, and react with it. This could preclude interactions between iron oxides and aluminum. Magma movement could disrupt the settling of the iron oxides, and the settling scenario depends upon several factors including viscosity of the magma, magma velocity, flow characteristics, and metal fragment sizes and shapes.

If any of the components to the thermite reaction are missing (i.e., unaltered aluminum and iron oxides), the thermite reaction will not occur. Because these materials will easily be incorporated into the magma or into secondary phases, the likelihood of having the unaltered aluminum and iron oxides in contact is very small. Therefore, this alternative conceptual model will not be analyzed further in this model.

6.4.3 Formation of Impermeable/Semi-Permeable Contact Metamorphic Aureole

During the intrusive and magma-cooling periods, propagation of dynamic pressures, fluid flow, conduction of heat and diffusion of volatile gases from Zone 1 drifts could induce a perturbed physical, thermal and chemical environment between Zones 1 and 2. Among the expected perturbations, is the formation of contact metamorphic aureole. For the contact aureole formation, magma fluids at high temperatures would interact with the drift wall rock (tuff), modifying the rock mineralogical composition, and weld the tuff, reducing the permeability and porosity of the contacted tuff. Field evidence of formation of metamorphic aureoles at the contacts of igneous intrusions and the intruded rocks which has a direct bearing on the intrusive scenario at the repository is the field study by Lichtner et al. (1999) at Paiute Ridge, located on the northeastern boundary of the Nevada Test Site. According to the authors, commonly, the tuff within 0.5 to 1.0 meter of the contact, at intrusive temperatures of 1000° to 1200°C, was completely fused to gray to black vitrophyre. From 1 to 3 meters from the contact, the degree of contact welding decreased to a sintered or original texture. From 2 meters of the contact, beginnings of devitrification of the volcanic glass shards and pumice to silicate phases (cristobalite and K-rich feldspars) was observed. Devitrification was observed to increase with increasing distance from the contact (Lichtner et al. 1999, p. 9). Based on this, at least one-meter wide contact metamorphic aureole could form at the intrusive-tuff contact. Because there is an uncertainty in the development and uniformity of the contact metamorphic aureole, the base case model considers the contact zone produces no effects on permeability

Natural analogs indicate that at the contacts of basalt dikes with tuffs of the types found at Yucca Mountain there is extensive fusion and devitrification of glass to clays (Lichtner et al. 1999, pp. 8 and 9). This indicates there could be lower permeabilities in such a contact metamorphic aureole. However, it is not certain how uniformly such an aureole would form around a basalt-filled drift at Yucca Mountain. Because of this, its overall effects to permeability cannot be easily quantified. Therefore, this alternative conceptual model will not be analyzed further in this model.

6.4.4 Fragmentation of Waste Forms

Corroborative evidence in support of cladding and waste form fragmentation and granulation is found in the results of the tests conducted for determining the stability of containers during

transport accidents under different scenarios (see Section 6.5.1.1). Results of these tests have shown the presence of broken-down and crushed fragments and granules of cladding, fuel pellets and rods. Lyman (1995) explained that substantial releases of plutonium and uranium oxides could occur when the cladding and fuel rods were subjected to a high-velocity impact, followed by a moderate temperature fire (as low as 500°C). Since the projected magma intrusive conditions at the repository are far more severe than the test conditions, more fragmentation and granulation of waste forms are expected to result from intrusion.

Thermal-shock induced effects are also found to fracture and fragment the UO_2 pellets and other ceramic materials. The degree of fracture and fragmentation is dependent on the porosity of the materials and the intensity of thermal shock (see Oguma 1985). The thermal shock experiments conducted by Oguma (1985) in the temperature range 200°C to 550°C demonstrates considerable fracturing in the UO_2 pellets. The study results suggest that severe fracturing, fragmentation, and granulation of waste forms due to thermal shock induced by basaltic intrusion could occur.

The data presented in Attachment I of *Miscellaneous Waste-Form FEPs* (CRWMS M&O 2001) presents the distribution of different size fractions of ground (ground by mortar and pestle in the laboratory) UO_2 fuel including unaltered fuel (uncorroded and unoxidized), dry-air oxidized fuel, and aqueous corroded fuel. The mean diameter of particle ranged from 0.002 to 0.0002 cm with the unaltered fuel having the largest mean grain size and the aqueous corroded fuel having the smallest, though only slightly lower than the air-oxidized fuel.

In the case of high-level radioactive waste glass waste forms, when the waste canisters are damaged by the intrusion, the vitrified glass waste would also be incorporated into the magma body. If the glass had already devitrified somewhat prior to intrusion, the heat of the intrusion may revitrify the glass waste. In any case, the glass fragments may devitrify as the glass cools in the magma. The extent of devitrification and re-vitrification would depend on the composition of the glass, extent of magma contact, contact magma temperatures and cooling rate. However, the extent of glass devitrification is expected to be small, because of the borosilicate based composition of the glasses. According to *Defense High Level Waste Glass Degradation* (BSC 2001c, Section 6.5.5), minimum precipitation of the high-level radioactive waste glasses occurs while it is in molten form at about 1150°C and as it solidifies in the canister.

The possibility of revitrification and devitrification of waste forms in the presence of magma can be demonstrated by some natural analogs and vitrification technology. Transformation of tuffaceous host rock (at temperatures of 1000° to 1200°C) to completely annealed vitric material, along with devitrification, against the intrusive contact was found at Paiute Ridge, located on the northeastern boundary of the Nevada Test Site (Lichtner et al. 1999). According to these authors, a clear evidence of devitrification of the volcanic glass shards and pumice to silicate phases (cristobalite and K-rich feldspars) was found starting about two meters from the intrusive contact. From this finding, it appears that there is a high reasonable probability of occurrence of revitrification of fragmented and shards glass in the intrusive magma contact at/near 1150°C, followed by devitrification as the magma cools.

The size distribution presented in *Miscellaneous Waste-Form FEPs* (CRWMS M&O 2001) is based on particles crushed in the laboratory by mortar and pestle. After the UO_2 fuel was crushed the first time, it is noted that there were numerous large fragments (>0.015 cm), material

less than 0.0045 cm and a relatively small amount of particles between 0.0045 and 0.015 cm. The distribution of these three particle sizes was never attempted. The larger pieces were re-ground and the materials milled again. It is these re-crushed particles that were used to determine the distribution of the particle sizes. The introduction to Attachment I of *Miscellaneous Waste-Form FEPs* (CRWMS M&O 2001) also states that the discussion is "based on laboratory examinations of commercial spent nuclear fuels, which were conducted for purposes outside the realm of understanding particle size." Also, there is no correlation as to how particles obtained by grinding with a mortar and pestle relate to fragment sizes due to an igneous intrusion into an emplacement drift. For these reasons, the size of fragmented waste forms is still not considered to be specifically quantified. Therefore, this part of the alternative conceptual model will not be analyzed further in this model.

Based on this corroborative published literature and limited evidence of natural analogs, possible revitrification of fragmented glass waste forms, followed by devitrification, would be expected at intrusive liquidus-temperatures of at or below 1150°C. However, the uniformity of occurrence of such processes at the Yucca Mountain Repository is not certain. It is assumed that vitrification and devitrification can be either total or partial depending on the degree of contact of glass fragments with magma at those temperatures. The extent of devitrification and revitrification of high-level radioactive waste glass as well as products that may be formed is unknown at this time. Therefore, this part of the alternative conceptual model will also not be analyzed further in this model.

6.5   BASE-CASE CONCEPTUAL MODEL RESULTS

For assessing the impacts of igneous intrusion, a conservative approach is taken by considering sequential events and processes during and post-intrusive periods. Given the nature of the intrusive event and processes, the modeling and assessment of impacts are governed by aleatoric and epistemic uncertainties (aleatoric uncertainty refers to uncertainty for which sufficient knowledge is unobtainable such that the corresponding parameters are treated as chance of occurrences of FEPs. Epistemic uncertainty arises from a lack of knowledge about a parameter because the data are limited or there are alternative interpretations of the available data). A discussion of these uncertainties is presented in Section 6.7. To compensate for uncertainties, a conservative approach is taken in the modeling and assessing the impacts of igneous intrusion. This approach has considered bounding expected conditions such as intrusive temperature, pressure, flow velocity and volume, and total compression of waste packages, cladding and waste forms (see Assumptions 1, 2, 3, 4, 5, and 8). In addition, the results of this study are corroborated by relevant natural and industrial analog and/experimental data.

Each stage of the sequence of events and processes, and their resulting effects on waste packages (including drip shields and cladding), waste forms, and the in-drift environment of Zones 1 and 2 are described below.

6.5.1   Intrusion of Basalt-Magma into Zone 1 Emplacement Drifts

Magma intrusion into emplacement drift(s) would likely be a composite of forcefully injected pyroclastic debris, hot gases, and flowing magma. Based on the data provided in Table 4 of

Characterize Eruptive Processes at Yucca Mountain, Nevada (BSC 2001a). The effects of such an intrusion are outlined in the remainder of Section 6.5.1.

6.5.1.1   Impacts on Waste Packages

The basic TSPA assumption for the igneous intrusion event is that the waste packages and other barrier materials in Zone 1 will be damaged during the intrusion, failing to provide further protection to the waste forms. The summary below is further corroboration for this assumption.

Several lines of evidence support that the igneous intrusion would render the drip shields, waste packages and cladding in the Zone 1 emplacement drifts ineffective so they would provide no further protection to the waste. These evaluations are summarized below.

The temperature of the intruding magma may be as high as 1169ºC (BSC 2001a, Table 7). The melting temperatures of Alloy C-22 (1357ºC) and 316NG SS (1375ºC) (CRWMS M&O 1999, Section 5.1) are above the magma temperature, but the metals would certainly lose strength at the magma temperature.

Waste Package Behavior in Magma (CRWMS M&O 1999) provides calculations of the pressures that would develop within waste packages as the result of gas expansion at high temperatures. It concludes that as temperatures approach 1200ºC the resulting stresses on the packages would reach the tensile strength of the package materials. If a package has been corroded or otherwise weakened it would have a lower tensile strength that could be exceeded by the internal pressure developed at lower temperatures. This provides a possible mechanism for package breaching.

Evidence in support of such damage is seen in the tests conducted for determining the stability of containers under different scenarios of transport accidents and sabotage. These tests considered 120 miles per hour truck impact accidents (with linear forces of up to 100,000 pounds/ft), variable energy shocks and vibrations, engulfing fire at 800°C temperature and high energy explosions (Sanders et al. 1992, Appendix III; Fischer et al. 1987, Section 6; Sandoval et al. 1983). The tests have indicated that the containers would be damaged to varying degrees. Similarly, the findings of literature review on the performance of waste package and drip shield materials in magmatic environments, documented by Structural Integrity Associates (Gordon 2003), suggest that the structural integrity of these materials would be severely compromised and damage could occur. For example, Types 310 and 446 stainless steels, exposed to Hawaiian basaltic lava at 1300°C and 2 psi for 100 hours, was extensively reacted and damaged, while alloy 718 suffered a loss of structural integrity (Gordon 2003).

During the course of magma cooling, waste packages and canisters/assemblies may be subject to corrosion, the degree of which may vary depending on their composition, contact magma temperature, and in situ geochemical environment. Magma temperatures, pressures, and geochemical environment in the drift, influenced by the magma composition and volume of exsolving volatile gases, such as H_2O, H_2, CO_2, CO, SO_2, S_2, HCl, HF, and H_2S may have a significant impact on corrosion rates. Literature review findings related to oxidation, sulfidation and corrosion propensities and rates of Alloy 22 waste package materials, drip shield titanium

alloy, and similar alloys in magmatic environments shed some on the degree of corrosion (Gordon 2003, Section 5).

Kinetic corrosion rate calculations suggest that Zircaloy cladding can be significantly damaged by corrosion in a matter of days in the presence of water vapor at temperatures between 250°C to 360°C (Hillner et al. 1998; CRWMS M&O 2000). In the nuclear industry, it is well known that cladding embrittlement and failure occur in the presence of volatiles or oxygenated environment at temperatures above 1204°C. Based on this corroborative information, damage to cladding could also occur in a matter of minutes to hours after the intrusion of magma with exsolving volatiles.

One study of binary and ternary alloys, containing molybdenum and chromium and exposed to basaltic magma at 1150°C for periods of 24 and 96 hours, shows essentially no quantifiable corrosion; however, a linear oxidation/sulfidation rate of approximately 0.83 µm/h was suggested (Ehrlich and Douglass 1982). Another finding, from a qualitative study of various alloys in contact with Hawaiian basalt lava, indicate that Types 310 and 446 stainless steel reacted extensively with the degassed lava while Udimet 700 and alloy 718 suffered a loss of structural integrity (Gordon 2003). Findings from another study, conducted at 727°C for 96 hours, indicate that under reducing 1.5 percent H_2S plus 98.5 percent H_2, the corrosion is significantly higher than in oxidizing-sulfidizing environment with 59 percent Ar, 3 percent O_2, 36.5 percent H_2 and 1.5 percent H_2S (Gordon 2003). All these corroborative findings suggest that metals embedded in the cooling basalt magma would be subjected to variable corrosion.

Results of magma-metal/alloys compatibility tests, conducted in a volatile-rich rhyolite magma at 850°C and 15-200 MPa pressures for run-durations of 1 hour to 30 days also shed light on the reaction of metals in contact with the magma, and on the formation of polymorphic minerals and xenocrysts. Although, the volatile content and temperature of intrusive basaltic magma at Yucca Mountain are different from those considered in the tests, the test results are used to demonstrate the possibility of reaction of metallic fragments at the metal-magma contacts. Some pertinent results of the tests outlined by (Westrich 1990) include formation of Fe/Cr/Mn-oxides (e.g., magnetite-Fe_3O_4), silicates (e.g., fayalite-Fe_2SiO_4) and aluminum oxides (e.g., hercynite-$FeAl_2O_4$) and mobilization of sulfur from magma and steels.

The tests were conducted for periods ranging from several minutes to 22 days under conditions similar to the environment of a shallow rhyolitic magma (850°C and 100 MPa). The preliminary results for the high carbon steel, under vapor saturated conditions, indicated the initial growth of large euhedral crystals of fayalite (Fe_2SiO_4) outward from the magma-metal interfaces followed by growth of two spinel phases and initial phases of hercynite ($FeAl_2O_4$) and magnetite (Fe_3O_4). The results of the runs of longer duration showed continued growth of magnetite phases. The tests have also indicated that high carbon steel showed a zone of sulfidation far below the zone of Fe oxides.

6.5.1.2   Impact on Waste Forms

With the damage of the waste packages, the waste forms are also subject to disruption. Effects may include:

- Incorporation of waste forms into cooling magma

- Chemical interactions with magma and exuded fluids which could alter the solubility of the waste forms.

The types and extents of such changes would depend upon such factors as the degree and duration of magma contact with waste forms, the contact pressure, viscosity and temperature; the redox conditions at the time of intrusion and the physical and chemical characteristics of the waste forms. While there are no verifiable data on waste form changes due to basaltic magma, it is to be expected that phases that could result from interaction between dispersed waste and waste package materials would be refractory and of limited solubility. However, the exact properties of these phases are not known. Therefore, the waste is conservatively considered chemically unchanged.

The extent of fragmentation and size distribution of the fragmented waste forms cannot be delineated with any certainty. However, these fragments and granules are expected to be engulfed by the magma. The crushed material may form radionuclide bearing minerals by incorporation into crystallizing silicates minerals as suggested by natural analog data. The effects of such reactions are explored as an alternate conceptual model in Section 6.4.3.

6.5.1.3   Results of Base Case Model for Waste Form Properties in Basalt-Filled, Zone 1 Drifts

It is conservatively concluded that the igneous intrusion would render the drip shields, waste packages, and cladding in the Zone 1 emplacement drifts ineffective so they would provide no further protection to the waste form. This provides further corroboration to the TSPA assumption that the waste packages in Zone 1 provide no further protection to waste forms after an intrusive event.

It is also concluded that the waste form would be distributed throughout the cooled magma, though exactly how is unknown. Spent fuel is itself a refractory material and in the base case is considered to be chemically unaffected by exposure to the intruding magma. Likewise, waste glass is considered likely to be minimally affected because the thermal environment during a magma intrusion would be similar to that in which the glass was fabricated.

Because waste forms are conservatively considered chemically unchanged (see Section 6.5.1.2) in the base case model, the dissolved concentration of radioelements in water in the basalt would have the same dependency on water chemistry as does waste dissolving in regions not influenced by an igneous intrusion. Thus, the solubility tables given in *Dissolved Concentration Limits of Radioactive Elements* (BSC 2003g) should be used to determine concentrations of radionuclides in basalt-filled drifts the same way they are used in magma-free drifts.

6.5.2 Numerical Simulations of Heat and Gas Flow from Zone 1 Emplacement Drifts Filled with Basalt Magma

6.5.2.1 Numerical Simulations of Non-Steady State Heat Conduction with Radial Flow

The temperature distribution for a magma flow filling a Zone 1 emplacement drift can be estimated using a one-dimensional unsteady heat conduction in a rod model, subject to constant heat content. The magma is considered to be at an initial intrusive temperature of 1150°C (BSC 2001a). The magma fills the drift entirely (see Assumption 1) and the temperature dissipates both spatially and temporally. The temperature of the drift wall and the far-field is considered to be 25°C at the time of the intrusion. The heat transfer thermal properties of the magma are considered to be the same as those for the densely welded tuff (see Assumption 5.3.3) for a first order analysis. The logic flow for the heat conduction model is explained in more detail, along with pertinent equations, in Attachment I.

6.5.2.1.1 Results of Model Simulations

The model simulations and analysis consider four types of lithophysal and nonlithophysal units that comprise the repository horizon (Tptpul, Tptpmn, Tptpll, and Tptpln). All of these units are from the Topopah Spring Tuff (Tpt). The fourth letter in the unit designation represents the crystal poor zone of this tuff. The last two letters in each unit designator are defined as follows: ul = upper lithophysal zone, mn = middle nonlithophysal zone, ll = lower lithophysal zone, and ln = lower nonlithophysal zone. To cover a broad range of potential conditions, the analysis assumes different alternative thermal properties of the tuff matrix: saturated with water, and void of water (dry conditions). The model considers ideal saturations: completely saturated and completely dry (as opposed to real saturation conditions, which are somewhere in between). Simulations of radial conduction of intrusive heat into the areas surrounding the intruded emplacement drifts are carried out.

The magma intrudes into the Zone 1 emplacement drifts in a single instantaneous event at a temperature of 1150°C, and heat diffuses to the surrounding welded tuff units by radial heat conduction with constant heat content. The rate at which thermal diffusion takes place depends on the thermal conductivity, and the volumetric heat capacity of the welded tuff.

The results of the analysis for different repository horizon rock units for a period of 50 years are presented in Figures 6-1 and 6-2 for the wet and dry analysis for Tptpll. The results for the three other regions were so similar to the Tptpll results, that the differences can not be distinguished in the graphs, and only the results for Tptpll were plotted. These figures show a simplified configuration of intruded drift and the adjacent drift. The results show that the temperatures near the drift are high. However, the temperatures attenuate rapidly into the surrounding tuff. The peak temperature is reduced with radius and shifted out in time. For example, the peak temperature at a 10-meter radius is less than boiling, and is attained after one year while the peak temperature at a radius of 20 m is approximately 40°C after several years. Under either completely dry or completely wet conditions, the temperature reduces to about 30°C at drift center in about 30 years. Further, the analysis shows that the high temperatures after the magma event attenuate rapidly with distance. The maximum temperature rise in the adjacent emplacement drifts in Zone 2 is small (less than 10°C), and that the rock provides an effective

thermal insulation barrier to the impacts of high temperature magma intrusion. Therefore, the spatial and temporal heat conduction simulations and analysis suggest that the waste packages in Zone 2 emplacement drifts would not be affected by the heat conducting from the magma intruded into Zone 1 emplacement drifts.
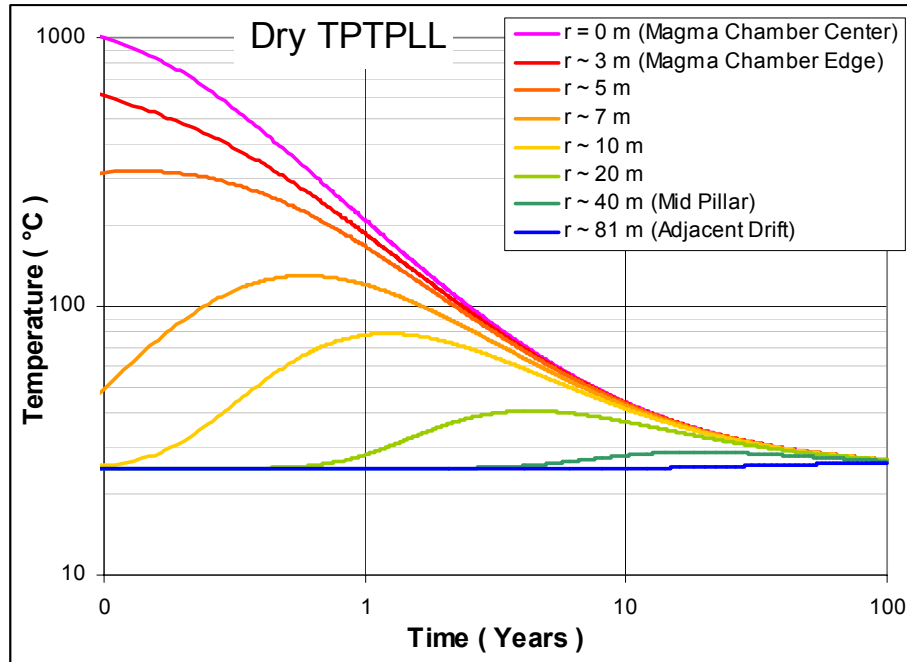
Figure 6-1. Heat Conduction from Magma Flow for Dry Tptpll
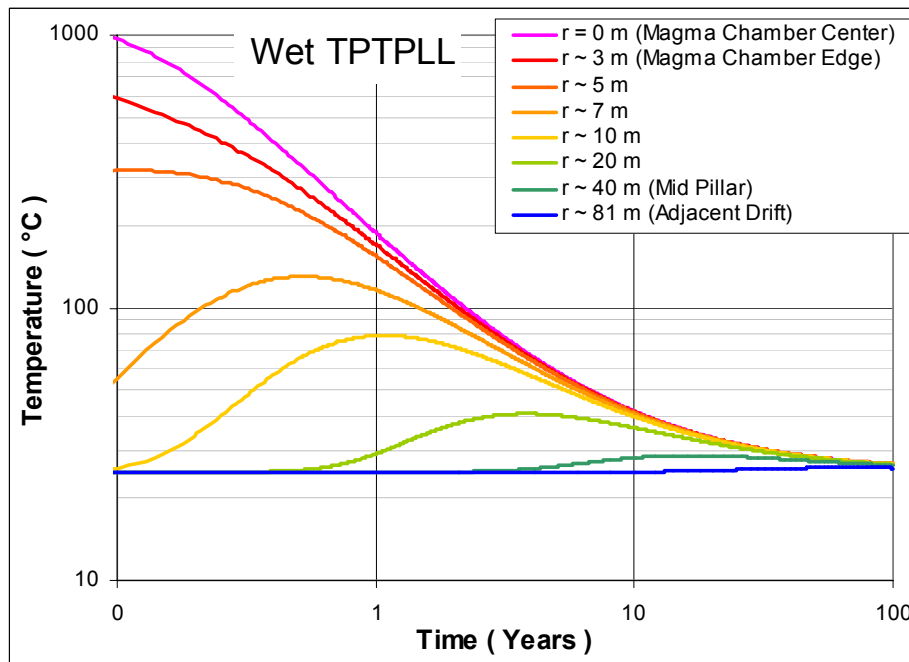
Figure 6-2. Heat Conduction from Magma Flow for Wet Tptpll

6.5.2.2   Simulations of Flow of Volatile Gas Components from Intrusive Magma

6.5.2.2.1   Volatile Gas Components

The data on the dissolved water content of post-Miocene basaltic magma in the Yucca Mountain region are sparse, and it is difficult to define a precise value distribution function for the dissolved water content for use in the TSPA-LA modeling of igneous consequences. *Characterize Eruptive Processes at Yucca Mountain, Nevada* (BSC 2001a, p. 29) recommended a distribution range of 0-4 weight percent dissolved water content for Yucca Mountain basalt magmas.   According to *Characterize Eruptive Processes at Yucca Mountain, Nevada* (BSC 2001a), between 1 and 3 percent, the probability should be uniform, reflecting the fact that this is most likely range of water contents. Between 3 and 4 weight percent of dissolved water, the probability decreases linearly so that it is zero at 4 weight percent, representing the expectation that at about 4 weight percent, basaltic magma would crystallize underground rather than erupt. Since this model report deals with the intrusive dike impacts, this study assumes that the upper bound of 4 weight percent initial dissolved water content initially exists in the intrusive magma. This initial mass of water is expected at depths around 9 km (BSC 2001a, Figure 1). As the magma ascends, it decompresses at lower pressures and as a result, crystallization of magma begins along with exsolving of water vapor. Owing to this, the initial dissolved mass of water in the magma is reduced. A value of 2 weight percent volatile water mass is considered to be the upper bound value for this study (see Assumption 4); therefore, it is conservative.

For purpose of simulating the transport of exsolving volatile gases away from the intrusive magma, the volatile water mass of 2 weight percent (see Assumption 2) and the mean values of volatile gases (H_2, CO_2, CO, SO_2, S_2, HCl, HF, and H_2S) are used. Using these values, the total mole volumes of all volatile components available for transport to the adjacent drifts from the total volume of intruded magma are computed by Microsoft Excel computational software. The details of these computations are given in Attachment IV (Microsoft Excel spreadsheet "gas flow analysis.xls"), and the total moles are given in Table 6-2.

Table 6-2. Total Moles of Volatile Components

Volatile Gas	Gram weight Concentration	Mole Fraction
H_2O	13.1688	0.7316
H_2	0.0234	0.0117
CO_2	6.2832	0.1428
CO	0.1596	0.0057
SO_2	6.048	0.0945
S_2	0.2624	0.0041
HCl	0.3171	0.0087
HF	0.0341	0.0017
H_2S	0.2516	0.0074

Source: BSC 2001a; Microsoft Excel spreadsheet Heat
Conduction - Dry Tptpll.xls in Attachment IV

6.5.2.2.2   Simulations of Volatile Gas Flow

The analysis considers the scenario of instant intrusion of magma into the Zone 1 emplacement drift and backfilled perimeter drifts. The fractured and porous rock as well as the crushed tuff used to backfill the perimeter drifts represents a possible path for gas flow resulting from magma intrusion. The Ideal Gas Law is used in the estimate of gas flow from a magma-filled drift to an adjacent emplacement drift.

For the purpose of this analysis, the diffusion through the backfill is neglected and the host rock material is described as an isotropic material (i.e., the diffusivity coefficient along the three principal axes is equal). The result is a concentration front moving radially outward from the magma filled drift into the surrounding host rock. The gas flow analysis is documented in Attachment II.

6.5.2.2.3   Results of Gas Flow Analysis

The gas flow analysis from Zone 1 to Zone 2 is detailed in Attachment II. The results of the gas flow analysis are found in Microsoft Excel spreadsheet "gas flow analysis.xls" in Attachment IV, and are plotted in Figures II-2 through II-7 in Attachment II. The main points from this analysis are summarized below.

Gas movement through the backfill is slower than the rock matrix and does not move as far as the flow in the rock matrix (Figures II-2 and II-3). For a given gas flux rate, the pore velocity of gas moving through a less porous material is faster because the flow of the gas occurs through a smaller area. This difference can be attributed to the difference in porosity between the two materials (host rock porosity = 0.154, backfill porosity = 0.545, see Table 4-4). In both cases, the velocity approaches zero around one year. As the pressure equilibrates to under 10 atmospheres, the gas flow rate decreases (Figure II-4). The movement of the gas front in the rock matrix and backfill is shown in Figure II-3. The gas front eventually stops at around 3.6 m in the host rock and 1.4 m in the backfill. Results of the advective flow analysis show that gas movement resulting from advection is minimal and is likely the result of the decreased permeability of the basalt intrusion.

While advective gas flow is one component of movement between the drifts during the first year, diffusion is still occurring and becomes the single mode of gas movement at some point during gaseous equilibration. Results from the analyses of gaseous diffusion from the magma filled emplacement drift show that the gas concentrations entering the adjacent Zone 2 emplacement drifts, would be low and begin to significantly reduce after about two years. The maximum number of moles that would enter the adjacent drift (Zone 2) is about 100 moles; the resulting concentration of the gases is presented in Table II-1. It is important to note that the calculated concentration of gases that would reach zone two is extremely conservative because the model neglects interactions of the gases with the host rock, and the models only considers flow in the horizontal direction. The acid components of the gases released from the magma will interact strongly with the rock between the drifts, so any gases that do migrate into adjacent drifts will be much less aggressive with respect to corrosion. In addition, much of the water vapor will condense in the rock, based on the temperatures calculated in Attachment I. The gases will migrate away from the intersected drift in all directions, so the actual amount of gas that moves

horizontally to the adjacent drifts will only be a fraction of the gas released. Therefore, it is concluded that the waste packages in Zone 2 emplacement drifts would not be impacted by the volatile gases exsolving from the basalt magma intruded into Zone 1 emplacement drifts.

6.5.3 Reaction of Seepage Water with Basalt After Reversion to Normal In-Drift Environmental Conditions

After post-intrusive magma cooling and reversion to normal in-drift environmental conditions, the seepage water is expected to flow through the contact metamorphic aureole and react first with the basalt in the intruded emplacement drifts, resulting in basalt-equilibrated seepage water. The geochemical interaction of seepage water with the basalt and the resulting hydrochemistry are simulated using EQ6 model.

The following sections provide calculated inputs into EQ6 simulations. All data for EQ6 simulation taken directly from controlled sources can be found in Sections 4.1.3 and 4.1.4. The results of the EQ6 simulations are located in Section 6.5.3.5.

The basalt composition provided in Table 4-5 is used in two ways representing the two end members of possible basalt cooling regimes. The first use is to convert the composition in oxides to moles of idealized minerals (for use as EQ6 reactants) shown in Table 6-3. The second use is the normalization of the oxides into a single material, called a "basalt-glass" (a homogenous mix of elements input into EQ6 in the form of the moles of individual elements) in this report. This is found in Table 6-4.

The normalized minerals were derived by normalization of the oxides from *Characterize Eruptive Processes at Yucca Mountain, Nevada* (BSC 2001a) to the modal composition of Crater Flat basalts recommended by Vaniman et al. (1982).

The normalization of basalt composition in oxides to composition in minerals was based on the following points:

- According to Vaniman et al. (1982), the primary minerals in basalts of Crater Flat include the plagioclases, pyroxenes, nepheline, and olivine. The plagioclase in the normative analysis was divided between the two end members of albite and anorthite. Although the orthopyroxene (enstatite) and olivine (fayalite) also are end members of a series, for ease of calculation only the end members mentioned here are used. This is because many of these minerals contain like elements (e.g., Mg, Fe) and since exact division of these to their respective minerals is unknown, the other end members (forsterite for olivine and ferrosilite for orthopyroxenes) were left out for simplicity in the normative analysis.

- The mineral sanidine was included to use the K_2O. This monoclinic disordered orthoclase feldspar is a very common constituent of acidic and alkaline volcanic rocks (Roberts et al. 1990, p. 754) and was considered justified for use.

- Cristobalite was used for the remaining SiO_2 in the analysis.

- Several of the minerals above can contain minor amounts of titanium. However, due to database constraints, this cannot be taken into account. Therefore, rutile was used to place the TiO_2 in the analysis. Though not a major mineral in basaltic rocks, it is known as an accessory mineral in many types of igneous rocks (Roberts et al. 1990, pp. 746 and 747).

- Vaniman et al. (1982) also mention minor amphibole (but not any particular one). However, due to the complexity of their chemical formulas, and once again not knowing the exact division of elements between minerals, no amphibole minerals were included in the normative analysis for ease of analysis.

Table 6-3. Idealized Mineral Composition of Basalt

EQ6 Minerals	EQ6 Mineral Formula	Mineral Molecular Weight	Wt%
Fayalite	Fe_2SiO_4	203.77	15.2326
Nepheline	$NaAlSiO_4$	142.05	8.3036
Sanidine_high	$KAlSi_3O_8$	278.33	11.1599
Albite_low	$NaAlSi_3O_8$	262.22	15.3279
Anorthite	$CaAl_2(SiO_4)_2$	278.21	25.0385
Diopside	$MgCaSi_2O_6$	216.55	14.5947
Enstatite	$MgSiO_3$	100.39	8.1375
Cristobalite(alpha)	SiO_2	60.08	0.2246
Rutile	TiO_2	79.87	1.9808

Source: Microsoft Excel spreadsheet Heat Conduction - Dry Tptpll.xls in Attachment IV

NOTE: All values above calculated in "basalt.xls" in Attachment IV.

Table 6-4. EQ6 Composition of Basalt as One Reactant "Basalt-Glass"

Element	Moles/100g	Element	Moles/100g
Si	0.8154	K	0.0395
Al	0.3317	Ti	0.0244
Fe	0.1471	P	0.0174
Mg	0.1461	Mn	0.0024
Ca	0.1549	O	2.7593
Na	0.1151		

NOTE: All values above calculated in "basalt.xls" in Attachment IV.

6.5.3.1   EQ6 Base-Case

EQ6 also requires the input of mineral surface areas and moles. These values, calculated in "basalt.xls" in Attachment IV are shown in Table 6-5. It should be noted that these values are based on having meter sized basalt blocks (see Assumption 7) in the fractured areas and a saturation index of 0.1 (saturation index of 0.12 from Table 4-5 rounded to 0.1).

Table 6-5. Surface Area and Moles of Mineral Reactants

Mineral	Moles	Surface Area (cm^2)
Fayalite	1.098E+02	4.46E+02
Nepheline	8.588E+01	2.43E+02
Sanidine	5.891E+01	3.27E+02
Albite	8.588E+01	4.49E+02
Anorthite	1.322E+02	7.33E+02
Diopside	9.901E+01	4.28E+02
Enstatite	1.191E+02	2.38E+02
Cristobalite	5.491E+00	6.58E+00
Rutile	3.644E+01	5.80E+01
"basalt-glass"	1.470E+03	2.929E+03

NOTE: Calculated in "basalt.xls" in Attachment IV

The dissolution rates of materials come from various literature sources and are presented in Tables 4.7 and 4-8. The calculated rates for EQ6 calculations using those rates from Tables 4-7 and 4-8 are presented in Table 6-6 and Attachment III. The rates for the minerals in the EQ6 cases were cast in the transition state theory formalism (Wolery and Daveler 1992, Section 3.3.3). The rate used for the "glass" material is a constant rate but was taken from the model for high-level radioactive waste glass for a pH of 8 (see Assumption 6), which is considered as an average pH of seepage water. The sources for the mineral dissolution rates are used here because they come from peer reviewed journals and in many cases they are the only source of information available for dissolution of minerals. A more in-depth discussion on the mineral dissolution rates can be found in Attachment III.

Table 6-6. Dissolution Rates of Basaltic Minerals and "Basalt-Glass"

Mineral	Acidic leg		Basic Leg	
	k$_1$	S1[b]	k$_2$	S2[b]
Anorthite	1.58E-11	0.91	2.0E-18	-0.3
Albite_low	7.94E-15	0.33	5.01E-19	-0.32
Nepheline	3.98E-08	1.0	7.94E-15	-0.2
Sanidine_high	Used same rate as albite			
Fayalite	7.94E-12	0.4	5.25E-15	0
Enstatite	1.58E-12	0.57	1.26E-19	-0.44
Diopside	3.16E-11	0.7	6.31E-16	0
Cristobalite(alpha)[a]	5.62E-17	0	3.16E-19	-0.3
Rutile	Used same rate as cristobalite[c]			
"Basalt-Glass"	Constant rate, 1.58E-15 moles/cm^2·s			

NOTES: Total Dissolution Rate = $k_1[H^+]^{S1} + k_2[H^+]^{S2}$ (moles/cm^2·s).

All values above were extrapolated in Microsoft Excel spreadsheets "Aluminosilicate rates.xls", "pyroxene rates.xls", "olivine rate.xls", "quartz rate.xls", and "HLWglass-2001.xls" in Attachment IV.

[a] Since cristobalite is composed of SiO_2 (Roberts et al. 1990), quartz values for dissolution were used to describe the dissolution of cristobalite.

[b] "S" represents the slope of the rates presented in this table and in Attachment III.

[c] Since rutile (TiO_2) is a simple metal oxide like cristobalite, cristobalite values are used for the dissolution of Rutile.

The rate for the "basalt-glass" was taken as a constant value equal to the corrosion of high-level radioactive waste glass at a pH of 8 ("HLWglass.xls" in Attachment IV; see Assumption 6). It needs to be noted that the pH dependence of the corrosion rate was abandoned for a simpler constant rate. Because of the uncertainty in the degradation rate of the basalt-glass material, the rate is taken as a constant value equal to the corrosion of high-level radioactive waste glass at a pH of 8 (see Assumption 6). Entering the "basalt-glass" to the input files instead of the database and the use of a constant dissolution rate were done for simplicity of the calculation and does not require further alteration of the thermodynamic database.

The composition of the water running through the basalt block (Table 6-7) is the EQ3-equilibrated Bin 8 seepage water from DTN: MO0304SPAEBSCB.001. The flow rate below was derived from an infiltration rate of 0.4 mm/year (DTN: LB0307AMRU0120.001) and is calculated in "basalt.xls" on Attachment IV.

Table 6-7. Water Composition and Flow Rate Used in the EQ3/6 Input Files of Water/Basalt Interaction

EQ3NR Input Composition Values				EQ6 Input File Composition[b]		
Element	Basis Switch	Concentration	Units	Element	Concentration	Units
redox		-0.7 [a]	$LogfO_2$	pH	7.94	pH
Na^+		168.0	mg/L	Na	7.31E-03	Moles/kg
$SiO_2(aq)$		108.0	mg/L	Si	1.90E-03	Moles/kg
Ca^{++}		23.0	mg/L	Ca	5.73E-04	Moles/kg
K^+		10.8	mg/L	K	2.76E-04	Moles/kg
Mg^{++}		2.07	mg/L	Mg	8.52E-05	Moles/kg
H^+		7.94	pH	O	5.55E+01	Moles/kg
HCO_3^-	$CO_2(g)$	-2.198	Log fugacity	C	6.95E-03	Moles/kg
F^-		12.2	mg/L	F	6.42E-04	Moles/kg
Cl^-		19.9	mg/L	Cl	5.61E-04	Moles/kg
NO_3^-	$NH_3(aq)$	2.46	mg/L	N	3.97E-05	Moles/kg
SO_4^{--}		34.1	mg/L	S	3.55E-04	Moles/kg
Al		4.05E-05	mg/L	Al	1.50E-09	Moles/kg
Fe^{++}		8.32E-08	mg/L	Fe	1.49E-12	Moles/kg
Flow Rate [c] = 1.726E-11 moles/s						

NOTES: [a] Equilibrium atmospheric levels of oxygen.
[b] These values are the output from EQ3NR for input into EQ6 input files.
[c] Calculated in Microsoft Excel spreadsheet "basalt.xls".

6.5.3.2   Sensitivity Cases

The base-case EQ6 run for basalt/water interactions having meter sized basalt blocks in the fractured areas and a saturation index of 0.1. As indicated in Section 4.1.3.4, seven sensitivity cases were examined that involve changing parameters to the base case that include water type, flow rate of water (flux), available reactive surface area of minerals, saturation index (fraction of pore saturation), and pore fraction.

Two different water types were used for the sensitivity analysis. The EQ6 Input file composition of Bin 11 seepage-water and J-13 well water (from EQ3NR output) are presented in Table 6-8.

Table 6-8. Water Composition Used in the EQ3/6 Input Files of Water/Basalt Interaction for Sensitivity Cases

EQ6 Input File Composition					
Bin11 Seepage Water			J-13 Well Water		
Element	Concentration	Units	Element	Concentration	Units
pH	7.73	pH	pH	8.1	pH
Na	4.78E-03	Moles/kg	Na	1.99E-03	Moles/kg
Si	1.19E-02	Moles/kg	Si	1.02E-03	Moles/kg
Ca	3.43E-04	Moles/kg	Ca	3.24E-04	Moles/kg
K	7.49E-04	Moles/kg	K	1.29E-04	Moles/kg
Mg	6.34E-06	Moles/kg	Mg	8.27E-05	Moles/kg
O	5.55E+01	Moles/kg	O	5.55E+01	Moles/kg
C	1.21E-03	Moles/kg	C	2.07E-03	Moles/kg
F	1.38E-03	Moles/kg	F	1.15E-04	Moles/kg
Cl	1.30E-03	Moles/kg	Cl	2.01E-04	Moles/kg
N	1.26E-04	Moles/kg	N	1.42E-04	Moles/kg
S	7.30E-04	Moles/kg	S	1.92E-04	Moles/kg
Al	3.10E-09	Moles/kg	Al	1.00E-16	Moles/kg
Fe	3.31E-12	Moles/kg	Fe	1.00E-16	Moles/kg

Table 6-9 presents the rest of the values used for the sensitivity analyses compared to the value used in the base case.

Table 6-9. Parameter and Values Changes for Sensitivity Cases versus Base-Case for Basalt/Water Interaction

Parameter	Sensitivity Value	Base Case Value
Flux (mm/year)	3.8 mm/year[a]	0.4 mm/year
	0.04 mm/year[b]	
Saturation Index	1.0[a,c]	0.1
Pore Fraction	0.13[a,c]	0.17
Surface Area of Minerals	0.1 times values in Table 4-6	Values in Table 4-6 of this report

NOTES: [a] From Section 4.1.3.4.
[b] Taken as 0.1 times base case rate.
[c] Note that when the values for the saturation index or pore fraction change, the surfaces areas and moles of minerals (like those in Table 6-7) also change. These values can be found in Microsoft Excel spreadsheet "basalt.xls" in Attachment IV.

6.5.3.3   All EQ6 Cases

For EQ3 and EQ6 runs, a trace concentration of elements is added to Bin 8 seepage water, Bin 11 seepage water and J-13 well water composition that are not in the original composition, but are in the composition of the basalt. This is to ensure numerical stability in EQ6 runs. The trace elements added are found in Table 6-10.

Table 6-10. Elements Added as "Trace" to Water

Ti[a]	P[a]	Mn[a]	Al[b]	Fe[b]

NOTES: [a] Added to all three water types as trace.
[b] Added only to J-13 well water as trace.

During EQ6 simulations, upon reaction with basalt, mineral phases precipitate from solution into the fractures within the basalt. Several minerals are suppressed from forming in the EQ6 runs because, though thermodynamically favored, they are kinetically unlikely to form upon reaction of water with cooled basalt. The following minerals were suppressed (not allowed to form) in all EQ6 runs:

Quartz	Tridymite	$CaZrO_3$	Muscovite	Celadonite
Dolomite	Dolomite-dis	Dolomite-ord	Annite	Phlogopite

The micas (muscovite, annite, celadonite, and phlogopite), quartz, and tridymite are high temperature (>500°C) minerals (Roberts et al. 1990) and not expected to form. Celadonite can form at low temperatures, but this is due to either diagenesis of pre-existing material, very low grade metamorphic processes, or concentration of the liquid environment through evaporation (Li, Peacor, et al. 1997; Li, Lowenstein, and Blackburn 1997), so celadonite is not expected to form. Dolomite is usually derived by secondary mineralization. Since it rarely occurs as a primary mineral, it was also suppressed. (Klein and Hurlbut 1999).

6.5.3.4   EQ6 Nomenclature for Water/Basalt Cases

The name for EQ6 cases contains various numbers and letters describing the inputs into that particular case. This nomenclature is defined here.

The first part of the EQ6 case names are indicative of the water type reacted with the basalt indicated with:

- bin11 = Bin 11 Seepage Water, bin8 = Bin 8 Seepage Water, and j13 = J-13 well water.

The letter in the file name immediately following the water type is indicative of the conditions in which the run was carried out as indicated below:

- b = base case where saturation index = 0.1, flux = 0.4 mm/year, pore fraction = 0.17, and the basalt is fractured into meter sized particles.

- p = pore fraction of base case changed to 0.13.

- a = surface area of minerals decreased by 0.1 times from the base case.

- s = saturation index of base case changed to 1.0.

- f1 = flux rate of base case changed to 3.8 mm/year.

- f2 = flux rate of base case decreases 0.1 times.

The final set of letters in the case name is indicative of the material with which the water was reacted as indicated by:

- m = basalt modeled as normalized minerals

- gm = basalt modeled as a homogenous mix of elements (Table 6-4) called "basalt-glass" in this model.

6.5.3.5 Results of EQ6 Simulations of Crown Seepage Water Reaction with Cooled Basalt

Due to the great amount of output generated through the EQ6 simulations of crown seepage water reaction with cooled basalt in an emplacement drift, these files are located on Attachment IV. The results of the abstraction of values (pH, fluoride content, ionic strength, pO_2, and pCO_2) for use in TSPA-LA can be found in Section 6.7.3.

6.6 DISCUSSION OF UNCERTAINTIES

The inferences/assumptions and the results presented in this model report are based on the conceptual models (base-case and alternative) governed by a hypothetical igneous intrusive event, and associated processes and conditions that could occur in the repository. Given the nature of the events and processes associated with igneous intrusion scenario, the prediction of impacts on the repository system and, in particular, on the waste packages and waste forms is complex. To compensate for uncertainties, the model simulations and analyses are based on conservative assumptions/estimates and bounded/maximum parameter values, and supported by corroborative natural and industrial analogs or experimental results.

The model simulations and analyses are based on conservative assumptions/estimates and bounding parameter values.

6.6.1 Uncertainty in Heat Conduction Analysis

The range of thermal conductivities for wet and dry conditions for the four units (Tptpul, Tptpmn, Tptpll, and Tptpln) cover a broad range of porosities, would bracket and compensate for any uncertainty in the results of radial heat conduction simulations. While detailed analyses have not been performed, based on Figures 6-1 and 6-2, it is likely that temperatures would exceed boiling only in the first few meters from the drift, and that the temperature of most of the rock is below boiling. A source of uncertainty is due to the fact that the thermal conductivity of the solid phase is several times larger than the thermal conductivity of water. Since the thermal gradients within the pore space are more likely to be influenced by liquid water, the effective thermal gradients for a uniform heat flux would be higher. The volumetric heat capacity is reduced with a reduction in saturation or water content because water with a high specific heat is substituted for air with a low specific heat capacity. Theoretical considerations indicate that the thermal gradients are much higher, depending on the spatial variations in the properties of the rock media between the drifts. Additionally, the idea that the magma is subject to constant heat content excludes any heat that may be generated by exothermic reactions. Though this heat is expected to be small compared to the heat of the magma, it still introduces a small amount of uncertainty.

These variation cannot be realistically captured for heat conduction modeling; however, any additional data collected for reducing this uncertainty may not significantly change the simulated results. Compensation for any of this uncertainty can be achieved by a conservative approach in heat conduction model simulations. Such conservative approach considers an intrusive temperature of 1150°C as the starting temperature for heat conduction and ignores the endothermic reaction heat that would be dissipated in the formation of contact metamorphic aureole which was the approach taken in this report.

A detailed sensitivity analysis is shown to determine the overall uncertainty in the heat conduction simulations and these are presented in Attachment I. This analysis provides information on the percent contribution values of each model component to the heat conduction/flow system variance. The sensitivity of the heat flow model to the uncertainty in key inputs was investigated using the Delta Method, as described in Attachment I. The variance shows that the resulting peak temperature at a distance of 10 m is sensitive only to the initial temperature. Therefore, the uncertainty in the initial temperature was used to calculate its variance, and that change in the peak temperature, ±3°C sampled as a uniform distribution, is used as the uncertainty in the temperature output provide in Tables 6-14 and 8-1.

6.6.2   Uncertainty in Volatile Gas Flow Analysis

There are two primary sources of uncertainty in the volatile gas flow: a) the spatial variation in the rock porosity and permeability between the drifts and the backfill, which affect the gas diffusivity and b) limitations of equations used for gas diffusion simulations. Gas diffusion due to spatial variation could also vary. While additional spatial data may reduce this type of uncertainty, it is not necessary because the conservative approaches taken for the model simulation bracket and compensate for the uncertainty. These approaches are outlined in the following:

1. In the gas diffusion model simulation, the entire volume of exsolving volatile gases was used for the transport calculation.

2. For calculating the total moles of exsolving volatile gases, the maximum volume of magma intruded into Zone 1 emplacement drifts is considered, which is calculated by subtracting the volume of waste packages from the total volume of the intruded drifts (see Assumption 1).

3. A maximum water content of 2 percent was assumed to be exuded from the intruded magma (see Assumption 2).

4. For flow simulations, the initial advective flow is considered to be linear, not radial, and this advective flow is considered as the mechanism of transport of gases into the Zone 2 drifts (see Assumption 4).

5. Although the diffusing volatile gases have a tendency to chemically react with rock material along the path of gas transport and consequently attenuate their concentration, this chemical reaction is not factored into the model simulation.

In the calculations, mean mole percents of volatile gases are used. These values are found in Table 4-4 along with their corresponding uncertainty values. Using conservative assumptions and parameters to model gas flow from Zone 1 to Zone 2 shows that only a small amount of volatile gases reach the Zone 2 drifts and that this will have no effect on the waste packages there. Therefore, the uncertainty in these particular values become inconsequential since so very little of the gas reaches the Zone 2 drifts.

6.6.3   Uncertainty in the Geochemical Modeling Using EQ6

6.6.3.1   Uncertainty in EQ6 Inputs

Uncertainties related to geochemical modeling using the EQ6 code may arise in inputs to the base case may arise including: pore fraction, reactive surface area of materials, flow rate of water through the basalt, saturation index, composition of oxides that make up the basalt, CO_2 and O_2 fugacity, and type of water flowing through the basalt. Several of these parameters are included in sensitivity cases which were used in the pH abstractions and are thus already incorporated into the model output. These parameters, as well as the range of values used, are:

- Pore Fraction: 0.13 through 0.17.
- Flow Rate (flux): 0.04mm/year through 3.8 mm/year.
- Surface Area: all surfaces are available and 10 percent of all surfaces available.
- Saturation Index: 0.1 through 1.0.

The composition of oxides that make up the basalt was taken from DTN: LA0107GV831811.001. These values are derived from 45 samples collected from the Lathrop Wells Cone. Materials from the Lathrop Wells Cone represent the most recent eruptive event (0.3 million years, Vaniman et al. 1982) in the Yucca Mountain region. Therefore it may better represent the composition of the hypothetical igneous intrusion than older volcanic centers in the area ranging in age from approximately 1.1 million to 3.7 million years (Vaniman et al. 1982). The composition of the Lathrop Well Cone along with corresponding uncertainty is presented in Table 6-11.

Table 6-11. Composition of Lathrop Wells Cone Basalt

Basalt Composition					
Oxide	Mean Wt%	Standard Deviation	Oxide	Mean Wt%	Standard Deviation
SiO_2	48.5	0.58	K_2O	1.84	0.04
Al_2O_3	16.74	0.22	TiO_2	1.93	0.06
Fe_2O_3	1.74	0.03	P_2O_5	1.22	0.03
MgO	5.83	0.11	MnO	0.17	0.00
CaO	8.6	0.22	FeO	8.9	0.17
Na_2O	3.53	0.09			

DTN: LA0107GV831811.001

Because of the small deviations from the mean, any differences arising in water chemistry from basalt water interactions with a slightly different basalt composition would be very small due to

the low dissolution rates of basaltic minerals. Therefore, no change to the water chemistry from that presented for reaction with mean basalt composition is expected.

The base-case water type reacted with the basalt was Bin 8 seepage water from DTN: MO0304SPAEBSCB.001. To determine the effects that other water types had on the pH, ionic strength, and fluoride content of water reacted with basalt, the basic base-case EQ6 run (see Section 6.5.3.4 for definition of this run) was run with Bin 11 seepage water from DTN: MO0304SPAEBSCB.001 and J-13 well water from DTN: MO0006J13WTRCM.000. These two water types represent seepage waters that are 1) more concentrated and 2) more dilute than the Bin 11 seepage water. The EQ6 output (Attachment IV) shows that the values for ionic strength are exactly the same. Variations in pH are noticed but these are very small with Bin 8 seepage water being the most conservative of the three. Therefore, the values presented with Bin 8 water are considered to have a probability of 1 when compared to other water types.

The EQ6 cases for this report were run at atmospheric condition for the repository horizon (log f_{CO2} = -3 and log f_{O2} = -0.7). To use the solubility look-up table in *Dissolved Concentration Limits of Radioactive Elements* (BSC 2003g), a constant value for these parameters must be used for any abstraction. Only one value for each was used here. Abstracted values at different concentrations of these gases can be explored in further revisions of this model report. For the time being, it will carry the constraint of being useful for these two gas parameter values.

6.6.3.2   Uncertainty in EQ6 Outputs

The water chemistry parameters required for use in TSPA are temporal values for pH, ionic strength, and fluoride content. As pointed out in Section 6.7, many EQ6 simulations of basalt/water interactions show no change in fluoride content. Therefore, the fluoride content of the aqueous fluid is dependent solely on the content that is already in the fluid as it contacts the basalt. The temporal variation of mean pH and ionic strength along with their corresponding uncertainty in the form of maximum and minimum values are presented in Tables 6-12 and 6-13.

Table 6-12. Temporal Mean, Maximum, and Minimum Values for pH and Ionic Strength for Basalt Modeled as Normalized Minerals

Time Period*	pH			Ionic Strength		
	Mean	Maximum	Minimum	Mean	Maximum	Minimum
0 - 15 years	8.9	9.1	8.6	2.28E-02	3.33E-02	1.02E-02
15 - 200 years	9.2	9.2	9.1	4.34E-02	4.81E-02	3.42E-02
200-300 years	9.2	9.2	9.2	4.81E-02	4.81E-02	4.80E-02
300-2000 years	9.2	9.2	9.2	4.81E-02	4.81E-02	4.80E-02
2000-5000 years	9.3	9.4	9.2	5.38E-02	8.24E-02	4.81E-02
5000 - 20000 years	9.3	9.5	9.2	6.62E-02	1.52E-01	4.81E-02

NOTE: * Time period represents time after re-establishment of seepage flow.

Table 6-13. Temporal Mean, Maximum, and Minimum Values for pH and Ionic Strength for Basalt Modeled as a Glass

Time Period*	pH			Ionic Strength		
	Mean	Maximum	Minimum	Mean	Maximum	Minimum
0 - 15 years	8.5	8.5	8.5	8.31E-03	8.41E-03	8.20E-03
15 - 200 years	8.6	8.6	8.5	9.28E-03	1.05E-02	8.42E-03
200-300 years	8.6	8.7	8.5	1.03E-02	1.23E-02	8.65E-03
300-2000 years	8.8	9.0	8.6	1.61E-02	2.40E-02	9.27E-03
2000-5000 years	8.9	9.2	8.6	2.57E-02	5.46E-02	1.02E-02
5000 - 20000 years	8.9	9.4	8.7	3.84E-02	1.20E-01	1.05E-02

NOTE: * Time period represents time after re-establishment of seepage flow.

6.7   IMPLEMENTATION OF IGNEOUS INTRUSION MODEL FOR TSPA-LA

6.7.1   Igneous Intrusion Impacts on Zone 1 Materials

Sections 6.5.1 shows, conservatively, that the igneous intrusion would render the drip shields, waste packages, and cladding in the Zone 1 emplacement drifts ineffective so they would provide no further protection to the waste forms. This would allow the waste form to be distributed throughout the cooled magma. Because the waste is considered chemically unchanged in the base case model, the dissolved concentration of radioelements in water in the basalt would have the same dependency on water chemistry as does waste dissolving in regions not influenced by an igneous intrusion. Thus, the solubility tables given in *Dissolved Concentration Limits of Radioactive Elements* (BSC 2003g) are appropriate to determine concentrations of radionuclides in basalt-filled emplacement drifts.

As the waste forms in Zone 1 will be inside the magma body, whether as bare waste forms or contained within damaged waste packages, then the temperature of those waste forms can be considered the same as the temperature of the cooling magma. These values are presented in the lookup-table (Table 6-11) for magma cooling temperatures found below. Because of the rapid change in temperature early in time combined with the large TSPA time-step of 10 years, the temperatures for times between 0-10 years should be sampled uniformly. The temperatures for times from 10 to 100 years should be taken directly from Table 6-14. The uncertainty in the temperature, as indicated in Section 6.6.1, is ±3°C for the temperature output. These values are warehoused in DTN: MO0307SPAHWCIG.000.

Table 6-14. Temperature of Waste Forms Inside Intruded Magma Body

Time (t)	For an Intrusion into a Repository at 25°C		For an Intrusion into a Repository at 50°C		For an Intrusion into a Repository at 100°C		For an Intrusion into a Repository at 150°C		For an Intrusion into a Repository at 200°C	
Years*	$T_{r=0m}$	$T_{r=3m}$	$T_{r=0m}$	$T_{r=3m}$	$T_{r=0m}$	$T_{r=3m}$	$T_{r=0m}$	$T_{r=3m}$	$T_{r=0m}$	$T_{r=3m}$
0	1150	1150	1150	1150	1150	1150	1150	1150	1150	1150
0.1	977	592	1006	620	1012	644	1019	668	1026	692
0.2	702	462	749	494	768	524	786	553	804	583
0.3	530	382	577	416	603	449	629	483	655	516
0.4	422	326	467	360	498	396	529	432	560	468
0.5	351	284	394	318	428	356	462	394	497	431
0.6	301	252	341	286	378	325	415	364	452	403
0.7	264	226	303	260	341	300	380	341	418	381
0.8	236	206	273	239	313	281	353	322	392	363
0.9	213	189	249	222	290	264	331	306	372	349
1	195	175	230	208	272	251	314	293	356	336
2	111	106	142	136	187	182	233	228	279	274
3	82.8	80.4	111	109	158	156	206	203	253	251
4	68.4	67.0	96.0	94.5	144	142	192	190	240	238
5	59.7	58.9	86.8	85.8	135	134	183	183	232	231
6	54.0	53.4	80.7	80.0	129	129	178	177	227	226
7	49.8	49.4	76.3	75.8	125	125	174	173	223	222
8	46.7	46.4	73.0	72.6	122	122	171	171	220	220
9	44.3	44.0	70.5	70.2	120	119	169	168	218	217
10	42.4	42.2	68.4	68.2	118	117	167	167	216	216
20	33.7	33.6	59.2	59.2	109	109	158	158	208	208
30	30.8	30.8	56.1	56.1	106	106	156	156	205	205
30	29.3	29.3	54.6	54.6	104	104	154	154	204	204
50	28.5	28.5	53.7	53.7	104	104	153	153	203	203
60	27.9	27.9	53.1	53.1	103	103	153	153	203	203
70	27.5	27.5	52.6	52.6	103	103	152	152	202	202
80	27.2	27.2	52.3	52.3	102	102	152	152	202	202
90	26.9	26.9	52.0	52.0	102	102	152	152	202	202
100	26.7	26.7	51.8	51.8	102	102	152	152	202	202

Source: Calculated in "Heat Conduction Lookup Table.xls" in Attachment IV

NOTES: $T_{r=0}$ is the centerline temperature and $T_{r=3}$ is the temperature at the edge of the dike.
*Time (t) represents time from the igneous intrusive event.

6.7.2   Igneous Intrusion Impacts on Zone 2

Thermal and gas transfer calculations (Sections 6.5.2.1.1 and 6.5.2.2.3) show that the effects of intrusions on Zone 2 would be negligible. Therefore, the TSPA-LA treatment of the waste packages in Zone 2 emplacement drifts should be the same as that under the nominal scenario.

6.7.3   Crown Seepage Reaction with Cooled Basalt

The chemistry of water seeping into Zone 1 drifts is considered the same as if there had been no intrusion. However, the chemistry of the incoming seepage may be affected by basalt-water reactions within the drift. The effects of these reactions on a typical crown seepage water have been modeled (Section 6.5.3). The output water chemistry parameters ionic strength and pH are warehoused in DTN: MO0307SPAHWCIG.000.

Tables 6-12 and 6-13 in Section 6.6.3.2 show the abstracted values for minimum, mean, and maximum pH and ionic strength. The two end members, basalt modeled as minerals and basalt modeled as a glass, were used in the analysis of basalt/water interactions because an actual composition of the basalt is unknown, but will lie somewhere in between the two modeled end members. Typically, basalt contains very little glass (Detournay et al. 2003). Therefore, the values for basalt reacted as minerals are the recommended values for use in TSPA.

The values presented in Tables 8-2 and 8-3 (from Table 6-12) do not represent an absolute range, but the range of values for the parameters expressed in Section 6.6.3.1. If those ranges were slightly modified, it is expected that the pH and ionic strength values may change slightly. Therefore, it is recommended that TSPA use the minimum, mean, and maximum values in Table 8-2 in a triangular distribution. Uncertainties in pH after 15 years are minimal. Therefore, a reasonable approach for TSPA implementation would be to use the mean values

Several EQ6 cases (see Attachment IV for output files) show that fluoride can drop from solution from precipitation of mineral phases containing fluoride. However, this is highly dependent on the phosphorus content of the fluid. Many EQ6 simulations of basalt/water interactions show no change in fluoride content. Therefore, it is recommended that the fluoride content used for TSPA be the initial fluoride content of the water entering the drift.

The EQ6 simulations of basalt/water interactions were carried out at atmospheric condition (log f_{CO2} = -3 and log f_{O2} = -0.7).

As the seepage water flows through the basalt, it will come into contact with the waste forms. Formation of secondary mineral phases (commonly called rind) form on the waste forms making the radionuclides available for release. The rind volume for the commercial spent nuclear fuel waste form is described in *Clad Degradation – Summary and Abstraction for LA* (BSC 2003h). This model accounts for rind volume of commercial spent nuclear fuel fuel in both nominal and volcanic cases. In the volcanic case, no credit is taken for cladding so that the waste form rind volume is essentially modeled from the bare fuel. Rind volume for high level waste glass is discussed in *Defense High Level Waste Glass Degradation* (BSC 2003i). In this model report, the rind volume is obtained using bare glass logs without any protection from the steel glass pour canister. Since it was modeled the same as the commercial spent nuclear fuel for the volcanic case, the rind volume for the glass is also considered appropriate for use in the igneous intrusion event. For the specifics on the rind volume and how they should be applied to the TSPA, refer to the individual model reports cited here: *Clad Degradation – Summary and Abstraction for LA* (BSC 2003h) and *Defense High Level Waste Glass Degradation* (BSC 2003i).

7. MODEL VALIDATION

The purpose of this process model is to assess the potential impacts of igneous intrusion on waste packages and waste forms, including deleterious dynamic, thermal, hydrologic, and chemical impacts. This assessment constitutes the waste package and waste form impacts submodel of the TSPA-LA model assessing the impacts of a potential igneous intrusion event on system performance.

Technical Work Plan for Waste Form Degradation Modeling, Testing, and Analyses in Support of SR and LA (BSC 2003a) lists eleven criteria, as required by AP-SIII.10Q, Section 5.4, to be used to determine whether the required level of confidence has been documented (BSC 2003a, Section 2.1.4.3).

The criteria from the technical work plan (BSC 2003a) used to validate this model (in Section 7.1) are as follows:

Criterion One: Corroboration of model results with data acquired from the laboratory, field experiments, analog studies, or other relevant observations, not previously used to develop or calibrate the model.

Criterion Three: Corroboration with data published in referenced journals or literature.

The technical work plan (BSC 2003a) defines the level of confidence by the number of criteria met to validate the model. At least one criteria must be met to show a required low level of confidence has been met. For Level II confidence (high confidence), more than one criterion must be met. As indicated in Section 2.1.4.4 of the technical work plan (BSC 2003a), the Igneous Intrusion Impacts Model requires a fairly high confidence level and, therefore, it is required to satisfy at least two criteria for model validation. Thus, criteria 1 and 3 dealing with corroboration by laboratory analog, or field data and corroboration with published data were selected as being appropriate criteria for this model report.

7.1 CORROBORATION

In the assessment of potential impact of igneous intrusion on the waste packages and waste forms in Zone 1 emplacement drifts, it is was conservatively shown that the drip shields, cladding, and waste packages would be damaged, failing to provide protection for the waste forms. The confidence in this conservative approach is augmented by corroborative information. Consideration of melting points of Stainless Steel Type 304 and 316 canisters (1400°C and 1450°C, respectively) and of zirconium alloy cladding (about 1850°C), suggest that, although the intrusive temperature (1150°C) is lower than the melting points of steel and nickel/zirconium alloys, the structural integrity of these engineered materials can be diminished upon an intrusive event. Softening, creeping, and breaking down of engineered materials are expected at the intrusive temperature, in combination with the shear forces of the viscous magma moving at sufficient velocities (see Section 6.5.1).

Damage to waste packages is also corroborated by the evidence from the tests conducted for determining the stability of containment of containers under different scenarios of transport

accidents and saboteur attacks. These tests considered 120 miles per hour truck impact accidents (with linear forces of up to 100,000 pounds/ft), variable energy shocks and vibrations, engulfing fire at 800°C temperature and high energy explosions (Sanders et al. 1992, Appendix III; Fischer et al. 1987, Section 6; Sandoval et al. 1983). The tests have indicated that the containers will be damaged to varying degrees. Similarly, the findings of literature review on the performance of waste package and drip shield materials performance in magmatic environments, documented by Structural Integrity Associates (Gordon 2003), suggested that the structural integrity of these materials will be compromised. For example, Types 310 and 446 stainless steels, exposed to Hawaiian basaltic lava at 1300°C and 2 psi for 100 hours, extensively reacted and were damaged, while alloy 718 suffered a loss of structural integrity (Gordon 2003). Thus, it is predicted the damage due to igneous intrusion is expected to be significant to the point of failure of the waste packages to contain the waste forms. This prediction is further corroborated by the nuclear industry tests, which strongly indicated that cladding embrittlement and failure occur in the presence of volatiles or oxygenated environment and at temperatures above 1204°C (for more details, see Section 6.5.1). Based on this corroborative information, damage to cladding could also occur in a matter of minutes to hours after the intrusion at temperature of 1150°C with exsolving volatiles.

In summary, model validation shows that the model predictions been corroborated, where necessary, with pertinent natural and industrial analogs, published journal articles/literature and experimental results and the criterion have been met. Therefore, the level of confidence required for this model has been obtained.

7.2 SUPPORTING VALIDATION CRITERIA

The model has met the criterion for a high level of confidence per the technical work plan (BSC 2003a), as discussed above in Section 7.1. Additional observations are discussed here for further verification and corroboration.

Has the model been validated by demonstrating that it is conservative?

Given the nature of the hypothetical igneous intrusion event and processes, the prediction of impacts on waste packages and waste forms is quite complex. The impact assessment, model simulations and analyses are based on conservative assumptions/estimates and bounded parameter values, and augmented by corroborative natural and industrial analogs or experimental results. Consequently, compensation is provided for the uncertainties and confidence in the results/conclusions is increased. For assessing the impacts of igneous intrusion on waste packages and waste forms, two conceptual models: base-case and alternative conceptual models are considered, and these are based on the igneous intrusion event and the resulting processes that potentially impact the Zone 1 emplacement drifts (see Sections 6.3 and 6.4). In this assessment, maximum/bounding conditions of intrusive magma are considered. Owing to these bounding conditions of igneous intrusion, the drip shield, cladding, and waste packages in Zone 1 fail to provide protection for the waste forms after the intrusion (see Section 6.5.1). The bounding conditions of intrusive magma considered are high temperature of 1150°C, viscosity (2.678 log poise units), density (2663 kg/m^3) and rapid ascent flux (1×10^6 kg s^{-1} m^{-1} or volumetric velocity of 2.15×10^3 m^3 s^{-1}) of magma. These are higher than those determined at 2 weight percent water (BSC 2001a, Table 4). These conditions are estimated mostly from the

published literature and analogs of basalt intrusions in the Yucca Mountain region and partly from the literature from other parts of the United States (BSC 2001a, Table 4). By assuming that the magma occupies the entire intruded drift, a bounding or maximum volume of basalt magma is established (see Assumption 1). This maximum volume is considered for assessing the impacts of heat and exsolving volatile gases on waste packages in Zone 2 emplacement drifts.

The conservative approach taken in the assessment includes the potential impacts of conductive heat loss and exsolution of volatile gases from the intruded magma on the waste packages in Zone 2 emplacement drifts. The approach used a high initial intrusive temperature of 1150°C and an average weight percent of volatile water component (2 percent), containing the corrosive gases (see Assumption 2).

For modeling the chemical interaction of seepage water with the basalt a conservative approach was taken. For example, since the nature and extent of fracturing of the solidifying basalt are unknown and there are no data on the permeability of the intruding basalt, the basalt in the intersected drifts was assumed to have permeability at least as great as the drift wall rock (see Assumption 3). This assumption is conservative because, it ensures that the cooled magma does not act as a barrier to the flow of seepage water from the rock above the drifts to the waste forms after reversion to normal conditions. The degree to which the seepage water equilibrates during its movement through the basalt is unknown, although some degree of chemical interaction based equilibration is expected.

For assessing the effects of exsolving volatile gases, a conservative approach was also taken. For example, although, coupled advective-diffusive-chemical reactive processes tend to transport the volatile gases to a relatively short distance away from the source, only the advection transport was used for maximum transport of exsolving gases from the intruded magma.

In summary, model validation shows that the model is conservative and this corroborative criterion has been met.

Has the model considered a credible scientific approach, principles and concepts?

This process model has considered probable igneous intrusion and consequential processes during intrusion, cooling of intrusion and post-cooling of intrusion. Based on these sequential processes, two conceptual models, with conservative assumptions, were considered: a) Base-Case Conceptual Model and b) Alternative Conceptual Models.

The base-case conceptual model was based on the igneous intrusion event and resulting processes stated in Section 6.3.

In contrast to the base-case model scenario, an alternative conceptual model was developed to cover other possibilities that may be relevant for igneous intrusive event impacts on the waste packages and waste forms. These include the scenarios presented in Section 6.4 of this report.

Since the calculated hydrochemistry of basalt interacted seepage water is based on the probable conceptual model and there are no relevant natural/experimental data to compare with the calculated results, the model for basalt water interactions cannot be quantitatively validated.

However, qualitative validation is done by assessing the sequential process of interaction of seepage water with the accepted seepage water chemistry of the nominal scenario.

Due to the vast uncertainty of the parameters involved in the alternative conceptual models, they were analyzed briefly only in Section 6.4.

In summary, model validation shows that the model considers credible scientific approaches, principles, and concepts and the corroborative criterion has been met.

8. CONCLUSIONS

The characteristics of a basaltic igneous intrusion, should it occur, are given in *Characterize Eruptive Processes at Yucca Mountain, Nevada* (BSC 2001a). These characteristics support the assumption that each drift intersected by an intrusion would be filled with magma (Section 5.1, Assumption 2).

Two zones of impact of igneous intrusions are considered: Zone 1, comprising the entirety of the drifts intersected by the intrusion, and Zone 2, comprising all other parts of the repository. Impacts of the intrusion to waste packages and waste forms as well as analysis of heat and gas flow from Zone 1 to Zone 2 were conducted to assess the impacts to waste packages and waste forms in Zone 2. Further analysis was conducted on the change in seepage water composition that may occur after the basalt cools and seepage water flow is re-established allowing it to react with the intruded basalt in Zone 1.

8.1   MODEL OUTPUT

The information in Section 6.5.1.1 supports the use of the TSPA assumption that waste packages in Zone 1 emplacement drifts no longer provide protection for the waste forms. The fuel, glass, and other waste would be entrained into the magma. The full detail of effects of magma intrusion on waste packages and cladding are not known. However, these results are conservative because it does not take credit for any residual waste-shielding effects of remaining waste package or cladding material.

The impacts of magmatic heat conduction and volatile gas diffusion on the waste packages in Zone 2 emplacement drifts were modeled. Temperatures were modeled by numerical simulations of Non-Steady State heat conduction with radial flow. Advective diffusion modeling was used to track the movement of volatile gases exolved from the magma.

The simulation modeling of heat conduction away from the intruded drifts demonstrates that the initial 1150°C temperature reduces to about 30°C at the center of the drift in about 30 years, and the maximum temperature rise expected in the Zone 2 emplacement drifts is less than 1°C. The drift-rock in Zone 2 provides an effective thermal insulation barrier to the impacts of high temperature of intruded magma and there would not be any impact of igneous heat on the waste packages in Zone 2 emplacement drifts.

Diffusion modeling of volatile gas components exsolving from the intruded basalt magma showed that no more than a mole (100) of volatile gases would diffuse into the Zone 2

emplacement drifts. Since H_2O is the major component of the volatile gases, the percent of other corrosive gases in this diffused concentration is expected to be too low to be significant. These low gas concentrations are not expected to affect the waste packages in the Zone 2 emplacement drifts.

Since the thermal and gas transfer calculations show that the effects of intrusions on Zone 2 would be negligible, TSPA-LA treatment of the barrier capability of waste packages in Zone 2 emplacement drifts should be the same as that under the nominal scenario.

As the waste forms are expected to be distributed throughout the magma body, then the temperature of those waste forms can be considered the same as the temperature of the cooling magma. These values are presented in the lookup-table (Table 6-11) for magma cooling temperatures found below. Because of the rapid change in temperature early in time combined with the large TSPA time-step of 10 years, the temperatures for times between 0 to 10 years should be sampled uniformly. The temperatures for times from 10 to 100 years should be taken directly from Table 8-1 (from Table 6-14). The uncertainty in the temperature, as indicated in Section 6.6.1, is ±3°C sampled as a uniform distribution. These values are warehoused in DTN: MO0307SPAHWCIG.000.

Processes accompanying magma intrusion and cooling may influence environmental conditions affecting radionuclide release from Zone 1. These processes include physical damage and disruption of the drift walls, formation of a contact metamorphic aureole and the filling of the drift with solid basalt. Based on consideration of the properties of natural analogs of contact metamorphic aureoles and of the development of fractures in cooling basalt, it was assumed (Assumption 3) that seepage rate through the basalt-filled, Zone 1 drifts would be the same as if no intrusion had occurred. With respect to contact metamorphic aureoles, this assumption is conservative in that the properties of such aureoles lead to lower permeabilities. *Abstraction of Drift Seepage* (BSC 2003j) indicates that it is reasonable to use non-degraded drift water inflow as the estimated water flow after an igneous event. Additional conservatism can be added by using the seepage for a collapsed drift. For the aqueous chemistry of the in-drift environment, it is appropriate to use the non-degraded configuration.

The chemistry of water seeping into Zone 1 drifts is also assumed to be the same as if there had been no intrusion. However, the chemistry of the incoming seepage may be affected by basalt-water reactions within the drift. The effects of these reactions on a typical crown seepage water have been modeled in Section 6.5.3 and the results of the abstraction for feed to TSPA are outlined in Section 6.7.3 and are reiterated below.

Tables 6-12 and 6-13 in Section 6.6.3.2 show the abstracted values for minimum, mean, and maximum pH and ionic strength. The two end members, basalt modeled as minerals and basalt modeled as a glass, were used in the analysis of basalt/water interactions because an actual composition of the basalt is unknown, but will lie somewhere in between the two modeled end members. Typically, basalt contains very little glass (Detournay et al. 2003). Therefore, the values for basalt reacted as minerals are the recommended values for use in TSPA.

Table 8-1. Look-Up Tables for Temperature of Waste Forms

Time (t)	For an Intrusion into a Repository at 25°C		For an Intrusion into a Repository at 50°C		For an Intrusion into a Repository at 100°C		For an Intrusion into a Repository at 150°C		For an Intrusion into a Repository at 200°C	
Years*	$T_{r=0m}$	$T_{r=3m}$	$T_{r=0m}$	$T_{r=3m}$	$T_{r=0m}$	$T_{r=3m}$	$T_{r=0m}$	$T_{r=3m}$	$T_{r=0m}$	$T_{r=3m}$
0	1150	1150	1150	1150	1150	1150	1150	1150	1150	1150
0.1	977	592	1006	620	1012	644	1019	668	1026	692
0.2	702	462	749	494	768	524	786	553	804	583
0.3	530	382	577	416	603	449	629	483	655	516
0.4	422	326	467	360	498	396	529	432	560	468
0.5	351	284	394	318	428	356	462	394	497	431
0.6	301	252	341	286	378	325	415	364	452	403
0.7	264	226	303	260	341	300	380	341	418	381
0.8	236	206	273	239	313	281	353	322	392	363
0.9	213	189	249	222	290	264	331	306	372	349
1	195	175	230	208	272	251	314	293	356	336
2	111	106	142	136	187	182	233	228	279	274
3	82.8	80.4	111	109	158	156	206	203	253	251
4	68.4	67.0	96.0	94.5	144	142	192	190	240	238
5	59.7	58.9	86.8	85.8	135	134	183	183	232	231
6	54.0	53.4	80.7	80.0	129	129	178	177	227	226
7	49.8	49.4	76.3	75.8	125	125	174	173	223	222
8	46.7	46.4	73.0	72.6	122	122	171	171	220	220
9	44.3	44.0	70.5	70.2	120	119	169	168	218	217
10	42.4	42.2	68.4	68.2	118	117	167	167	216	216
20	33.7	33.6	59.2	59.2	109	109	158	158	208	208
30	30.8	30.8	56.1	56.1	106	106	156	156	205	205
30	29.3	29.3	54.6	54.6	104	104	154	154	204	204
50	28.5	28.5	53.7	53.7	104	104	153	153	203	203
60	27.9	27.9	53.1	53.1	103	103	153	153	203	203
70	27.5	27.5	52.6	52.6	103	103	152	152	202	202
80	27.2	27.2	52.3	52.3	102	102	152	152	202	202
90	26.9	26.9	52.0	52.0	102	102	152	152	202	202
100	26.7	26.7	51.8	51.8	102	102	152	152	202	202

Source: Calculated in "Heat Conduction Lookup Table.xls" in Attachment IV

NOTES: $T_{r=0}$ is the centerline temperature and $T_{r=3}$ is the temperature at the edge of the dike.
　　　　*Time (t) represents time from the igneous intrusive event.

The values presented in Tables 8-2 and 8-3 (from Table 6-12) do not represent an absolute range, but the range of values for the parameters expressed in Section 6.6.3.1. If those ranges were slightly modified, it is expected that the pH and ionic strength values may change slightly. Therefore, it is recommended that TSPA use the minimum, mean, and maximum values in Table 8-2 in a triangular distribution. Uncertainties in pH after 15 years are minimal. Therefore, a reasonable approach for TSPA implementation would be to use the mean values. These values are warehoused in DTN: MO0307SPAHWCIG.000.

Table 8-2. Look-Up Table of Temporal Mean, Maximum, and Minimum Values for pH

Time Period[*]	Mean pH	Maximum pH	Minimum pH	Distibution
0 - 15 years	8.9	9.1	8.2	Triangular
15 - 200 years	9.2	9.2	9.1	Single value-mean
200-300 years	9.2	9.2	9.2	Single value-mean
300-2000 years	9.2	9.2	9.2	Single value-mean
2000-5000 years	9.3	9.4	9.2	Single value-mean
5000 - 20000 years	9.3	9.5	9.2	Single value-mean

NOTE: * Time period represents time after re-establishment of seepage flow.

Table 8-3. Look-Up Table of Temporal Mean, Maximum, and Minimum Values for Ionic Strength

Time Period[*]	Mean Ionic Strength	Maximum Ionic Strength	Minimum Ionic Strength	Distibution
0 - 15 years	2.28E-02	3.33E-02	1.02E-02	Triangular
15 - 200 years	4.34E-02	4.81E-02	3.42E-02	Triangular
200-300 years	4.81E-02	4.81E-02	4.80E-02	Triangular
300-2000 years	4.81E-02	4.81E-02	4.80E-02	Triangular
2000-5000 years	5.38E-02	8.24E-02	4.81E-02	Triangular
5000 - 20000 years	6.62E-02	1.52E-01	4.81E-02	Triangular

NOTE: * Time period represents time after re-establishment of seepage flow.

Several EQ6 cases (see Attachment IV for output files) show that fluoride can drop from solution from precipitation of mineral phases containing fluoride. However, this is highly dependent on the phosphorus content of the fluid. Many EQ6 simulations of basalt/water interactions show no change in fluoride content. Therefore, it is recommended that the fluoride content used for TSPA be the initial fluoride content of the water entering the drift.

Water seeping through the cooled, fractured basalt would contact the spent fuel and waste entrained in it and begin to dissolve them. The solubility of the waste forms would depend on the chemistry of the water as described in *Dissolved Concentration Limits of Radioactive Elements* (BSC 2003g). This report gives tables of the solubilities of elements with safety-relevant radionuclides over a range of values of pH and pCO_2. Variations in other water chemistry parameters including temperature and fluoride concentrations are included in the uncertainties associated with the solubilities.

As the seepage water flows through the basalt and comes into contact with the waste forms, it may form secondary mineral phases (commonly called rind) on the waste forms making the radionuclides available for release. Instructions for the use of these rinds in the TSPA-LA can be found in Section 6.7.3. These instructions dictate that the TSPA-LA should refer to the individual model reports cited here: *Clad Degradation – Summary and Abstraction for LA* (BSC 2003h) and *Defense High Level Waste Glass Degradation* (BSC 2003i). See Section 6.7.3 for more information.

DTN: MO0307MWDIGINT.000 is assigned to the model information used to develop the model report.

8.2 OUTPUT UNCERTAINTY

8.2.1 Heat Flow Calculation

Uncertainties from various sources have been addressed in this model report (Attachment I and Section 6.6.1). They consist of thermal conductivity, grain density, specific heat capacity, matrix porosity, saturation, lithophysal porosity, and initial temperature. Of these, it was shown that only the initial temperature had any effect. The uncertainty in the temperature, as indicated in Section 6.6.1, is $\pm 3°C$ for the temperature output.

8.2.2 EQ6 Calculations

Uncertainties from various sources have been addressed in this model report (Section 6.6.3). They consist of: pore fraction, reactive surface area of materials, flow rate of water through the basalt, saturation index, composition of oxides that make up the basalt, CO_2 and O_2 fugacity, and type of water flowing through the basalt. The uncertainty in the output for reaction of basalt and seepage waters is summarized in Tables 6-12 and 6-13.

8.3 RESTRICTIONS

As discussed in Section 6.6.3, the pH and ionic strength values developed in this model report for reaction of seepage water and basalt are valid for certain parameter ranges. These are provided in Table 8-4.

Table 8.4. Valid Range of pH and Ionic Strength Reported in This Model Report

Parameter	Value or Range of Values Used
Pore fraction	0.13 through 0.17
Flow rate (flux)	0.04mm/year through 3.8 mm/year
Surface area	All surfaces are available and 10% of all surfaces available
Saturation index	0.1 through 1.0
Log f_{CO2}	-3
Log f_{O2}	-0.7

8.4 YUCCA MOUNTAIN REVIEW PLAN ACCEPTANCE CRITERIA

The purpose of the Waste Package and Waste Form Impacts model (TSPA-LA submodel) is to provide an analytical framework to evaluate the potential effects of a hypothetical, future basaltic igneous intrusion that intersects the repository. Of specific interest are potentially deleterious dynamic, thermal, hydrologic, and chemical impacts that could result from the intrusion of a basaltic dike into one or more repository drifts. The TSPA-LA approach to implementing the models for waste package and waste form response during and following an igneous intrusion is based on the identification of damage zones. Zone 1 includes the emplacement drift intruded by the basalt dike. Zone 2 includes the emplacement drifts adjacent to Zone 1 but not directly intersected by a dike. The model describes:

- Impacts of magma intrusion on components of engineered barrier system (drip shields, cladding and waste packages) in Zone 1, and the fate of waste forms

- Impacts of intrusion-related thermal conduction/convection and migrating magmatic gases on the drip shields, cladding and waste packages in Zone 2 emplacement drifts, adjacent to the intruded drift

- Impacts of intrusion on in-drift thermal and geochemical environments, including seepage hydrochemistry, which may affect the release, and fate and transport of radionuclides.

The following description identifies information in this report that addresses acceptance criteria and/or review methods from *Yucca Mountain Review Plan, Final Report* (NRC 2003, Section 2.2.1.3.2.3) that are related to the integrated sub-issue of mechanical disruption of engineered barriers.

Acceptance Criterion 1: System description and model integration are adequate

The objectives for modeling magma-waste package/waste form interactions are described in Section 6.1 of the model report. The main objective of this model is to assess the potential impacts of an igneous intrusion on waste package and waste form performance, including:

- Mechanical and thermal impacts of basalt magma intrusion on the waste packages and waste forms of the intersected emplacement drifts of zone

- Temperature and pressure trends of basaltic magma intrusion intersecting the Zone 1 and their potential effects on waste packages and waste forms in Zone 2 emplacement drifts

- Geochemical conditions, due to basaltic magma intrusion intersecting the Zone 1 drift(s), and their potential effects on waste packages and waste forms in Zones 1 and 2

- Deleterious volatile gases, exsolving from the intruded basalt magma and their potential effects on waste packages of Zone 2 emplacement drifts

- Post-intrusive physical-chemical environment and seepage water alteration by reaction with intruded basalt.

(1) Total system performance assessment adequately incorporates important design features, physical phenomena, and couplings, and uses consistent and appropriate assumptions throughout the mechanical disruption of engineered barrier abstraction process.

The report documents the base-case conceptual model (Section 6.3) for magma-waste package/waste form interactions and alternative conceptual models (Section 6.4). Results from exercise of the base-case model are described in Section 6.5. Impacts on waste packages in Zone 1 are described in Section 6.5.1.1 and impacts on waste forms in Zone 1 are discussed in Section 6.5.1.2. The numerical simulations of heat flow around Zone 1 are described in Section 6.5.2.1. Results of the heat flow modeling are described at the end of Section 6.5.2.1. Effects of thermal disturbances, volatile gases, and the geochemical

interaction of seepage water with basalt and fragmented waste are described in Section 8. The results indicate the waste packages in Zone 2 would not be affected by heat conducted from magma in drifts in Zone 1.

Section 6.5.2.2 describes simulations of flow of volatile components from an intruding magma, and the enumeration of the model is described in Section 6.5.2.2. Results of the modeling are described at the end of Section 6.5.2.2 and show that emplacement drifts and their contents in Zone 2 would not be affected by volatile constituents exsolving from a basaltic magma that intrudes Zone 1 drifts.

Based on the description in Sections 6.5.2.1 and 6.5.2.2, there is little basis or need to define damage Zone 2 (as described in TSPA-SR) peripheral to Zone 1 for TSPA-LA.

Section 6.5.3 describes EQ6 modeling of post-intrusion geochemical interactions of seepage water with basalt (Zone 1) after cooling of the basalt.

(2) The description of geological and engineering aspects of design features, physical phenomena, and couplings, that may affect mechanical disruption of engineered barriers, is adequate. For example, the description may include materials used in the construction of engineered barrier components, environmental effects (e.g., temperature, water chemistry, humidity, radiation, etc.) on these materials, and mechanical failure processes and concomitant failure criteria used to assess the performance capabilities of these materials. Conditions and assumptions in the abstraction of mechanical disruption of engineered barriers are readily identified and consistent with the body of data presented in the description.

Properties of the basalt are described in Section 4.1.3 and presented in Tables 4-5 through 4-8. The material properties of the basalt are used to model changes in water that contacts the basalt.

Numerical simulation of heat flow around Zone 1 emplacement drifts is describe in Section 6.5.2, and the simulation results indicate that the increase in temperatures in the surrounding drifts (in Zone 2) is small (< 10°C). This result is interpreted to show that the rocks provide an effective thermal barrier (insulation) and would limit the effects from a high temperature intrusion of basaltic magma. Hence, the results indicate that waste packages in Zone 2 would not be affected by heat transfer from Zone 1 drifts.

The simulation of the movement of volatile gases from Zone 1 are described in Section 6.5.2.2. Results show that waste packages in Zone 2 would not be impacted by volatile gases exsolving from basaltic magma intruded into Zone 1 drifts.

(3) The abstraction of mechanical disruption of engineered barriers uses assumptions, technical bases, data, and models that are appropriate and consistent with other related U.S. Department of Energy abstractions. For example, assumptions used for mechanical disruption of engineered barriers are consistent with the abstraction of degradation of engineered barriers (Section 2.2.1.3.1 of *Yucca Mountain Review Plan, Final Report* [NRC 2003]). The descriptions and technical bases provide transparent and traceable support for the abstraction of mechanical disruption of engineered barriers.

This model report documents the development of the conceptual models, model enumeration, and simulations of interactions between basaltic magma, and waste packages and waste forms in emplacement drifts intersected by a dike and adjacent to the intersected drifts. The material properties of the basalt (from Section 4.1.3) are used to model changes in water that contacts basalt.

Inputs for heat flow calculations and model simulations are described in Section 4.1.1, and inputs for volatile gas calculations and flow model simulations are described in Section 4.1.2. Inputs for EQ6 simulation of water/basalt reaction hydrochemistry are described in Section 4.1.3. General inputs that are used in all EQ6 calculations are described in Section 4.1.4.

Documentation of assumptions specific to the intrusive event and its effects on waste packages and waste forms is provided in Section 5.1. Assumptions specific to volatile gas flow model simulations are described in Section 5.2, and assumptions specific the EQ3/6 simulations are documented in Section 5.3. For the EQ3/6 simulations, assumptions about the basalt glass degradation rate are described in Section 5.3.1 and block size in fractures are described in Section 5.3.2.

(4) Boundary and initial conditions used in the total system performance assessment abstraction of mechanical disruption of engineered barriers are propagated throughout the abstraction approaches.

Basalt properties are described in Section 4.1.3 and presented in Tables 4-5 through 4-8. The material properties of the basalt are used to model changes in water that contacts the basalt. Inputs for heat flow calculations and model simulations are described in Section 4.1.1, and inputs for volatile gas calculations and flow model simulations are described in Section 4.1.2. Inputs for EQ6 simulation of water/basalt reaction hydrochemistry are described in Section 4.1.3. General inputs that are used in all EQ6 calculations are described in Section 4.1.4.

Documentation of assumptions specific to the intrusive event and its effects on waste packages and waste forms is provided in Section 5.1. Assumptions specific to volatile gas flow model simulations are described in Section 5.2, and assumptions specific the EQ3/6 simulations are documented in Section 5.3.

(5) Sufficient data and technical bases to assess the degree to which features, events, and processes have been included in this abstraction are provided.

FEPs that are specifically addressed by information in this model report are identified in Table 6-1. One FEP, 1.2.04.04.0A, Igneous intrusion interacts with EBS components, is addressed in this model report. The table identifies sections of the report in which disposition of the FEP is described and includes a summary of the TSPA-LA disposition. Basically, the output of the model provides descriptions of physical and chemical conditions for application in the TSPA-LA in-drift sub-models.

(6) The conclusion, with respect to the impact of transient criticality on the integrity of the engineered barriers, is defensible.

This model report does not address the impact of transient criticality on the integrity of the engineered barriers.

(7) Guidance in NUREG-1297 (Altman et al. 1988a) and NUREG-1298 (Altman et al. 1988b), or other acceptable approaches, is followed.

NUREG-1297 (Altman et al. 1988a) describes the generic technical position with respect to the use of peer reviews on high-level waste repository programs. Peer review was not used in the development of the report. NUREG-1298 (Altman et al. 1988b), describes the generic technical position with respect to qualification of existing data. This report does not document the results of qualification of existing data.

Acceptance Criterion 2: Data are sufficient for model justification

(1) Geological and engineering values, used in the license application to evaluate mechanical disruption of engineered barriers, are adequately justified. Adequate descriptions of how the data were used, and appropriately synthesized into the parameters are provided.

The basalt properties are described in Section 4.1.3 and presented in Tables 4-5 through 4-8. The material properties basalt are used to model changes in water that contacts basalt. Inputs for heat flow calculations and model simulations are described in Section 4.1.1, and inputs for volatile gas calculations and flow model simulations are described in Section 4.1.2. Inputs for EQ6 simulation of water/basalt reaction hydrochemistry are described in Section 4.1.3. General inputs that are used in all EQ6 calculations are described in Section 4.1.4.

Documentation of assumptions specific to the intrusive event and its effects on waste packages and waste forms is provided in Section 5.1. Assumptions specific to volatile gas flow model simulations are described in Section 5.2, and assumptions specific the EQ3/6 simulations are documented in Section 5.3.

(2) Sufficient data have been collected on the geology of the natural system, engineering materials, and initial manufacturing defects, to establish initial and boundary conditions for the total system performance abstraction of mechanical disruption of engineered barriers.

The basalt properties are described in Section 4.1.3 and presented in Tables 4-5 through 4-8. The material properties basalt are used to model changes in water that contacts basalt. Inputs for heat flow calculations and model simulations are described in Section 4.1.1, and inputs for volatile gas calculations and flow model simulations are described in Section 4.1.2. Inputs for EQ6 simulation of water/basalt reaction hydrochemistry are described in Section 4.1.3. General inputs that are used in all EQ6 calculations are described in Section 4.1.4.

(3) Data on geology of the natural system, engineering materials, and initial manufacturing defects, used in the total system performance assessment abstraction, are based on appropriate techniques. These techniques may include laboratory experiments, site-specific field measurements, natural analog research, and process-level modeling studies. As appropriate, sensitivity or uncertainty analyses used to support the U.S. Department of

Energy total system performance assessment abstraction are adequate to determine the possible need for additional data.

The basalt properties are described in Section 4.1.3 and presented in Tables 4-5 through 4-8. The material properties basalt are used to model changes in water that contacts basalt. Inputs for heat flow calculations and model simulations are described in Section 4.1.1, and inputs for volatile gas calculations and flow model simulations are described in Section 4.1.2. Inputs for EQ6 simulation of water/basalt reaction hydrochemistry are described in Section 4.1.3. General inputs that are used in all EQ6 calculations are described in Section 4.1.4.

(4) Engineered barrier mechanical failure models for disruption events are adequate. For example, these models may consider effects of prolonged exposure to the expected emplacement drift environment, material test results not specifically designed or performed for the Yucca Mountain site, and engineered barrier component fabrication flaws.

The objectives of the modeling of igneous intrusion impacts on the waste package and waste form are described in Section 6.1. The base-case conceptual model and alternative conceptual models are described, respectively, in Sections 6.3 and 6.4. Identification of the software codes used in the analysis and their applicability to the modeling of magma-waste package and magma-waste form interactions are described in Section 3.1. Table 2 compares the specifics of the EQ3/6 and EQ6 codes. Simulation conditions for the base-case conceptual model are described in Section 6.2, and results of numerical simulations of heat flow around Zone 1 emplacement drifts filled with basalt magma are described in Section 6.5.2.1. Results of simulations of flow of volatile components from a basaltic intrusion are described in Section 6.5.2.2, and results of post-intrusion geochemical interactions of seepage water with basalt is described in Section 6.5.3.

Acceptance Criterion 3: Data uncertainty is characterized and propagated through the model abstraction

Data and parameters used for the analysis of magma-waste package and magma-waste form interactions is described in Section 4.1.

(1) Models use parameter values, assumed ranges, probability distributions, and bounding assumptions that are technically defensible, reasonably account for uncertainties, and variabilities, and do not result in an under-representation of risk.

Inputs for heat flow calculations and model simulations are described in Section 4.1.1, and inputs for volatile gas calculations and flow model simulations are described in Section 4.1.2. Inputs for EQ6 simulation of water/basalt reaction hydrochemistry are described in Section 4.1.3. General inputs that are used in all EQ6 calculations are described in Section 4.1.5. The uncertainty in inputs as they are propagated in the calculation in the model is described in Section 6.6.

The representation of risk is a TSPA-LA responsibility. This report describes no results that could be used to evaluate the representation of risk from magma-drift and magma-waste package interactions.

(2) Process-level models used to represent mechanically disruptive events, within the emplacement drifts at the proposed Yucca Mountain repository, are adequate. Parameter values are adequately constrained by Yucca Mountain site data, such than the estimates of mechanically disruptive events on engineered barrier integrity are not underestimated. Parameters within conceptual models for mechanically disruptive events are consistent with the range of characteristics observed at Yucca Mountain.

The base-case conceptual model and alternative conceptual models are described, respectively, in Sections 6.3 and 6.4. Identification of the software codes used in the analysis and their applicability to the modeling of magma-waste package and magma-waste form interactions are described in Section 3.1. Table 2 compares the specifics of the EQ3/6 and EQ6 codes. Simulation conditions for the base-case conceptual model are described in Sections 4.1.1, 4.1.2, 4.1.3, 4.1.4, 6.5.1, 6.5.2, and 6.5.3, and results of numerical simulations of heat flow around Zone 1 emplacement drifts filled with basalt magma are described in Section 6.5.2.1. Results of simulations of flow of volatile components from a basaltic intrusion are described in Section 6.5.2.2, and results of post-intrusion geochemical interactions of seepage water with basalt are described in Section 6.5.3.

Assumptions needed to support the modeling of magma-waste package and magma-waste form interactions are described in Section 5. Section 5.1 describes assumptions specific to the intrusive event and potential resulting effects. Section 5.2 describes assumptions specific to the simulation of volatile gas flow. Section 5.3 describes assumptions specific to the EQ3/6 simulations about the physical and chemical properties of basalt degradation and dissolution rates and size of basalt blocks inside fracture system.

Inputs for heat flow calculations and model simulations are described in Section 4.1.1, and inputs for volatile gas calculations and flow model simulations are described in Section 4.1.2. Inputs for EQ6 simulation of water/basalt reaction hydrochemistry are described in Section 4.1.3. General inputs that are used in all EQ6 calculations are described in Section 4.1.5.

Modeling results are consistent with assuming that once intrusion occurs, waste packages in Zone 1 provide no further protection for the waste. However, for packages in Zone 2, Section 6.5.2.1 and 6.5.2.2 show that the intrusion will have minimal effect.

(3) Uncertainty is adequately represented in parameter development for conceptual models, process-level models, and alternative conceptual models considered in developing the assessment abstraction of mechanical disruption of engineered barriers. This may be done either through sensitivity analyses or use of conservative limits.

Alternative conceptual models that were considered in the development of the model of igneous intrusion impacts on waste packages and waste forms are described in Section 6.4. Uncertainties in the modeling are described in Section 6.6, and specific descriptions are provided of process level uncertainties, including uncertainty in heat conduction analysis (Section 6.6.1), uncertainty in volatile gas flow analysis (Section 6.6.2), and uncertainty in geochemical modeling using EQ6 (Section 6.6.3). The restrictions to the use of the output data are located in Section 8.3.

Attachment IV contains the verification for heat conduction and verification of the calculations used in assessing the effects of magma intrusion for regions in the repository host horizon.

(4) Where sufficient data do not exist, the definition of parameter values and conceptual models is based on appropriate use of expert elicitation, conducted in accordance with NUREG-1563 (Kotra et al. 1996). If other approaches are used, the U.S. Department of Energy adequately justifies their use.

Expert elicitation was not used in the development of the model of igneous activity impacts on waste packages and waste forms.

Acceptance Criterion 4: Model uncertainty is characterized and propagated through the model abstraction

(1) Alternative modeling approaches of features, events, and processes are considered and are consistent with available data and current scientific understanding, and the results and limitations are appropriately considered in the abstraction.

Alternative conceptual models that were considered in the development of the model of igneous intrusion impacts on waste packages and waste forms are described in Section 6.4. Uncertainties in the modeling are described in Section 6.6, and specific descriptions are provided of process level uncertainties, including uncertainty in heat conduction analysis (Section 6.6.1), uncertainty in volatile gas flow analysis (Section 6.6.2), and uncertainty in geochemical modeling using EQ6 (Section 6.6.3). The restrictions to the use of the output data are located in Section 8.3.

(2) Consideration of conceptual model uncertainty is consistent with available site characterization data, laboratory experiments, field measurements, natural analog information and process-level modeling studies; and the treatment of conceptual model uncertainty does not result in an under-representation of the risk estimate.

Alternative conceptual models that were considered in the development of the model of igneous intrusion impacts on waste packages and waste forms are described in Section 6.4. Uncertainties in the modeling are described in Section 6.6, and specific descriptions are provided of process level uncertainties, including uncertainty in heat conduction analysis (Section 6.6.1), uncertainty in volatile gas flow analysis (Section 6.6.2), and uncertainty in geochemical modeling using EQ6 (Section 6.6.3). The restrictions to the us of the output data are located in Section 8.3. The documentation includes conservatism incorporated in the consideration of uncertainties and bounding values that result.

The representation of risk is a TSPA-LA responsibility. This report describes no results that could be used to evaluate the representation of risk from magma-drift and magma-waste package interactions.

(3) Appropriate alternative modeling approaches are investigated that are consistent with available data and current scientific knowledge, and appropriately consider their results and limitations using tests and analyses that are sensitive to the processes modeled.

Alternative conceptual models that were considered in the development of the model of igneous intrusion impacts on waste packages and waste forms are described in Section 6.4.

Attachment IV contains verification for heat conduction and verification of the calculations used in assessing the effects of magma intrusion for regions in the repository host horizon.

Acceptance Criterion 5: Model abstraction output is supported by objective comparisons

(1) Models implemented in this total system performance assessment abstraction provide results consistent with output from detailed process-level models and/or empirical observations (laboratory and field testing and/or natural analogs).

The waste package damage model for Zone 1 conservatively shows that all waste packages contacted by magma are damaged to the extent that they provide no further protection for the waste. Analog studies at erupting basaltic volcanoes suggest that this damage is possible. Waste packages in Zone 2 are expected to show no effects from conducted heat and volatile gases because the repository host rocks provide good insulation around the Zone 1 drifts, and corrosive gases are not expected to reach Zone 2 in concentrations that would damage the waste packages. The consistency of these results with site conditions and process models is described in Section 7.

(2) Outputs of mechanical disruption of engineered barrier abstractions reasonably produce or bound the results of corresponding process-level models, empirical observations, or both.

For waste packages in Zone 1, TSPA-LA assumes that the waste packages are damaged to the extent that they provide no further protection for the waste. This assumption represents a bound on process-level modeling further corroborated by the information in Section 6.5.1.1. Waste form modifications are consistent with documented experimental petrology studies and are, therefore, considered reasonable representations of processes that could occur following intrusion.

Waste packages in Zone 2 are expected to show no effects from conducted heat and volatile gases because the repository host rocks provide good insulation around the Zone 1 drifts, and corrosive gases are not expected to reach Zone 2 in concentrations that would damage the waste packages. The consistency of these results with site conditions and process models is described in Section 7.

(3) Well-documented procedures, that have been accepted by the scientific community to construct and test the mathematical and numerical models are used to simulate mechanical disruption of engineered barriers.

The basis for the selection of EQ3/6 Version 7.2B and EQ6 Version 7.2bLV for the modeling of seepage water/basalt interactions is documented in Sections 3.1.1 and 3.1.2. Validation of the model and consistency with well-understood processes are described in Section 7. Documentation of the consistency of the development of the EQ3/6 code with documented procedures for the development of software is beyond the scope of this report. Such documentation should be available in the EQ6 manual (CRWMS M&O 1998).

(4) Sensitivity analyses or bounding analyses are provided to support the total system performance assessment abstraction of mechanical disruption of engineered barriers that cover ranges consistent with site data, field or laboratory experiments and tests, and natural analog research.

Results from analyses using the base-case model are documented in Sections 6.5.1, 6.5.2, and 6.5.3. Consistency of the model with data from site studies, field and laboratory experiments and tests, and natural analog research are described in Section 7. Additional information about consistency of specific model components with site features and processes is provided in Section 6.6 in the discussion of uncertainties.

9. INPUTS AND REFERENCES

9.1 DOCUMENTS CITED

Altman, W.D.; Donnelly, J.P.; and Kennedy, J.E. 1988a. *Peer Review for High-Level Nuclear Waste Repositories: Generic Technical Position*. NUREG-1297. Washington, D.C.: U.S. Nuclear Regulatory Commission. TIC: 200651.

Altman, W.D.; Donnelly, J.P.; and Kennedy, J.E. 1988b. *Qualification of Existing Data for High-Level Nuclear Waste Repositories: Generic Technical Position*. NUREG-1298. Washington, D.C.: U.S. Nuclear Regulatory Commission. TIC: 200652.

Audi, G. and Wapstra, A.H. 1995. *Atomic Mass Adjustment, Mass List for Analysis*. Upton, New York: Brookhaven National Laboratory, National Nuclear Data Center. TIC: 242718.

Bird, R.B.; Stewart, W.E.; and Lightfoot, E.N. 1960. *Transport Phenomena*. New York, New York: John Wiley & Sons. TIC: 208957.

Brady, P.V. and Walther, J.V. 1989. "Controls on Silicate Dissolution Rates in Neutral and Basic pH Solutions at 25°C." *Geochimica et Cosmochimica Acta*, *53*, 2823-2830. New York, New York: Pergamon Press. TIC: 235216.

Brady, P.V. and Walther, J.V. 1990. "Kinetics of Quartz Dissolution at Low Temperatures." *Chemical Geology*, *82*, 253-264. Amsterdam, The Netherlands: Elsevier. TIC: 235349.

Brantley, S.L. and Chen, Y. 1995. "Chemical Weathering Rates of Pyroxenes and Amphiboles." Chapter 4 of *Chemical Weathering Rates of Silicate Minerals*. White, A.F. and Brantley, S.L., eds. Reviews in Mineralogy Volume 31. Washington, D.C.: Mineralogical Society of America. TIC: 222496.

BSC (Bechtel SAIC Company) 2001a. *Characterize Eruptive Processes at Yucca Mountain, Nevada*. ANL-MGR-GS-000002 REV 00 ICN 01. Las Vegas, Nevada: Bechtel SAIC Company. ACC: MOL.20020327.0498.

BSC 2001b. *Multiscale Thermohydrologic Model*. ANL-EBS-MD-000049 REV 00 ICN 02. Las Vegas, Nevada: Bechtel SAIC Company. ACC: MOL.20020123.0279.

BSC 2001c. *Defense High Level Waste Glass Degradation*. ANL-EBS-MD-000016 REV 00 ICN 02. Las Vegas, Nevada: Bechtel SAIC Company. ACC: MOL.20011015.0502.

BSC 2002a. *Total System Performance Assessment-License Application Methods and Approach*. TDR-WIS-PA-000006 REV 00. Las Vegas, Nevada: Bechtel SAIC Company. ACC: MOL.20020923.0175.

BSC 2002b. *Thermal Conductivity of the Potential Repository Horizon Model Report*. MDL-NBS-GS-000005 REV 00. Las Vegas, Nevada: Bechtel SAIC Company. ACC: MOL.20020923.0167.

BSC 2002c. *Geochemistry Model Abstraction and Sensitivity Studies for the 21 PWR CSNF Waste Packages*. MDL-DSU-MD-000001 REV 00. Las Vegas, Nevada: Bechtel SAIC Company. ACC: MOL.20021107.0154.

BSC 2003a. *Technical Work Plan for Waste Form Degradation Modeling, Testing, and Analyses in Support of SR and LA*. TWP-WIS-MD-000008 REV 02 ICN 01. Las Vegas, Nevada: Bechtel SAIC Company. ACC: DOC.20030731.0001.

BSC 2003b. *Repository Design Project, RDP/PA IED Typical Waste Package Components Assembly 1 of 9*. 800-IED-WIS0-00201-000-00A. Las Vegas, Nevada: Bechtel SAIC Company. ACC: ENG.20030702.0001.

BSC 2003c. *Repository Design Project, RDP/PA IED Typical Waste Package Components Assembly (2)*. 800-IED-WIS0-00202-000-00A. Las Vegas, Nevada: Bechtel SAIC Company. ACC: ENG.20030702.0002.

BSC 2003d. *Repository Design Project, Repository/PA IED Emplacement Drift Configuration 1 of 2*. 800-IED-EBS0-00201-000-00A. Las Vegas, Nevada: Bechtel SAIC Company. ACC: ENG.20030630.0002.

BSC 2003e. *Repository/PA IED Subsurface Facilities (2)*. 800-IED-WIS0-00102-000-00Aa. Las Vegas, NV: Bechtel SAIC Company. ACC: MOL.20030728.0199. TBV-5311

BSC 2003f. *Ventilation Model and Analysis Report*. ANL-EBS-MD-000030 REV 03 ICN 01. Las Vegas, NV: Bechtel SAIC Company. ACC: DOC.20030804.0003.

BSC 2003g. *Dissolved Concentration Limits of Radioactive Elements*. ANL-WIS-MD-000010 REV 02 Las Vegas, Nevada: Bechtel SAIC Company. ACC: DOC.20030624.0003.

BSC 2003h. *Clad Degradation – Summary and Abstraction for LA*. ANL-WIS-MD-000021 REV 00. Las Vegas, Nevada: Bechtel SAIC Company. ACC: DOC.20030626.0002.

BSC 2003i. *Defense High Level Waste Glass Degradation*. ANL-EBS-MD-000016 REV 01F. Las Vegas, Nevada: BSC. ACC: MOL.20030728.0197.

BSC 2003j. *Abstraction of Drift Seepage*. MDL-NBS-HS-000019 REV 00C. Las Vegas, Nevada: Bechtel SAIC Company. ACC: MOL.20030728.0198.

Canori, G.F. and Leitner, M.M. 2003. *Project Requirements Document*. TER-MGR-MD-000001 REV 01. Las Vegas, Nevada: Bechtel SAIC Company. ACC: DOC.20030404.0003.

Carnahan, B.; Luther, H.A.; and Wilkes, J.O. 1990. *Applied Numerical Methods*. Malabar, Florida: Krieger Publishing. TIC: 224042.

Chapman, A.J. 1974. *Heat Transfer*. 3rd Edition. New York, New York: Macmillan Publishing. TIC: 245061.

Chou, L. and Wollast, R. 1985. "Steady-State Kinetics and Dissolution Mechanisms of Albite." *American Journal of Science*, *285*, 963-993. New Haven, Connecticut: Yale University, Kline Geology Laboratory. TIC: 223169.

CRWMS M&O (Civilian Radioactive Waste Management System Management and Operating Contractor) 1998. *Software Qualification Report (SQR) Addendum to Existing LLNL Document UCRL-MA-110662 PT IV: Implementation of a Solid-Centered Flow-Through Mode for EQ6 Version 7.2B*. CSCI: UCRL-MA-110662 V 7.2b. SCR: LSCR198. Las Vegas, Nevada: CRWMS M&O. ACC: MOL.19990920.0169.

CRWMS M&O 1999. *Waste Package Behavior in Magma*. CAL-EBS-ME-000002 REV 00. Las Vegas, Nevada: CRWMS M&O. ACC: MOL.19991022.0201.

CRWMS M&O 2000. *Clad Degradation – FEPs Screening Arguments*. ANL-WIS-MD-000008 REV 00 ICN 01. Las Vegas, Nevada: CRWMS M&O. ACC: MOL.20001208.0061.

CRWMS M&O 2001. *Miscellaneous Waste-Form FEPs*. ANL-WIS-MD-000009 REV 00 ICN 01. Las Vegas, Nevada: CRWMS M&O. ACC: MOL.20010216.0006.

Cutlip, M.B. and Shacham, M. 2000. *Problem Solving in Chemical Engineering with Numerical Methods*. Upper Saddle River, New Jersey: Prentice Hall. TIC: 254281.

Detournay, E.; Mastin, L.G.; Pearson, J.R.A.; Rubin, A.M.; and Spera, F.J. 2003. *Final Report of the Igneous Consequences Peer Review Panel*. Las Vegas, Nevada: Bechtel SAIC Company. ACC: MOL.20030325.0227.

Domenico, P.A. and Schwartz, F.W. 1990. *Physical and Chemical Hydrogeology*. New York, New York: John Wiley & Sons. TIC: 234782.

Ehrlich, S.A. and Douglass, D.L. 1982. *The Effect of Molybdenum Plus Chromium on the Corrosion of Iron-, Nickel, and Cobalt-Base Alloys in Basaltic Lava and Simulated Magmatic Gas at 1150°C*. SAND82-7055. Albuquerque, New Mexico: Sandia National Laboratories. ACC: MOL.19981028.0003.

Einziger, R.E.; Marschman, S.C.; and Buchanan, H.C. 1991. "Spent-Fuel Dry-Bath Oxidation Testing." *Nuclear Technology*, *94*, 383-393. Hinsdale, Illinois: American Nuclear Society. TIC: 246459.

Fischer, L.E.; Chou, C.K.; Gerhard, M.A.; Kimura, C.Y.; Martin, R.W.; Mensing, R.W.; Mount, M.E.; and Witte, M.C. 1987. *Shipping Container Response to Severe Highway and Railway Accident Conditions*. NUREG/CR-4829. Volume 1. Washington, D.C.: U.S. Nuclear Regulatory Commission. ACC: NNA.19900827.0230.

Freeze, R.A. and Cherry, J.A. 1979. *Groundwater*. Englewood Cliffs, New Jersey: Prentice-Hall. TIC: 217571.

Gordon, B.M. 2003. *Literature Review of Waste Package and Drip Shield Materials' Corrosion Performance in Magmatic-Type Environments*. SIR-02-168, Rev. 0. San Jose, California: Structural Integrity Associates. ACC: MOL.20030414.0260.

Hahn, G.J. and Shapiro, S.S. 1967. *Statistical Models in Engineering*. New York, New York: John Wiley & Sons. TIC: 247729.

Hillner, E.; Franklin, D.G.; and Smee, J.D. 1998. *The Corrosion of Zircaloy-Clad Fuel Assemblies in a Geologic Repository Environment*. WAPD-T-3173. West Mifflin, Pennsylvania: Bettis Atomic Power Laboratory. TIC: 237127.

Hofmann, P. and Kerwin-Peck, D. 1984. "UO_2/Zircaloy-4 Chemical Interactions from 1000 to 1700°C under Isothermal and Transient Temperature Conditions." *Journal of Nuclear Materials*, *124*, 80-105. New York, New York: North-Holland. TIC: 253983.

Incropera, F.P. and DeWitt, D.P. 2002. *Fundamentals of Heat and Mass Transfer*. 5th Edition. New York, New York: John Wiley & Sons. TIC: 254280.

Jury, W.A.; Gardner, W.R.; and Gardner, W.H. 1991. *Soil Physics*. 5th Edition. New York, New York: John Wiley & Sons. TIC: 241000.

Klein, C. and Hurlbut, C.S., Jr. 1999. *Manual of Mineralogy*. 21st Edition, Revised. New York, New York: John Wiley & Sons. TIC: 246258.

Knauss, K.G.; Nguyen, S.N.; and Weed, H.C. 1993. "Diopside Dissolution Kinetics as a Function of pH, CO_2, Temperature, and Time." *Geochimica et Cosmochimica Acta*, *57*, (2), 285-294. New York, New York: Pergamon Press. TIC: 253990.

Kotra, J.P.; Lee, M.P.; Eisenberg, N.A.; and DeWispelare, A.R. 1996. *Branch Technical Position on the Use of Expert Elicitation in the High-Level Radioactive Waste Program*. NUREG-1563. Washington, D.C.: U.S. Nuclear Regulatory Commission. TIC: 226832.

Li, G.; Peacor, D.R.; Coombs, D.S.; and Kawachi, Y. 1997. "Solid Solution in the Celadonite Family: The New Minerals Ferroceladonite, $K_2Fe^2{}_2+Fe^3{}_2+Si_8O_{20}(OH)_4$, and Ferroaluminoceladonite, $K_2Fe^2{}_2+Al_2Si_8O_{20}(OH)_4$." *American Mineralogist*, *82*, (5-6), 503-511. Washington, D.C.: Mineralogical Society of America. TIC: 252472.

Li, J.; Lowenstein, T.K.; and Blackburn, I.R. 1997. "Responses of Evaporite Mineralogy to Inflow Water Sources and Climate During the Past 100 k.y. in Death Valley, California."

Geological Society of America Bulletin, 109, (10), 1361-1371. Boulder, Colorado: Geological Society of America. TIC: 247723.

Lichtner, P.C.; Keating, G.; and Carey, B. 1999. *A Natural Analog for Thermal-Hydrological-Chemical Coupled Processes at the Proposed Nuclear Waste Repository at Yucca Mountain, Nevada*. LA-13610-MS. Los Alamos, New Mexico: Los Alamos National Laboratory. TIC: 246032.

Lyman, E.S. 1995. "Behavior of Mixed-Oxide Fuel Under Transport Accident Conditions." Washington, D.C.: Nuclear Control Institute. Accessed May 6, 2003. TIC: 254231. http://www.nci.org/i/ib8596a.htm

NRC (U.S. Nuclear Regulatory Commission) 2003. *Yucca Mountain Review Plan, Final Report*. NUREG-1804, Rev. 2. Washington, D.C.: U.S. Nuclear Regulatory Commission, Office of Nuclear Material Safety and Safeguards. TIC: 254568.

Oguma, M. 1985. "Integrity Degradation of UO_2 Pellets Subjected to Thermal Shock." *Journal of Nuclear Materials*, *127*, (1), 67-76. New York, New York: North-Holland. TIC: 253982.

Parrington, J.R.; Knox, H.D.; Breneman, S.L.; Baum, E.M.; and Feiner, F. 1996. *Nuclides and Isotopes, Chart of the Nuclides*. 15th Edition. San Jose, California: General Electric Company and KAPL, Inc. TIC: 233705.

Roberts, W.L.; Campbell, T.J.; and Rapp, G.R., Jr. 1990. *Encyclopedia of Minerals*. 2nd Edition. New York, New York: Van Nostrand Reinhold. TIC: 242976.

Sanders, T.L.; Seager, K.D.; Rashid, Y.R.; Barrett, P.R.; Malinauskas, A.P.; Einziger, R.E.; Jordan, H.; Duffey, T.A.; Sutherland, S.H.; and Reardon, P.C. 1992. *A Method for Determining the Spent-Fuel Contribution to Transport Cask Containment Requirements*. SAND90-2406. Albuquerque, New Mexico: Sandia National Laboratories. ACC: MOV.19960802.0116.

Sandoval, R.P.; Weber, J.P.; Levine, H.S.; Romig, A.D.; Johnson, J.D.; Luna, R.E.; Newton, G.J.; Wong, B.A.; Marshall, R.W., Jr.; Alvarez, J.L.; and Gelbard, F. 1983. *An Assessment of the Safety of Spent Fuel Transportation in Urban Environs*. SAND82-2365. Albuquerque, New Mexico: Sandia National Laboratories. ACC: NNA.19870406.0489.

Schott, J.; Berner, R.A.; and Sjöberg, E.L. 1981. "Mechanism of Pyroxene and Amphibole Weathering—I. Experimental Studies of Iron-Free Minerals." *Geochimica et Cosmochimica Acta*, *45*, (11), 2123-2135. New York, New York: Pergamon Press. TIC: 253991.

Tole, M.P.; Lasaga, A.C.; Pantano, C.; and White, W.B. 1986. "The Kinetics of Dissolution of Nepheline $(NaAlSiO_4)$." *Geochimica et Cosmochimica Acta*, *50*, (3), 379-392. New York, New York: Pergamon Press. TIC: 253992.

Vaniman, D.T.; Crowe, B.M.; and Gladney, E.S. 1982. "Petrology and Geochemistry of Hawaiite Lavas from Crater Flat, Nevada." *Contributions to Mineralogy and Petrology*, *80*, 341-357. Berlin, Germany: Springer-Verlag. TIC: 201799.

Weast, R.C., ed. 1984. *CRC Handbook of Chemistry and Physics*. 65th Edition. Boca Raton, Florida: CRC Press. TIC: 206666.

Westrich, H.R. 1990. "Materials Compatibility Studies for the Magma Energy Extraction Project." *Geothermics*, *19*, (4), 341-357. Elmsford, New York: Pergamon Press. TIC: 254234.

Wogelius, R.A. and Walther, J.V. 1991. "Olivine Dissolution at 25°C: Effects of pH, CO_2, and Organic Acids." *Geochimica et Cosmochimica Acta*, *55*, (4), 943-954. New York, New York: Pergamon Press. TIC: 236732.

Wolery, T.J. and Daveler, S.A. 1992. *EQ6, A Computer Program for Reaction Path Modeling of Aqueous Geochemical Systems: Theoretical Manual, User's Guide, and Related Documentation (Version 7.0)*. UCRL-MA-110662 PT IV. Livermore, California: Lawrence Livermore National Laboratory. ACC: MOL.19980701.0459.

YMP (Yucca Mountain Site Characterization Project) 2001. *Q-List.* YMP/90-55Q, Rev. 7. Las Vegas, Nevada: Yucca Mountain Site Characterization Office. ACC: MOL.20010409.0366.

9.2 CODES, STANDARDS, REGULATIONS, AND PROCEDURES

10 CFR 63. Energy: Disposal of High-Level Radioactive Wastes in a Geologic Repository at Yucca Mountain, Nevada. Readily available.

AP-SI.1Q, Rev. 5, ICN 1. Software Management. Washington, D.C.: U.S. Department of Energy, Office of Civilian Radioactive Waste Management. ACC: DOC.20030708.0001.

AP-SIII.10Q, Rev. 1, ICN 2. *Models*. Washington, D.C.: U.S. Department of Energy, Office of Civilian Radioactive Waste Management. ACC: DOC.20030627.0003.

ASTM C 1174-97. 1998. *Standard Practice for Prediction of the Long-Term Behavior of Materials, Including Waste Forms, Used in Engineered Barrier Systems (EBS) for Geological Disposal of High-Level Radioactive Waste*. West Conshohocken, Pennsylvania: American Society for Testing and Materials. TIC: 246015.

9.3 SOURCE DATA, LISTED BY DATA TRACKING NUMBER

LA0107GV831811.001. Parameters for Igneous Consequences Analysis. Submittal date: 07/11/2001.

LB0207REVUZPRP.002. Matrix Properties for UZ Model Layers Developed from Field and Laboratory Data. Submittal date: 07/15/2002.

LB0307AMRU0120.001. Supporting Calculations and Analysis for Seepage Abstraction and Summary of Abstraction Results. Submittal date: 07/17/2003.

LB990861233129.001. Drift Scale Calibrated 1-D Property Set, FY99. Submittal date: 08/06/1999.

MO0006J13WTRCM.000. Recommended Mean Values of Major Constituents in J-13 Well Water. Submittal date: 06/07/2000.

MO0302SPATHDYN.000. Thermodynamic Data Input Files - Data0.YMP.R2. Submittal date: 02/05/2003.

MO0304SPAEBSCB.001. EBS Chemistry Binning Abstraction Results of the THC Seepage Model. Submittal date: 04/08/2003.

SN0208T0503102.007. Thermal Conductivity of the Potential Repository Horizon Rev 3. Submittal date: 08/26/2002.

SN0303T0510902.002. Revised Heat Capacity of Yucca Mountain Stratigraphic Units. Submittal date: 03/28/2003.

9.4   OUTPUT DATA, LISTED BY DATA TRACKING NUMBER

MO0307MWDIGINT.000. Model Information for Igneous Intrusion Impacts on Waste Packages and Waste Forms. Submittal date: 07/31/2003.

MO0307SPAHWCIG.000. Heat and Water Chemistry Output from Igneous Intrusion. Submittal date: 07/31/2003.

9.5   SOFTWARE CODES

Software Code: ASPRIN. V1.0. 10487-1.0-00.

Software Code: EQ3/6. V7.2b. LLNL: UCRL-MA-110662.

Software Code: EQ6, Version 7.2bLV. V7.2bLV. 10075-7.2bLV-00.

10. ATTACHMENTS

Attachment I	Verification of Heat Conduction Model Simulation Calculations
Attachment II	Computations of Moles of Volatile Water and Gases Exsolving from Basaltic Magma Intruded into Emplacement Drift
Attachment III	EQ6 Mineral Dissolution Rates
Attachment IV	Attached CD-ROM
Attachment V	File Listing of Attached CD-ROM

ATTACHMENT I

I.1 HEAT FLOW MODEL

A one-dimensional second order partial differential equation (Chapman 1974, p. 137), subject to initial temperature (due to the constant heat content) and a far field temperature boundary condition applies to the problem magma intrusion:

$$k\left[\frac{1}{r}\cdot\frac{\partial T}{\partial r}+\frac{\partial^2 T}{\partial r^2}\right]=\rho\cdot C_p\cdot\frac{\partial T}{\partial t} \qquad\text{(Eq. I-1)}$$

The temperature distribution for a magma flow filling a Zone 1 emplacement drift can be estimated using a one-dimensional unsteady radial heat conduction model, subject to constant heat content. The magma is considered to be at an initial intrusive temperature of 1150°C (BSC 2001a [DIRS 160130]). The magma fills the drift entirely and instantaneously, and then the temperature spatially and temporally dissipates. The temperature of the drift wall and the far-field is considered to be 25°C at the time of the intrusion. The heat transfer thermal properties of the magma are considered to be the same as those for the densely welded tuff for a first order analysis.

Carnahan et al. (1990, p. 462) provides finite difference expression approximations to first and second order derivatives for the radial heat conduction problem. The governing equation may be expressed as:

$$\frac{1}{r_i}\cdot\left(\frac{T'_{i+1}-T'_{i-1}}{2\cdot\Delta r}\right)+\frac{1}{\Delta r^2}\cdot\left[T'_{i+1}+T'_{i-1}-2\cdot T_i'\right]=\frac{1}{\alpha}\cdot\frac{T_i-T'_i}{\Delta t} \qquad\text{(Eq. I-2)}$$

Using the following definition of thermal diffusivity (Incropera and DeWitt 2002, p. 59):

$$\alpha=\frac{k}{\rho C_p} \qquad\text{(Eq. I-3)}$$

where
    Δt is the change in time (time-step) in years
    r_i is the total distance to the center of the cylinder (units: m)
    Δr is the change in distance from the center of the cylinder in one time-step (units: m)
    T_i is the temperature at distance r_i from the center of the cylinder (°C)
    T'_i is the temperature from the previous time-step at a distance of r_i from the center of the cylinder
    T'_{i+1} is the temperature from the previous time-step at a distance of r_{i+1} from the center of the cylinder
    T'_{i-1} is the temperature from the previous time-step at a distance of r_{I-1} from the center of the cylinder
    α is the thermal diffusivity of the rock mass (and thus the magma) (m²/year)
    k is the thermal conductivity of the rock mass (and thus the magma) (W/m·K)
    ρ is the density (kg/m³)

C_p is the specific heat (J/kg·K)

Factoring the expression to express T_i in terms of $T`_i$, $T`_{i-1}$, and $T`_{i+1}$ in an explicit finite difference calculation:

$$T_i = \alpha \cdot \Delta t \cdot \left[\frac{1}{r_i \cdot 2 \cdot \Delta r} + \frac{1}{\Delta r^2}\right] \cdot T'_{i+1} + \alpha \cdot \Delta t \cdot \left[\frac{-1}{r_i \cdot 2 \cdot \Delta r} + \frac{1}{\Delta r^2}\right] \cdot T'_{i-1} - \frac{2\alpha \cdot \Delta t \cdot T'_i}{\Delta r^2} + T'_i \qquad \text{(Eq. I-4)}$$

Radial Equation ($r_i > 0$)

A simple explicit finite difference calculation was set up in Microsoft Excel based upon the second order finite difference expression for radial flow. The explicit finite difference calculation can be simplified by defining the coefficients for T'_{i+1}, T'_{i-1}, and T'_i as α', β', and γ', respectively:

$$\alpha' = \left[\frac{1}{r_i \cdot 2 \cdot \Delta r} + \frac{1}{\Delta r^2}\right] \qquad \text{(Eq. I-4a)}$$

$$\beta' = \left[\frac{-1}{r_i \cdot 2 \cdot \Delta r} + \frac{1}{\Delta r^2}\right] \qquad \text{(Eq. I-4b)}$$

$$\gamma' = \left(-\frac{2}{\Delta r^2}\right) \qquad \text{(Eq. I-4c)}$$

The explicit finite difference expression (Equation I-4) then becomes:

$$T_i = \alpha \cdot \Delta t \cdot \left[\alpha' \cdot T'_{i+1} + \beta' \cdot T'_{i-1} + \gamma' \cdot T'_i\right] + T'_i \qquad \text{(Eq. I-5)}$$

The far-field temperature boundary condition at a distance of 150 meters (approximately 10 m less than twice the drift spacing) is set to a constant ambient temperature of 25°C.

Centerline Equation ($r_i = 0$)

To obtain an equation for the centerline temperature, a finite difference expression at the center of the model sets the insulated temperature boundary condition equal to the centerline temperature ($T`_{i-1} = T`_{i+1}$).

$$T_i = \alpha \cdot \Delta t \cdot \left[\frac{1}{r_i \cdot 2 \cdot \Delta r} + \frac{1}{\Delta r^2}\right] \cdot T'_{i+1} + \alpha \cdot \Delta t \cdot \left[\frac{-1}{r_i \cdot 2 \cdot \Delta r} + \frac{1}{\Delta r^2}\right] \cdot T'_{i+1} - \frac{2\alpha \cdot \Delta t \cdot T'_i}{\Delta r^2} + T'_i \qquad \text{(Eq. I-6)}$$

Simplifying this equation:

$$T_i = \left[\frac{2\alpha \cdot \Delta t}{\Delta r^2}\right] \cdot [T'_{i+1} - T'_i] + T'_i \qquad \text{(Eq. I-7)}$$

The model was implemented by entering Equations I-4 and I-7 into a Microsoft Excel spreadsheet ("Heat Conduction - [Dry / Wet] [TPTPUL / TPTPMN / TPTPLL / TPTPLN].xls" in Attachment IV). The required thermal diffusivity (α) was calculated using the method discussed below.

Thermal Diffusivity

Assessment of the effects of temperatures of intruded magma (intruded into Zone 1 drifts) on Zone 2 waste packages requires the rock mass thermal diffusivity, which in turn requires an estimate of the rock mass volumetric heat capacity and thermal conductivity of the welded tuff at the repository horizon.

The volumetric heat capacity was calculated using an equation derived in *Ventilation Model and Analysis Report* (BSC 2003f, Equation II-15).

$$C_{rock} = \frac{S \cdot \dfrac{\phi_m}{1-\phi_m} C_{vw} + \rho_g \cdot C_p}{\left(1 + \dfrac{\phi_m}{1-\phi_m} + \dfrac{\phi_l}{1-\phi_l} \cdot \left(1 + \dfrac{\phi_m}{1-\phi_m}\right)\right)} \qquad \text{(Eq. I-8)}$$

Simplifying this equation:

$$C_{rock} = \frac{S \cdot \dfrac{\phi_m}{1-\phi_m} C_{vw} + \rho_g \cdot C_p}{\left(1 + \dfrac{\phi_l}{1-\phi_l}\right) \cdot \left(1 + \dfrac{\phi_m}{1-\phi_m}\right)} \qquad \text{(Eq. I-9)}$$

where

C_{rock} volumetric heat capacity of the rock mass (J/m^3·K)
S   saturation (S = 0: dry; S = 1: wet)
ϕ_m matrix porosity
ϕ_L lithophysal porosity
C_{vw} volumetric heat capacity of water (J/m^3·K)
ρ_g grain density of solids (kg/m^3)
C_p specific heat capacity of solids (J/kg·K)

The saturation in this heat flow calculation is either completely dry (no water; S = 0), or completely wet (matrix is completely filled with water; S = 1). Real conditions of saturation are not so absolute; unsaturated conditions really lie between 10 and 20 percent saturation (DTN: LB0207REVUZPRP.002), and fully saturated conditions do not consider the lithophysae to be filled with water.

The Yucca Mountain Project assessed the thermal conductivity of the potential repository horizon for spatial variability and uncertainty of thermal conductivity in the host horizon (BSC

2002b, Table 7-10). Table I-1 presents the properties taken from that report for the rock units near the repository horizon.

Table I-1. Summary of Primary Thermal Conductivity Statistics

Stratigraphic Unit	Bulk Dry Rock Mass Thermal Conductivity (W/m·K) k_{rm}	Bulk Wet Rock Mass Thermal Conductivity (W/m·K) k_{rm}	Matrix Porosity ϕ_m	Lithophysal Porosity ϕ_L	Dry Bulk Density (kg/m³) ρ_{bd}	Specific Heat Capacity of Solids J/(kgK) C_p
Tptpul	1.18	1.77	0.17	0.12	1830	934
Tptpmn	1.42	2.07	0.13	0.03	2150	932
Tptpll	1.28	1.89	0.15	0.09	1980	933
Tptpln	1.49	2.13	0.11	0.03	2210	933

DTN: SN0208T0503102.007, SN0303T0510902.002

NOTE: Porosity is the ratio of void volume to total rock volume, and has units of m³ void/m³ rock.

The volume heat capacity of water (C_{vw}) is calculated for saturated water at 62°C by multiplying the density of water (kg/m³) to the specific heat of water (J/kg·K) (Incropera and DeWitt 2002, pp. 58 and 59). Such that:

$$C_{vw} = C_P \cdot \rho \qquad \text{(Eq. I-10)}$$

where

ρ density of water ($1/v_f$)   982.3 (kg/m³)
C_p specific heat capacity   4186 J/kg·K
(Incropera and DeWitt 2002, p. 924, Table A.6)

The grain density of solids can be calculated from the dry bulk density and the porosities of the matrix and lithophysae using the following equation from *Thermal Conductivity of the Potential Repository Horizon Model Report* (BSC 2002b, p. 41, Equation 6-4):

$$\rho_{bd} = (1 - \phi_L)(1 - \phi_m)\rho_g \qquad \text{(Eq. I-11)}$$

Solving for the grain density of solids:

$$\rho_g = \frac{\rho_{bd}}{(1 - \phi_L)(1 - \phi_m)} \qquad \text{(Eq. I-12)}$$

After plugging in the required values into Equation I-9 and solving for C_{rock}, the thermal diffusivity can be calculated by combining Equation I-3 with Equation I-10:

$$\alpha = \frac{k}{C_{rock}} \qquad \text{(Eq. I-13)}$$

Note: The units of watts are converted to joules (W=J/s), and then seconds converted to years, since Δt is in terms of years.

Table I-2 contains all of the values calculated using the values presented in Table I-1, and Equation 10 through Equation 13, which were then used in the heat transfer explicit finite difference calculation.

Table I-2. Summary of Volumetric Heat Capacity and Thermal Diffusivity Calculations

Stratigraphic Unit	Grain Density of Solids (kg/m³)	Dry Volumetric Heat Capacity (J/(m³·K)	Wet Volumetric Heat Capacity (J/(m³·K)	Dry Thermal Diffusivity (m²/yr)	Wet Thermal Diffusivity (m²/yr)
	ρ_g	C_{rock}	C_{rock}	α	α
Tptpul	2504	1709220.0	2335595.2	21.84	23.98
Tptpmn	2532	2003800	2528980	22.35	25.88
Tptpll	2551	1847340	2414589	21.84	24.69
Tptpln	2548	2061930	2491536	22.80	26.98

NOTE: Calculated in "Heat Conduction.xls" in Attachment IV.

I.2 HEAT FLOW MODEL UNCERTAINTY ANALYSIS OF PEAK TEMPERATURE IN THE ROCK MASS AT A DISTANCE OF 10 M

The generation of system moments allows a determination of the relative importance of each component variable by examining the magnitude of its partial derivative. Hahn and Shapiro (1967, p. 229) provide an expression for the mean system performance (for example the maximum temperature at a radius of 10 m from the drift with magma) through the expression under the assumption that the parameters are independent for the composite model:

$$E(z) = h((E(x_1), E(x_2),...E(x_n)) + \frac{1}{2} \cdot \sum_{i=1}^{n} \frac{\partial^2 h}{\partial x_i^2} \cdot Var(x_i)$$ (Eq. I-14)

where
   $E(z)$ = Expectation for the System Performance
   $E(x_I)$ = Expectation of the Component Variables
   $x_1...x_n$ = Component Variables
   $h()$ = Functional relationship between the component variables and the system performance

Hahn and Shapiro (1967, p. 231) present the following relationship for the variance in which the higher order moments are not used:

$$Var(z) = \sum_{i=1}^{n} \left(\frac{\partial h}{\partial x_i} \right)^2 \cdot Var(x_i)$$ (Eq. I-15)

This relation is frequently a satisfactory approximation to calculating the variance for independent parameters.

The peak temperature at a radius of 10 m for the constant heat content process depends on the rock mass thermal conductivity and thermal diffusivity that in turn depend on the solids thermal conductivity; the solids specific heat capacity; the solids grain density; the matrix porosity; the matrix saturation; and the lithophysal porosity. This set of parameters is taken as the independent set of parameters.

Table I-3 presents the input parameters for evaluation of the system variance. The values were obtained from *Ventilation Model and Analysis Report* (BSC 2003f, Section 6.11).

Table I-3. Sensitivity of Uncertainty in Input Parameters (with Standard Deviation for Use in Delta Method)

Input/Design Parameter	Mean Value	Standard Deviation	Rock Mass Thermal Conductivity		Rock Mass Thermal Diffusivity		Peak Temperature			Percent Contribution
			Plus	Minus	Plus	Minus	Plus	Minus	Variance	
Solids Thermal Conductivity (W/(m·K))	2.603	0.3413	2.02	1.62	26.68	21.48	78.17	78.12	5.55E-04	0%
Solids Grain Density (kg/m^3)	2593	138	1.82	1.82	23.14	25.16	78.13	78.15	8.54E-05	0%
Solids Specific Heat Capacity (J/(kg·K))	930	170	1.82	1.82	21.09	28.15	78.11	78.16	4.50E-04	0%
Matrix Porosity	14.86%	3.40%	1.74	1.91	22.59	25.79	78.13	78.16	2.08E-04	0%
Matrix Saturation	90.50%	10%	1.89	1.76	24.39	23.82	78.14	78.14	5.91E-06	0%
Lithophysal Porosity	8.83%	5.40%	1.72	1.93	24.13	24.09	78.14	78.14	1.92E-08	0%
Initial Temperature*	1150	35.51	1.82	1.82	24.11	24.11	73.23	79.04	2.81	100%
								Sum	2.81	100%
								Standard Deviation	1.68	

The Method of Moments provides information as to the source of uncertainty from the individual variables. In Equation I-13, the variance of each individual variable x_i is multiplied by the square of the derivative of the system function for that parameter. The square of the derivative represents the sensitivity of the system variance to the individual parameter. If the sensitivity, and the variance to an individual parameter are large, then the system variance is dominated by this contribution. Conversely, if the sensitivity, and the variance to an individual parameter are small, then the system variance is not influenced by this individual contribution.

Table I-3 represents the results of the analysis using the method of generating system moments. The analysis is performed by calculating the first order partial derivatives of temperature to the solids thermal conductivity (k_s); the solids specific heat capacity (C_p); the solids grain density (ρ_g); matrix porosity (ϕ_M); the matrix saturation (S_M); and the lithophysal porosity (ϕ_L). Each component is perturbed from it's mean value by plus or minus one standard deviation while the other components are evaluated at their mean value. The rock mass thermal conductivity and the thermal diffusivity are then calculated based upon the relations for thermal conductivity and thermal diffusivity presented previously. The finite difference calculations are then performed and the peak temperature at a radius of 10 m is evaluated for the parameters. The first order partial derivatives are approximated for the mean values plus or minus one standard deviation for each component and then substituted into Equations I-14.
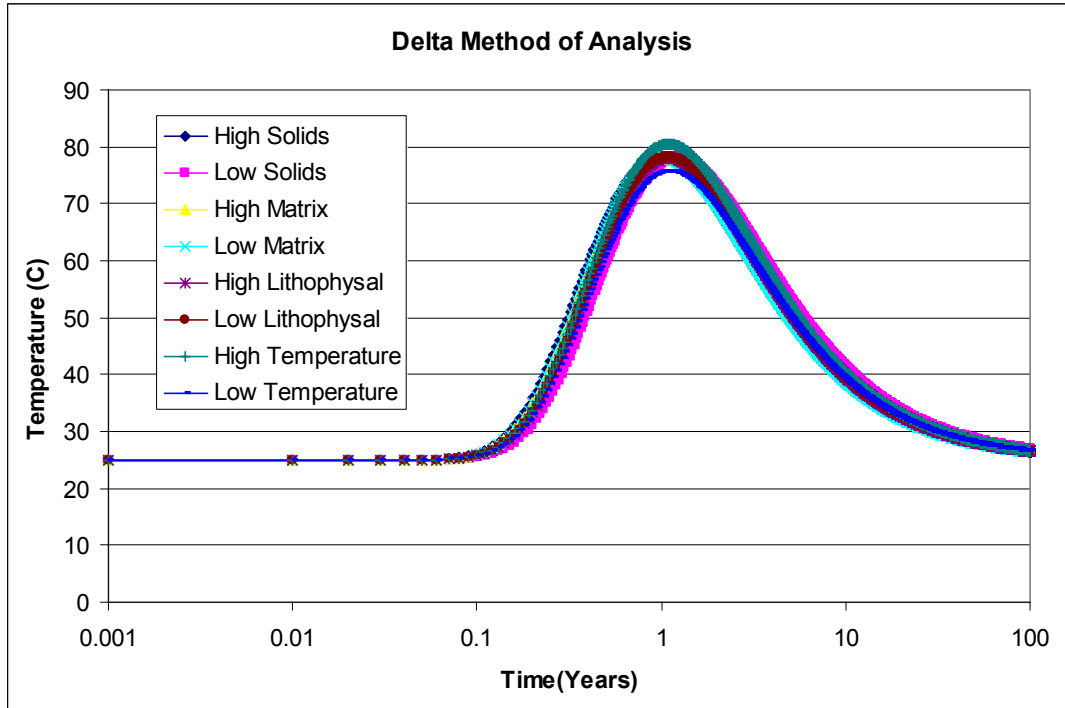
Figure I-1. Peak Temperatures for Variations in Key Inputs

Figure I-1 shows that variations in key inputs other than initial temperature result in a shift in the time when the peak temperature occurs, but the actual peak temperature remains the same.

The contributions to variance are then calculated for each component as the product of the sensitivity time the variance. The contributions are then summed. The analysis provides information on the percent contributions to system variance from each of the component variables. The analysis suggests that the principal source of uncertainty is the initial temperature (100 percent of the uncertainty). The variance caused by the uncertainty of the initial temperature should be used as the uncertainty of the output temperatures, which is ±3°C.

INTENTIONALLY LEFT BLANK

ATTACHMENT II

ANALYSIS OF GAS FLOW FROM ZONE 1 TO ZONE 2

II.1   PARAMETERS

Parameters used in the gas flow analysis are presented below.

Gas Viscosity (mu Gas): Since water in the volatile vapor makes up the majority of the gaseous mixture (73.16 percent), the viscosity of water vapor will be used to represent the viscosity of the gaseous mixture. The viscosity of water vapor at the highest temperature is 241.2 micro poises at 400°C (Table 4-4). The viscosity of water vapor at 400°C temperature is used because it is a conservative estimate of the viscosity of water vapor at elevated temperatures. The calculated water viscosity at 1150°C is 497.066 micro poises from an equation by Bird et al. (1960), which would cause a substantial reduction in gas flow.

Total Moles of Gases: Calculated total moles $= 9.58 \times 10^6$ moles. For calculating the total moles of volatile gas components, 2 weight percent volatile water is used (see Assumption 2).

Temperature over Time: The temperatures are based upon heat conduction through the rock mass presented in Section 6.5.2.1.

Rock Matrix permeability: Intrinsic permeability of mafic intrusion in rock matrix is estimated as an effective intrinsic permeability of 2.0×10^{-17} m^2, which is used to incorporate basalt (mafic) intrusion into the back-filled perimeter drifts.

Length between Drifts: Length of the space between two drifts (L) = 81 m (Table 4-4).

Emplacement Drift Dimensions: Average calculated length is 603 meters and diameter is 5.5 m (Table 4-4).

II.2   ANALYSIS

The analysis considers the scenario of instant intrusion of magma into the Zone 1 emplacement drift and backfilled perimeter drifts. Let X equal the distance between Zone 1 and Zone 2 drifts into the contact zone backfill and host rock. For the purpose of this calculation, it is assume that within this X distance, the contact zone rock matrix and backfill permeability has been affected. The air permeability of the backfill is k_b and that of the intruded host rock is k_r and the equivalent permeability for parallel flow through the backfill and host rock is given by Freeze and Cherry (1979, p. 34):

$$k_e = \frac{k_b \times A_b + k_r \times A_r}{A_{total}}$$ (Eq. II-1)

where

k_e = Effective air permeability (m^2)
k_b = Air permeability of backfill (m^2)

k_r = Air permeability of the host rock (m^2)
A_b = Area of flow through backfill (perimeter drift) (m^2)
A_r = Area of flow through host (m^2)
A_{total} = Total area of flow (m^2)

The effective permeability used in these calculations represents a magma intrusion of the rock and backfill (BSC 2002b; Lichtner et al. 1999). The intruded material has a low permeability to gas flow while the crushed tuff backfill and host rock are porous, and show a higher permeability. The Van der Waals Equation of State (Equation II-2) given by Cutlip and Shacham (2000, p. 1) can represent the gas pressure:

$$\left(P + \frac{a}{V^2}\right) \times (V - b) = n \times R \times T \qquad \text{(Eq. II-2)}$$

where

$$a = \frac{27}{64} \times \left(\frac{R^2 \times T_c^{\,2}}{P_c}\right)$$

$$b = \frac{R \times T_c}{8 \times P_c}$$

P = Pressure (atm)
V = Volume (L)
T = Temperature (K)
R = Gas constant (R= 0.08206 atm · L/(mol · K)
T_c = Critical temperature for the gas (K)
P_c = Critical pressure for the gas (atm)

Solving for the pressure in terms of the other variables, we obtain:

$$P = \frac{\left(\dfrac{a}{V} - \dfrac{a \times b}{V^2} - n \times R \times T\right)}{(V - b)} \qquad \text{(Eq. II-3)}$$

The fractured and porous rock as well as the crushed tuff used to backfill the perimeter drifts represents a possible path for gas flow resulting from magma intrusion. At the time magma flows into the drift, the initial pressure can be calculated from an estimate of the pore space, the number of moles of gas and the initial bounding temperature of 1150°C. The estimate can be made on the basis of Van der Waals Equation of state or the Ideal Gas Law. The Ideal Gas Law is used in the estimate of gas flow from a magma-filled drift to an adjacent emplacement drift (see Assumption 3).

For the purpose of this calculation, it is the void volume of the gas does not change in the magma and intruded drift. However, the pressure of the gas would change by gas flow from the magma into the intruded backfill and backfill, and by the reduction in temperature as predicted by the heat transfer analysis. Therefore, the time rate of change of the pressure is given by:

$$\frac{dP}{dt} = \frac{\left(\dfrac{a}{V} - \dfrac{a \times b}{V^2} - \dfrac{dn}{dt} \times R \times T\right)}{(V - b)} + \frac{\left(\dfrac{a}{V} - \dfrac{a \times b}{V^2} - \dfrac{dT}{dt} \times R \times n\right)}{(V - b)}$$

(Eq. II-4)

In the above differential equation, both the molar gas generation rate and the temperature change.

Figure II-1 shows that the Ideal Gas Law can be used in place of the Van der Waals Equation except at high pressures. Though the initial gas pressure was calculated at 640 atm in "Gas Flow Analysis.xls" (Attachment IV), this pressure drops off very quickly, and within 1.5 years is below 10 atm, as shown in Figure II-2. Therefore, this model uses the Ideal Gas Law.
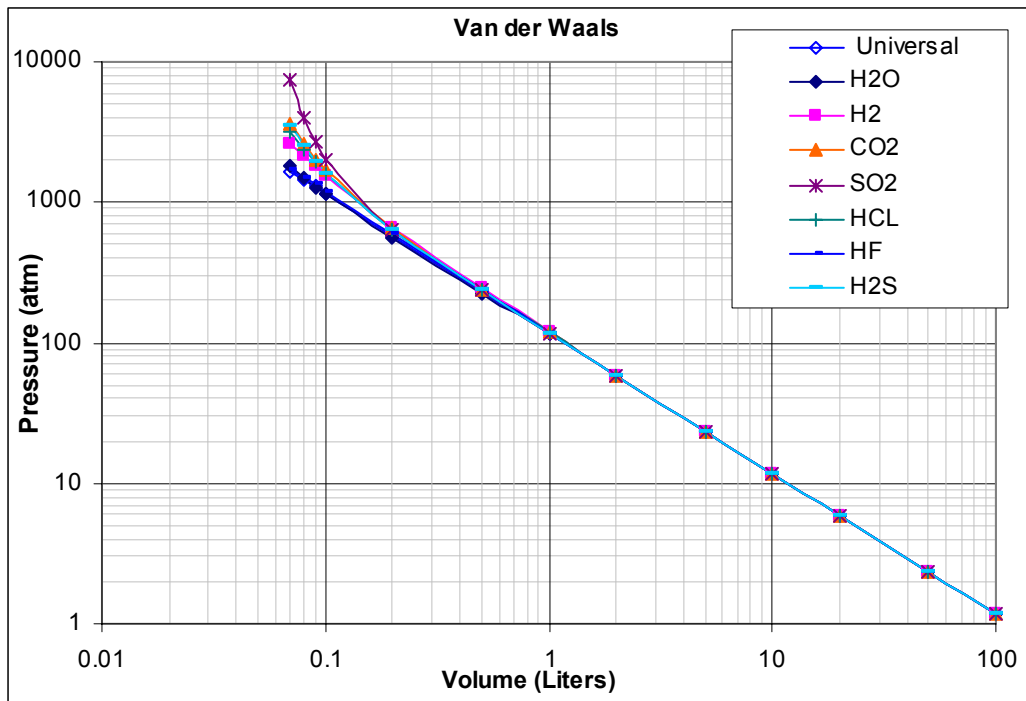
Figure II-1. Plot Showing Comparison of Van der Waals Equation and Universal Gas Constant
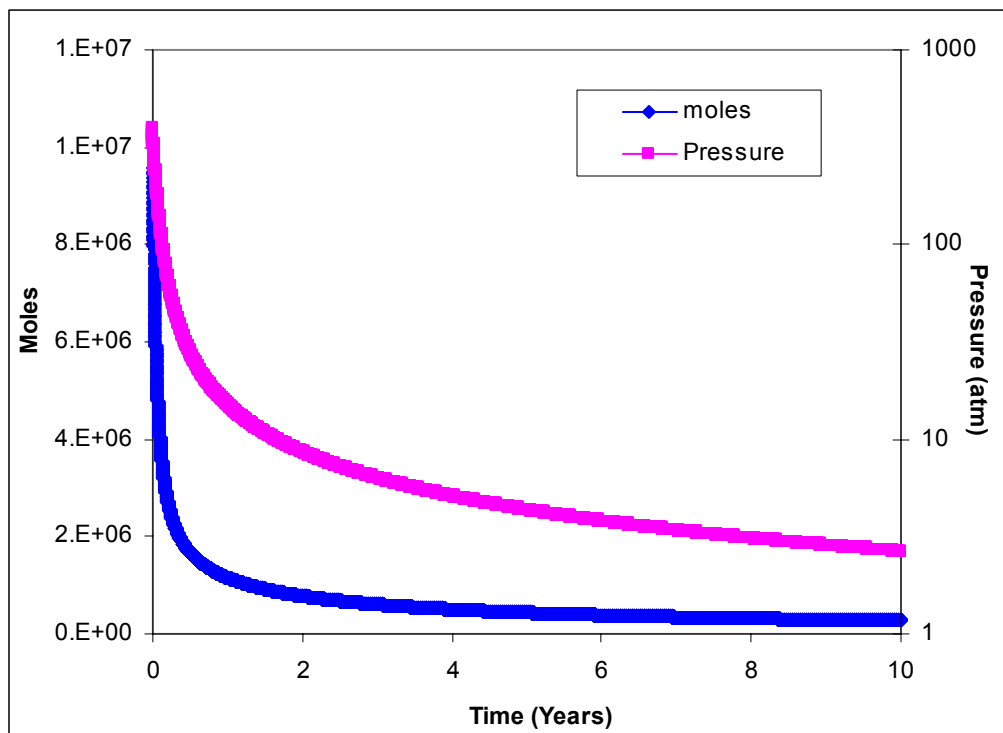
Figure II-2. Pressure and Moles Over Time

The temperature calculation presented in the report shows that there would only be a local temperature and therefore rock mass perturbation near the drift, and it would be expected that the rock mass fracture properties in the vadose zone would not be significantly altered. Since the system is open, any gas pressure from the magma intrusion would be expected to relieve quickly with time. The gas flow analysis using rock mass properties support this conclusion. It would not be realistic to expect the gas pressures to be lithostatic. This is validated in Figure II-1, which shows a plot of the pressures verses volumes calculated with the universal gas constant and the Van der Waals Equation for each gas constituent, and in Figure II-2, which shows pressure versus time. In using the Ideal Gas Law instead of the Van der Waals Equation, the constants "a" and "b" become zero in equations II-2, II-3, and II-4. The result is that the Ideal Gas Law is used to calculate pressure in place of the Van der Waals Equation.

For a given pressure, the density of the gas in (kg/m^3) is determined by solving the equation. The density is then multiplied by the volumetric flow rate to obtain the mass flow rate. By knowing the molecular weight for the gas, the flow rate of the moles of gas is determined through an application of Darcy's Law for incompressible gas flow:

$$\frac{dn}{dt} = \frac{\rho(p,T)}{MW} \times \left(-\frac{k_e}{\mu} \times A \times \frac{(p - p_{atm})}{L} \right)$$
(Eq. II-5)

where

      n   =   Number of moles
    MW =   Molecular weight (gm/mole)
      ρ =   Mass/m^3

μ = Dynamic viscosity (gm/(cm × sec))
A = Area (m^2)
k_e = Effective permeability (m^2)

Equation II-6 restates the Ideal Gas Law in terms of pressure (Jury et al. 1991, p. 172):

$$\frac{\rho(p,T)}{M} = \frac{p}{R \times T}$$ (Eq. II-6)

Equation II-5 can be rewritten to express the ratio $\rho(p, T)/M$ in terms of pressure:

$$\frac{dn}{dt} = \frac{p}{R \times T} \times \left(-\frac{k_e}{\mu} \times A \times \frac{(p - p_{atm})}{L} \right)$$ (Eq. II-7)

Equations II-4 and II-5 constitute a system of coupled ordinary nonlinear differential equations subject to initial conditions of pressure P, temperature T, and number of moles of gas. Using the simple Euler method solves the system of ordinary differential equations. Additionally, the average linear velocity of gas moving from the intruded drift to the adjacent drift is described by Darcy's law (Freeze and Cherry 1979, p. 16):

$$v = \left(-\frac{k_e}{n_e} \times \frac{(p - p_{atm})}{L \times \gamma} \right)$$ (Eq. II-8)

where

v = Velocity (m/s)
n_e = Porosity
γ = Specific Weight (kg/(m^2 × s^2))

While advection is one mode of gas movement (see Assumption 4), diffusion is the primary mode of movement when the pressure equilibrates between the intruded and adjacent drift. Diffusion of gas from the magma filled drift is calculated using the three dimensional transient solution of Fick's second law of diffusion (Freeze and Cherry 1979):

$$C(x,y,z,t) = \frac{M}{8(\pi t)^{3/2}\sqrt{D_x D_y D_z}} \exp\left(-\frac{x^2}{4D_x t} - \frac{y^2}{4D_y t} \frac{z^2}{4D_z t} \right)$$ (Eq. II-9)

where

C = Concentration (moles/m^3)
M = Initial mass or moles
x, y, z = Distance (m)
t = Time (yr)
D = Diffusivity coefficient

Equation II-9 describes radial diffusion along the three principal axes.

In the simulations of volatile gas diffusion, there are two main sources of uncertainty: a) the spatial variation in the diffusing media rock porosity and permeability between the drifts and the backfill, which affect the gas diffusivity and b) limitations of equations used for gas diffusion simulations. Gas diffusion due to spatial variation could also vary.

II.3 RESULTS

Results of the gas flow analysis are plotted in Figures II-3 and II-4, and show the advection and the gas front position over time resulting from the difference in pressure between the magma filled and adjacent drifts (Darcy flux) for the rock matrix (porosity = 0.154, DTN: LB990861233129.001) and the backfill (porosity = 0.545, DTN: MO0009SEPTIHMP.000). Gas movement through the backfill is slower and does not move as far as the flow in the rock matrix. This difference can be attributed to the difference in porosity between the two materials (i.e., the host rock porosity is less than that of the backfill). In both cases the velocity approaches zero at around one year, the gas front slows and stops at around 3.6 m in the host rock and 1.1 m in the backfill. Results of the advective flow analysis show that gas movement resulting from advection is minimal and is likely the result of the decreased permeability of the mafic intrusion.

While advective gas flow is one component of movement between the drifts during the first year, diffusion is still occurring and will become the single mode of movement at some point during gaseous equilibration. Results from an analysis of gaseous diffusion from the magma filled drift are provided in Figure II-5 and shows the maximum gas concentrations entering the adjacent drifts, 81 m away from the magma filled drift, would be low and will begin to fall off after about one year. It is important to note that the calculated concentration of gases that would reach zone two is extremely conservative because the model neglects interactions of the gases with the host rock, and the models only considers flow in the horizontal direction. The acid components of the gases released from the magma will interact strongly with the rock between the drifts, so any gases that do migrate into adjacent drifts will be much less aggressive with respect to corrosion. In addition, much of the water vapor will condense in the rock, based on the temperatures calculated in Attachment I. The gases will migrate away from the intersected drift in all directions, so the actual amount of gas that moves horizontally to the adjacent drifts will only be a fraction of the gas released. Therefore, it is concluded that the waste packages in Zone 2 emplacement drifts would not be impacted by the volatile gases exsolving from the basalt magma intruded into Zone 1 emplacement drifts.

Table II-1 gives the potential number of moles that could enter the adjacent drift. The gas concentration (moles/L) was calculated by dividing the number of moles that would enter the adjacent drift by the available drift volume (12,800 m^3, see Section 4.0).
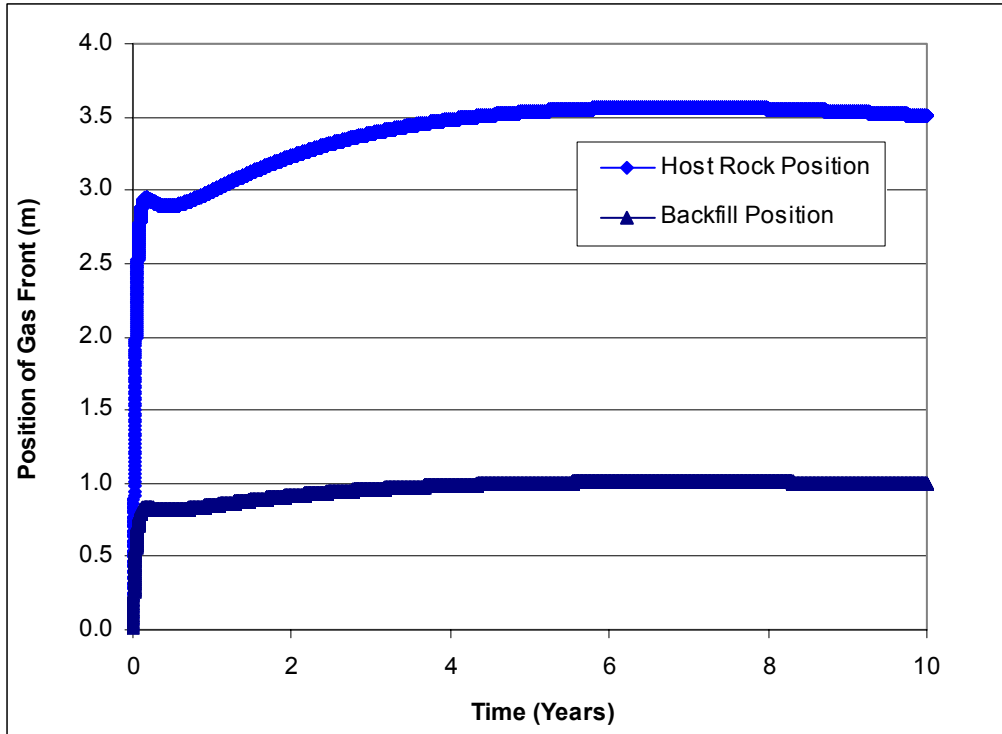
Figure II-3. Plot of Position of Gas Front Over Time for the Rock Matrix and Backfill
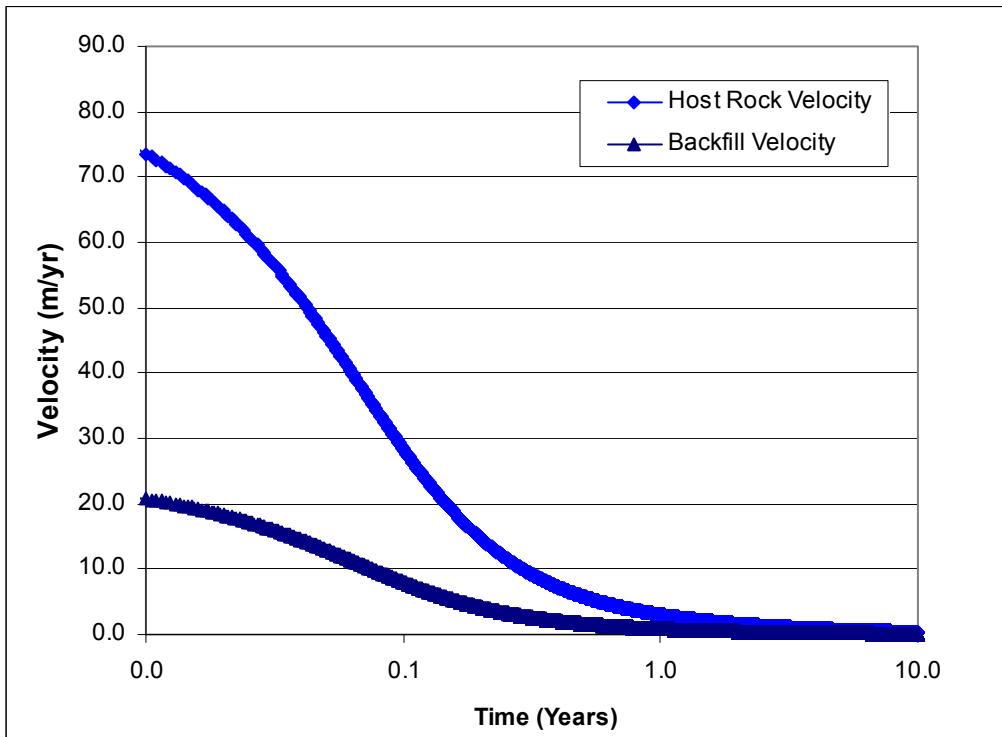
Figure II-4. Plot of Gas Velocity Over Time for the Rock Matrix and Backfill
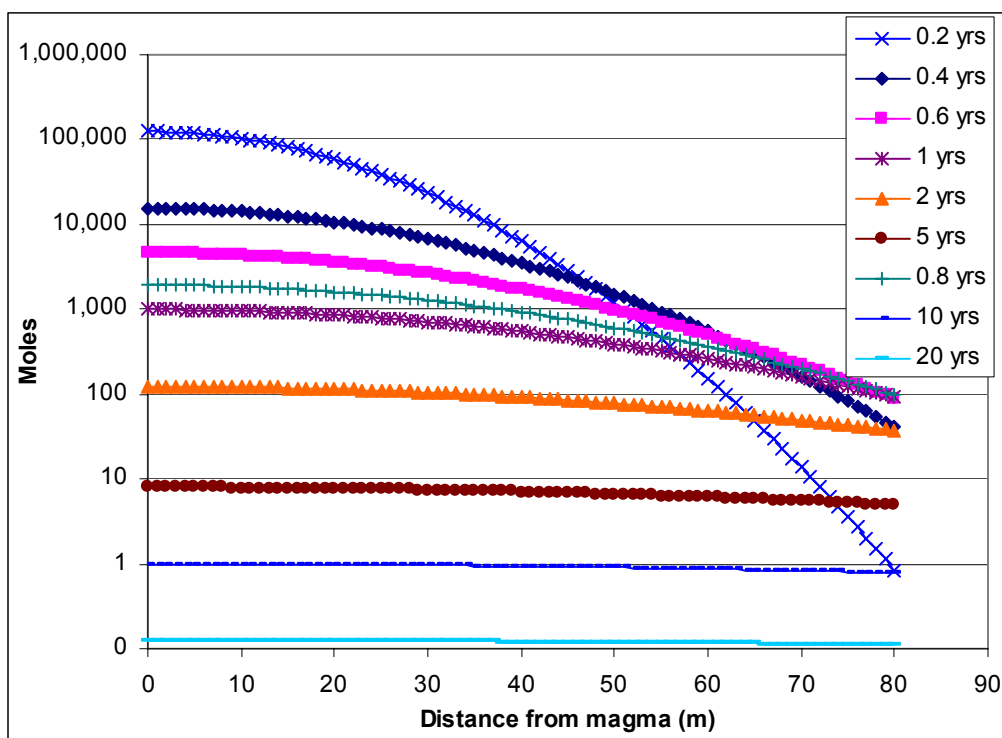
NOTES: The gaseous diffusivity is 2.13E-5 m^2/sec. Moles are expressed as a function of available drift volume: concentration (moles/m^3) $\times$ available drift volume (m^3).

Figure II-5. Plot of Moles Resulting from Radial Diffusion from the Magma-Filled Drift

The small amount of gas flow that does make it to Zone 2 results in the concentrations given in Table II-1.

Table II-1. Concentration of Gases That Reach Zone 2

Volatile gas	Mole %	moles/L
H_2O	0.7316	5.05E-06
H_2	0.0117	8.08E-08
CO_2	0.1428	9.86E-07
CO	0.0057	3.93E-08
SO_2	0.0945	6.52E-07
S_2	0.0041	2.83E-08
HCl	0.0087	6.01E-08
HF	0.0017	1.17E-08
H_2S	0.0074	5.11E-08
Total Moles	100 moles	

Source: "Gas Flow Analysis.xls" in Attachment IV

ATTACHMENT III

EQ6 MINERAL DISSOLUTION RATES

This attachment contains figures that show input values to, calculation of, and EQ6 rate comparisons of the rates for the dissolution of minerals in the EQ6 simulation of basalt/water interaction. Calculation of the mineral dissolution rates for EQ6 is as follows:

- Using Microsoft Excel, a trendline was added (linear) to each of the pH legs (i.e., low pH values were fit with one trendline and high pH values were fit with a different trendline). These linear fits are shown by the black trendlines in the figures. The linear equation for these lines is also presented as well as the rounded values used for the calculation of the rate for EQ6.

- EQ6 calculates the rate of dissolution at any pH by the following formula

$$\text{Total Dissolution Rate} = k_1[H^+]^{S1} + k_2[H^+]^{S2} \text{ (moles/cm}^2\cdot\text{s)} \qquad \text{(Eq. III-1)}$$

where k_1 and k_2 represent the exponential of the intercept and S1 and S2 values represent the slope of the trendlines.

- The EQ6 curve (pH dependent dissolution rate) is calculated by using the above stated values to calculate the dissolution rate for each pH leg. These values are then combined to create one dissolution rate by the model.
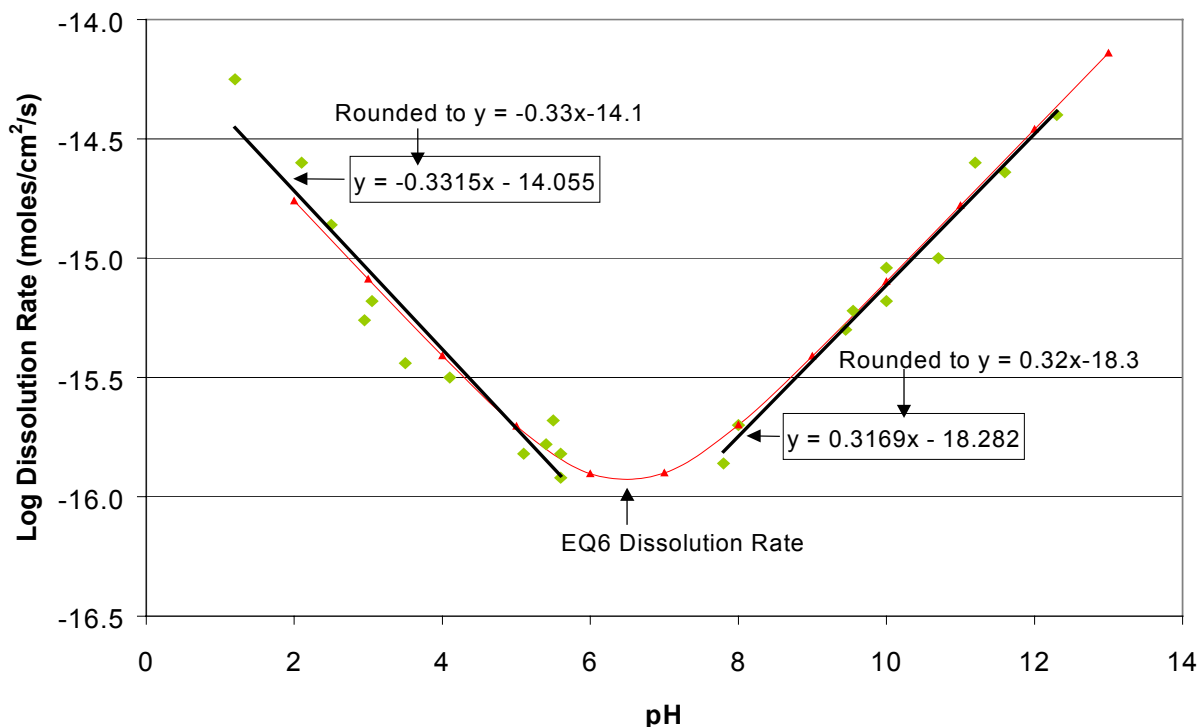
Figure III-1. EQ6 Dissolution Rate of Albite
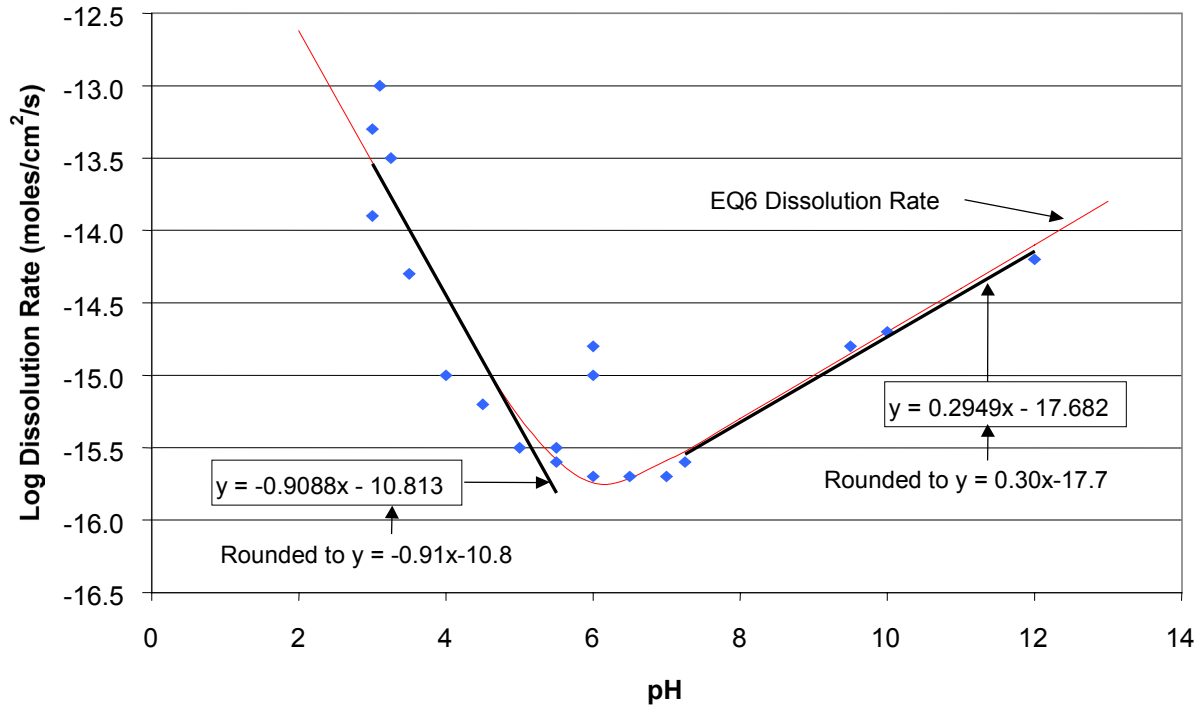
Figure III-2. EQ6 Dissolution Rate of Anorthite
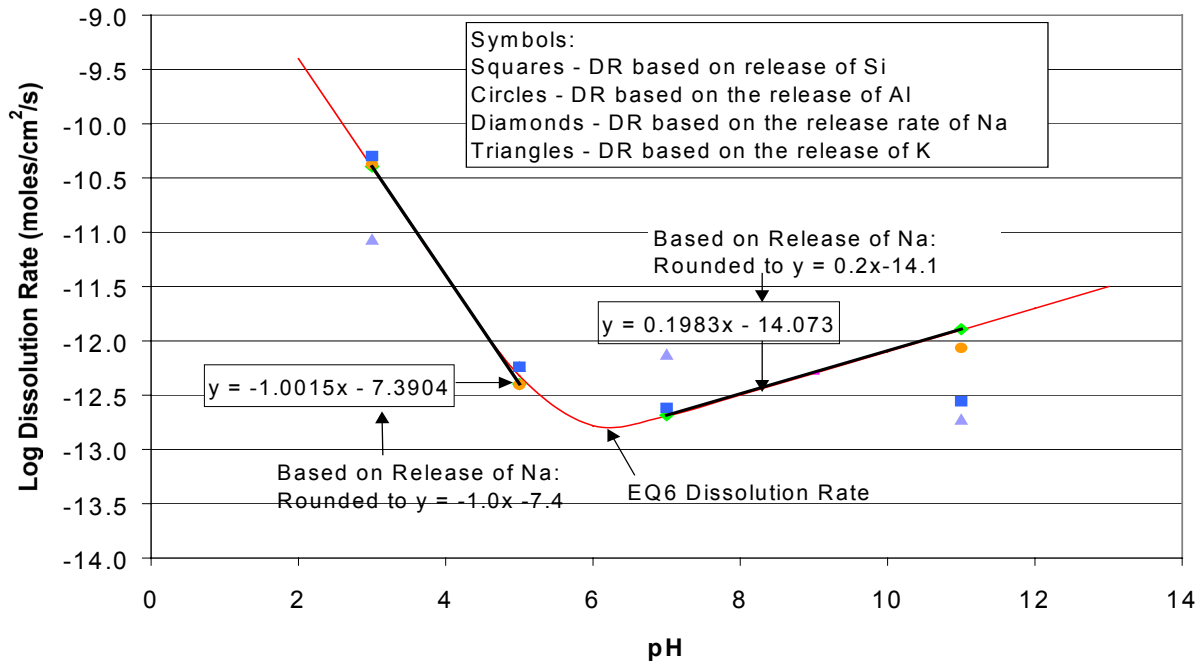
Figure III-3. EQ6 Dissolution Rate of Nepheline
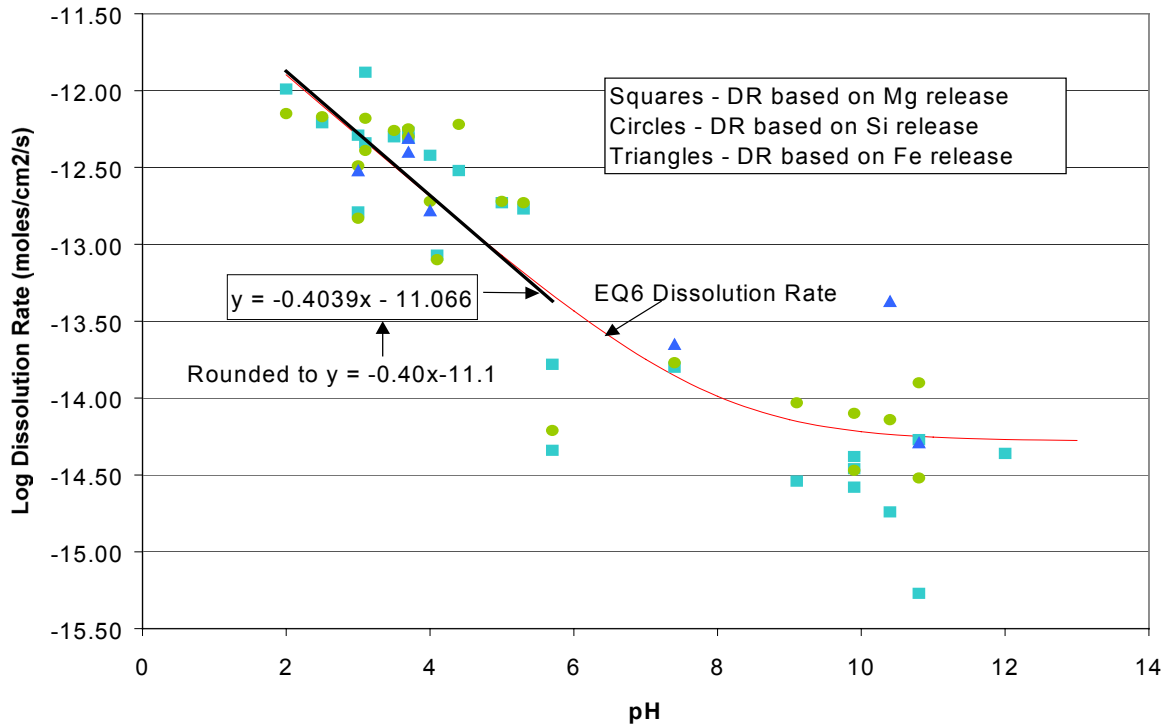
Figure III-4. EQ6 Dissolution Rate of Olivine
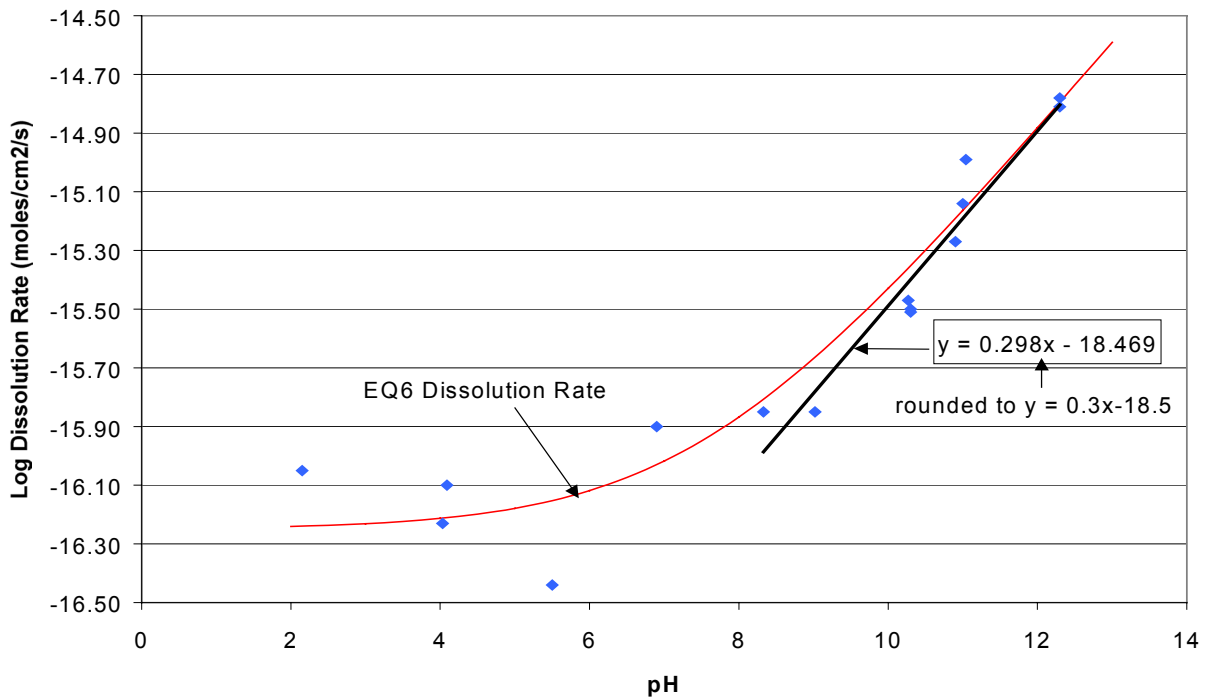
Figure III-5. EQ6 Dissolution Rate of Quartz
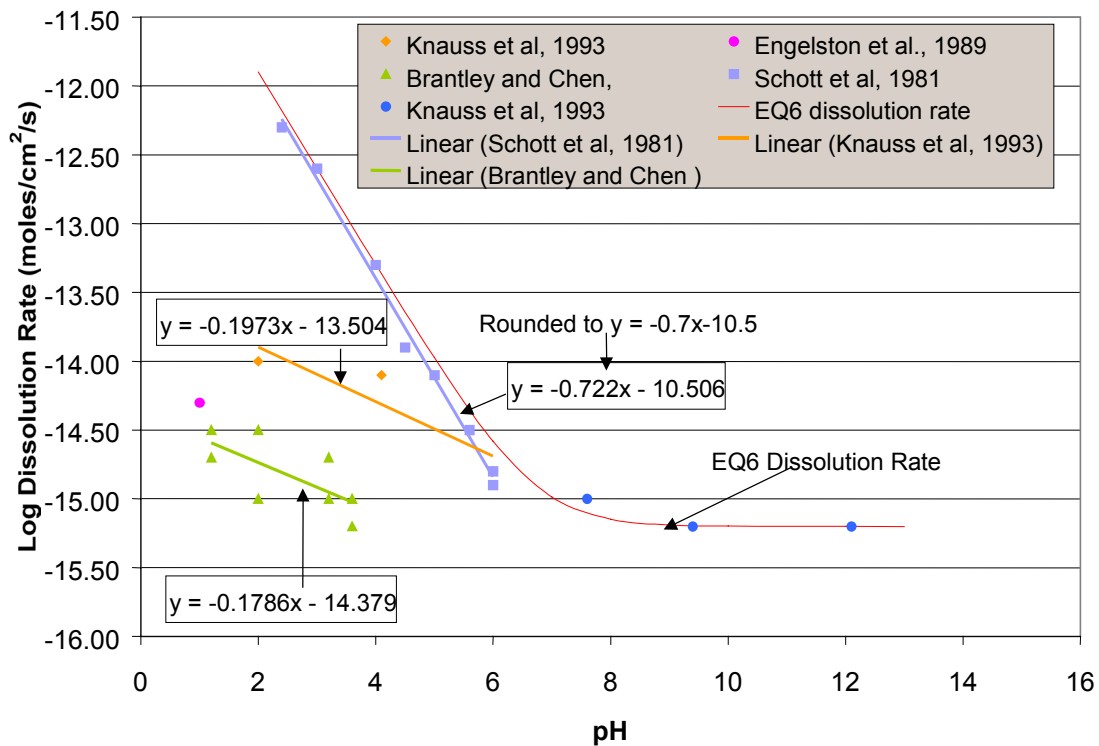
NOTE: All plotted data are from Table 1 of Brantley and Chen (1995), which is a compilation of dissolution data from different sources mentioned in the plot inset box.

Figure III-6. EQ6 Dissolution Rate of Diopside
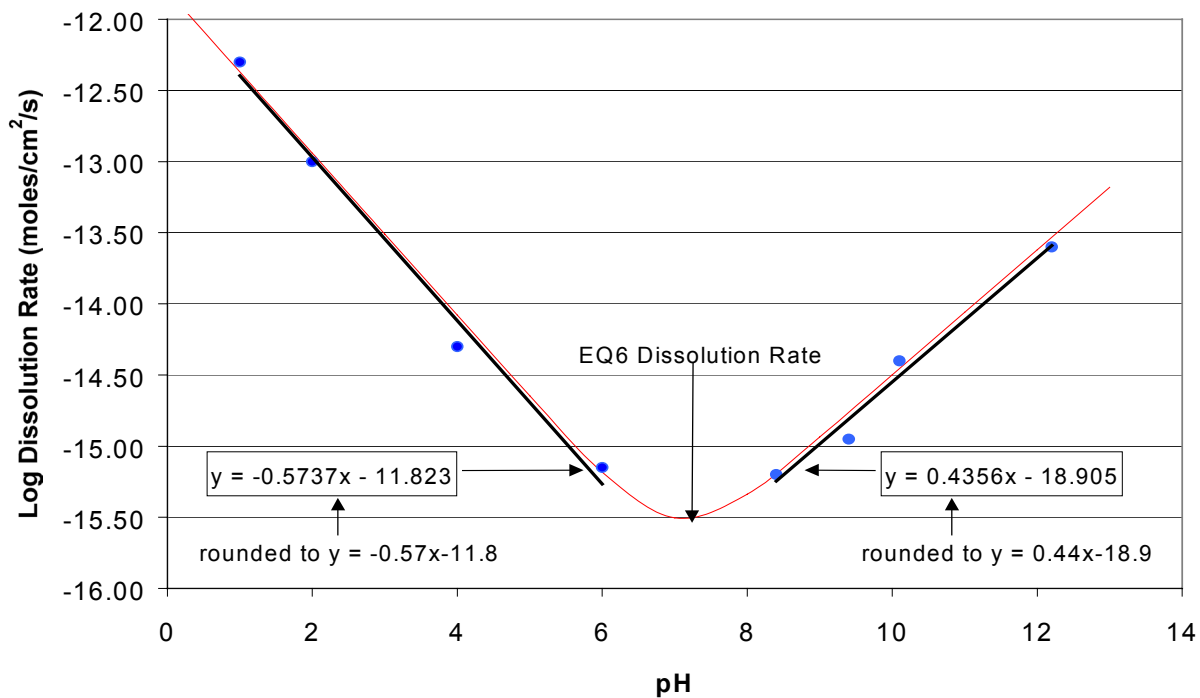
Figure III-7. EQ6 Dissolution Rate of Enstatite

ATTACHMENT IV

ATTACHED CD-ROM

Microsoft Excel Files for verification of calculations for the EQ6 are given on accompanied CD-ROM in the Attachment IV folder.

INTENTIONALLY LEFT BLANK

ATTACHMENT V

FILE LISTING OF ATTACHED CD-ROM

Volume in drive D is 030812_0939

 Volume Serial Number is BC50-4EBB

 Directory of d:\

07/31/2003 11:55a   3,718,047 EQ6 Files.zip

07/31/2003 11:56a   6,090,708 Gas Flow.zip

07/31/2003 12:00p   189,357,577 Heat Flow.zip

07/31/2003 11:57a   551,685 Uncertainty.zip

               4 File(s)   199,718,017 bytes

       Total Files Listed:

               4 File(s)   199,718,017 bytes

               0 Dir(s)   0 bytes free

INTENTIONALLY LEFT BLANK